University of California
Santa Barbara

# Improving Electron Transfer Across Membranes: Development of Redox Active COEs

A dissertation submitted in partial satisfaction
of the requirements for the degree

Doctor of Philosophy
in
Chemistry

By

Zachary David Rengert

Committee in charge:

Professor Guillermo C. Bazan, Co-Chair
Professor Thuc-Quyen Nguyen, Co-Chair
Professor Javier Read de Alaniz
Professor Mattanjah de Vries
Professor Frederick Dahlquist

June 2017

The Dissertation of Zachary David Rengert is approved.

---

Professor Javier Read de Alaniz

---

Professor Mattanjah de Vries

---

Professor Frederick Dahlquist

---

Professor Thuc-Quyen Nguyen, Co-Chair

---

Professor Guillermo C. Bazan, Co-Chair

May 2017

Improving Electron Transfer Across Membranes: Devolpment of Redox Active COEs



by

Zachary David Rengert

*To my father, David L. Rengert, who taught me to desire a life of my own choosing. To dream big, love much, and never give up.*

*R.I.P.*

*To my uncle, Steven J. Schaeffer, who taught me to stand up for what I believe in and to be generous with my time. For teaching me what it means to be a man, in my father's absence.*

*R.I.P.*

*To my mother, Susan E. Schaeffer, who sacrificed so much, so that I could pursue my dreams and a better life. For always believing in and supporting me, no matter how unorthodox my dreams where. For encouraging me to leave home to explore the world, myself, and the beauty of life. You are always in my heart.*

## Acknowledgements

At the completion of my Ph.D., I find myself at a bittersweet transition and I have a feeling reminiscent of when I first left home almost 9 years ago to pursue my education. That is, in many ways I again feel as though I am leaving home, leaving my family. My time at UCSB has, as anyone with a Ph.D. would likely agree, been filled with ups and downs, strikes and gutters. The amazing group of people that I have worked with over the past 5 years have been more than just colleagues, they have helped me through many tough times and, moreover, have always been more than enthusiastic in sharing my successes. We have seen each other almost everyday, many late nights, and many weekends. This group, of which I wish to acknowledge in grave detail, have been key in my learning and growth, both as a scientists and a member of the modern world. One of the great pleasures I have enjoyed over the past 5 years is working with people from all over the world, form literally every continent on this planet. They have taught me so much about myself though sharing their knowledge, culture, life experiences, and morality. When working with such a culturally diverse group, my beliefs and self-proclaimed truths have been challenged, allowing me to ask (and sometimes answer) some of the toughest questions in my life pertaining to my own desires and my view of the world as a whole. I know I am a better man through the experiences I have shared with them.

First and foremost, I would like to acknowledge the two people who first ignited my passion for chemistry and science: Professor Igor Alabugin and Dr. Wang Yong Yang. Yong was my TA for the first organic chemistry class I took at FSU and a grad student in Igor's lab. I was a bewildered undergrad that was desperately looking for a purpose and, to be perfectly honest, looking for a place to finally fit in. Yong was patient with my frantic excitement for chemistry and such a great mentor. We shared countless hours together as he meticulously trained me in the tenants of organic synthesis. He also taught

me much about handling stress and taking failure in stride. The bond we shared together is something I'll never forget.

Igor was a very dedicated mentor, refusing to give me an "undergrad project" and instead giving me a challenging project to freely explore, for that I am eternally grateful. He was patient when needed, but his tough attitude evoked my best. He would give me a look and say in an playfully sarcastic tone "Zach, a week in the lab can save you a day in the library", thus encouraging me to gather as much information about my work before attempting to learn the hard way. He was so supportive of my education, sending me to a conference and always being available to critique my presentations, posters, and, most importantly, data interpretation.

The Alabugin lab was also filled with individuals of the same character. I would like to acknowledge the support, mentorship, and friendship of Dr. Paul Peterson, Dr. Brian Gold, Dr. Kerry Gilmore, Dr. Phil Byers, Dr. Kemal Kaya, Dr. Runa Pal, Dr. Samuya Roy, Dr. Nikolay Shevchenko, and Dr. Abdulkader Baroudi. I would also like to acknowledge my fellow undergrad researchers; Natalie Bonus, Jason Kirincich, Matthew Gatcombe, Forat Lufti, Nalisha Minors, and Jeremiah Alicea. Last, but most importantly, I thank Dani Phrathep, who was a dear friend, working side by side on the same projects, your the man Dani!

Next, and most importantly, I would like to acknowledge my Ph.D. advisors, Professor Guillermo Bazan and Professor Thuc-Quyen Nguyen. It is to these two that I owe so much for their unending dedication to my education and their support of me as I grew into a scientist. I would like to thank them for giving me freedom in my research to pursue topics of my own interest and for guiding me along the way, I know at times I have pushed their patience. I am deeply grateful for the opportunities they have given me to travel to conferences to present my work in Italy, Seattle, and China. In fact, the first time I ever left the U.S. was on my conference to Italy, which was one of the most

exciting experiences of my life.

Gui's passion for science pushed me to require the best from myself and taught me to stay focused on the road to achieving a specific goal. His attention to detail has helped me to vigorously question my logic and to relentlessly look for deeper meanings in seemingly simple trends. He has helped me become a succinct, deliberate scientific writer and a polished, charismatic presenter. His, at times, tough character has brought resolve to dealing with my own shortcomings and toughened my skin.

Quyen has taught me much about being a leader; tough when needed and kind in general. She has constantly instilled a desire to do careful science and to work collaboratively with both my colleagues and other scientists in general, encouraging me to reach out to others in an effort to gain knowledge and to concomitantly have the bravery to tackle problems outside my comfort zone. She has always taken interest in my well being and was determined that all her students lead a healthy research lifestyle. She has shared countless life experiences and advice that have helped immensely with my skill set as a scientist and person.

I would like to thank Dr. Lei Ying, for being my mentor when I first started grad school and for being an awesome person in general. Lei taught me so much about organic semiconductor synthesis and characterization. Our short time together allowed me to start grad school on a strong note and allowed me to succeed early on in synthetic projects. My dear friend Dr. Ron Bakus was also so instrumental during my initial grad school years, teaching me numerous important details in synthesis and teaching me to properly maintain lab equipment in a environment that sometimes disregarded the value of "fix it yourself". Ron has so much knowledge in so many deep, dark corners of science, without his mentorship I would have spent years digging for answers buried in the vast expanse of scientific literature. Ron's generous, authentic personality afforded a friend who helped me through some tough times during my research, when my chemistry wasn't

working.

Dr. Nate Krichhofer was my partner in crime throughout grad school. He was the one who initially proposed the idea of redox active COEs and was the second half of the team that brought this project to life. We worked very closely together for almost 4 years and saw each other everyday. It is quite rare to have a someone in your life that your work exceptionally well with and can also be the best of friends. This is surely due to his exceptional character and unparalleled whit. Nate taught me electrochemistry in such great detail and I did my best to teach him organic synthesis (due to my shortcomings, not his intellect!). Nate also taught me to finally find a balance between my work and home lives, something that was in a decrepit state at the time.

To the same end, I am grateful to Dr. Chelsea Catania for our work together with the liposome project. Throughout my grad school career, Chelsea and I were very good friends, but it wasn't until the end of our time at UCSB that we had the opportunity to finally work on a project together. I found in Chelsea another great relationship that blended true friendship with intellectual productivity. We were able to bring our different backgrounds together to start to answer questions that had been looming in our lab for a few years. She taught me much about molecular biology and how to thoughtfully layout a project plan prior to execution. Indeed, the themes she instilled in my approach to solving a problem will be invaluable for the rest of my life.

Dr. Hengjing Yan and I collaborated on two COE projects and I am very grateful for her input, knowledge, and amazing attitude. Sam McCuskey and I worked together at the end of my Ph.D. and she has been such a pleasure to work with. Sam has been instrumental in helping to prove my hypothesis with regard to my double ferrocene molecules by performing all of the bioelectrochemical work.

There are a myriad of brilliant individuals who have helped me solve so many problems throughout the course of my Ph.D. and I would like to thank them for teaching me so

much. In the area of organic synthesis, I would like to thank Dr. Xiafeng Liu, Dr. Jianhua Liu, Dr. Cheng-Kang Mia, Dr. James Fennewald, Dr. Jessi Coughlin, Alex Moreland, Dr. Sam Helmy, Dr. Roscoe Linstadt, Dan Lippincott, Dr. Stephanie Fronk, Xiaofen Chen, Dr. Bruno Grimm, Dr. Andreas Lorbach, Dr. Kuburat Saliu, Prof. Surya Prakash Singh, Dr. Vishal Patil, and Dr. Yasuharu Hasegawa. In the area of device physics, I would like to thank Dr. Niva Ran, Dr. Sam Collins, Dr. Jack Love, Dr. Chris Proctor, Dr. Martjin Kuik, Dr. Hung Phan, Dr. Olex Mikhnenko, Dr. Mark Burgers, Dr. Yuanyuan Hu, Caitlin McDowell, Michael Ford, and Michael Hughes. In the area of bioelectronics, I would like to thank Dr. Jenny Du, Dr. Logan Garner, Dr. Alex Thomas, and Dr. Bing Wang.

I must also mention the amazing friendship I found in Dr. Niva Ran, Dr. Sam Collins, and Dr. Hung Phan. Niva is such an amazing person to have shared an office with for 4 years and has such a beautiful outlook on life, your presence has helped me through some tough times. Dr. Sam Collins is another person of great character and an amazing musician I must add, we had many good times revealing stress through our music together. Dr. Hung Phan, although originating from across the world in Vietnam, shares so many similar life experiences with myself. I have always been amazed at how similar we are in so many ways, our adventure together during the Seattle conference was one of the best I've had.

I also thanks all of my friends and colleagues in both Bazan and Nguyen groups; Michael Hughes, Akchheta Karki, Ben Luginbuhl, Alex Lil, Tyler Postel, David Cao, Katie Rosenthal, Brett Yurash, Jianfei Huang, Dr. Lijiao Ren, Dr. Seo-Jin Ko, Martin Seifrid, Dr. Ming Wang, and Zichao Zhang.

**Thank you so, so, so much to my amazing girlfriend, Apoorva Chiplunkar, for always being there for me, always loving me, and being my best friend. I love you!**

The family I found at UCSB involved so many people, that I know I will inevitably leave someone off, for that I am sincerely sorry. I must mention my mazing friends outside of the lab, for without you I could not have done this. Particularly I want to mention my best friends in the world; Eric Engel, Alex Pavellas, Cory Lund, Josh Sheltzer, Elmer Guzman, and Carl Peterson, you guys are the best friends anyone could ask for. Also, thank you to Chris Gabriel, John Eickhoff, Brett Cook, Alicia Lund, Jill Denison, Lauren Covey, Dr. Sam Helmy, Marcela Areyano, and so many more.

Last, thank you to my **real** family, which is too large to name here, you know who you are and I love you more than anything!

*This dissertation was supported by the National Science Foundation (NSF) Graduate Research Fellowship Program (GRFP) and a doctoral scholars fellowship from the graduate division of UCSB.*

# Curriculum Vitæ

Zachary David Rengert

## Education

| | |
|---|---|
| 2017 | Doctor of Philosophy in Chemistry (Materials Chemistry), University of California, Santa Barbara, CA 93106 USA. |
| 2012 | Bachelor of Science in Biochemistry, The Florida State University, Tallahassee, Fl, 32306, Honors: *magna cum laude* |
| 2012 | Bachelor of Science in Environmental Chemistry, The Florida State University, Tallahassee, Fl, 32306, Honors: *magna cum laude* |

## Publications

| | |
|---|---|
| 2017 | *The Role of Electrostatic Interactions in Governing Conjugated Oligoelectrolyte Association with Liposomes*, Zachary D. Rengert, Chelsea Catania, Thuc-Quyen Nguyen, and Guillermo C. Bazan. *To be submitted* |
| 2017 | *Impact of Aggregation on the Redox Properties of Ferrocene-containing Conjugated Oligoelectrolytes*, Zachary D. Rengert, Mengwen Zhang, Matthew E. Helgeson, Thuc-Quyen Nguyen, and Guillermo C. Bazan. *Submitted* |
| 2017 | *Membrane-intercalating molecules modify microbial dynamics in biofilms and enhance energy generation from wastewater*, Hengjing Yan, Zachary D. Rengert, Frederick Dahlquist, and Guillermo C. Bazan. *Submitted* |
| 2017 | *Acceleration of Yeast Biocatalysis with Conjugated Oligoelectrolytes*, Stephanie L. Fronk, Bing Wang, Zachary D. Rengert, and Guillermo C. Bazan. *To be submitted* |
| 2017 | *A Ferrocene-Based Conjugated Oligoelectrolyte Catalyzes Bacterial Electrode Respiration*, Nathan D. Kirchhofer*, Zachary D. Rengert*, Frederick W. Dahlquist, Thuc-Quyen Nguyen, and Guillermo C. Bazan. *Chem* **2**, 240 (2017). [DOI]*Co-first Author |
| 2017 | *Observing Ion Motion in Conjugated Polyelectrolytes with Kelvin Probe Force Microscopy*, Samuel D. Collins, Oleksandr V. Mikhnenko, Thanh Luan Nguyen, Zachary D. Rengert*, Guillermo C. Bazan, Han Young Woo, and Thuc-Quyen Nguyen. *Adv. Electron. Mater.*, 1700005 (2017). [DOI] |
| 2016 | *Influence of molecular structure on the antimicrobial function of phenylenevinylene conjugated oligoelectrolytes*, Hengjing Yan, Zachary D. Rengert, Alexander W. Thomas, Carolin Rehermann, |

Jamie Hinks, and Guillermo C. Bazan. *Chem. Sci.* **7**, 5714 (2016). [DOI]

2014 *Operational Mechanism of Conjugated Polyelectrolytes*, Daniel Tordera, Martijn Kuik, Zachary D. Rengert, Enrico Bandiello, Henk J. Bolink, Guillermo C. Bazan, and Thuc-Quyen Nguyen. *J. Am. Chem. Soc.* **136**, 8500 (2014). [DOI]

2011 *Engineering pH-Gated Transitions for Selective and Efficient Double Strand DNA Photocleavage in Hypoxic Tumors*, Wang-Yong Yang, Saumya Roy, Boondaniwon Phrathep, Zachary D. Rengert, Rachael Kenworthy, Diego Zorio, Igor Alabugin. *J. Med. Chem.* **54**, 8501 (2011). [DOI]

**Selected Honors**

2013 Phi Lambda Upsilon Award, University of California, Santa Barbara

2013 National Science foundation (NSF) Graduate Research Fellowship Program (GRFP)

2012 Doctoral Scholars 2-Year Fellowship: UCSB Graduate Division

2012 Undergraduate Research Award: FSU Department of Chemistry and Biochemistry

2011 $1^{st}$ place: ACS-Florida Annual Meeting and Exposition (FAME) undergraduate poster competition. Presentation titled, Photoadditions of Acetylenes: Dimerization, Homoquadracyclane Formation, and Double-Stranded DNA Cleavage

2008 Florida Bright Futures- Medallion Scholarship

## Abstract

Improving Electron Transfer Across Membranes: Devolpment of Redox Active COEs

by

Zachary David Rengert

Biotic-abiotic interfaces play crucial roles in bioelectrochemical systems, where the transport of electrons across membranes to or from an electrode is a key challenge which limits device performance. In electrogenic bacteria, this process is assisted by transmembrane proteins which utilize redox centers to shuttle electrons to extracellular electron acceptors. However, electrogenic bacteria are quite rare in nature and imparting electrogenic phenotypes to broad classes of bacteria represents an understudied strategy, especially with respect to real world applications of bioelectrochemical systems.

Drawing inspiration from the naturally occurring electron transporting proteins found in *Shewanella oneidensis*, we designed a redox active conjugated oligoelectrolyte (COE) which mimics the properties of these proteins in a small organic molecule, DSFO+. The properties of DSFO+ allow it to spontaneously intercalated into a lipid bilayer, have a redox potential that is biologically relevant, and catalyze transmembrane electron transfer in a non-toxic manner. The design, synthesis, and characterization of DSFO+ with relevant comparison to previous COE architectures will be discussed in detail . The ability for DSFO+ to catalyze transmembrane electron transfer in wild type and mutant strains of *Shewanella oneidensis* lacking key transmebrane redox proteins will then be discussed. These results afford the description of DSFO+ to be akin to a synthetic protein prosthetic.

The design of a $2^{nd}$ generation of redox active COEs bearing two redox centers will then be discussed and characterization of their electrochemical properties will be inves-

tigated. Intermolecular interactions play a large role in the observed electrochemical response of these materials and these effects will be deconvoluted from single molecule properties. Fluorinating the semiconducting backbone modulates electochemical properties, allowing for studying the effect of redox potential on bioelectrochemical performance with minimal change in COE structure. Preliminary results using our $2^{nd}$ generation redox active COEs in bioelectrochemical devices will be presented.

In the last section, the interaction of non-redox active COEs is investigated with model lipid bilayers in the form of liposomes. Cationic and anionic COEs were used to stain liposomes containing neutral or anionic lipids. Electrostatic interactions were found to play a large role in governing the favorability of COE intercalation and the amount of COE incorporated into a liposome was found to closely correlate with changes in the surface potential of the liposome. The mole percent of COEs in model systems were found to be much lower than what was previously found in living systems, hinting at the possibility of more complex COE-cell interaction than what can be accounted for in a simple membrane intercalation model. These results indicate that COE intercalation is governed not only by solubilization of the hydrophobic core of COEs in the lipid bilayer, but that COE-COE and COE-lipid electrostatic interactions play an important role in governing the favorability of COE intercalation.

# Contents

# List of Figures

# Chapter 1

# Renewable Energy: The Scientific Holy Grail at the Turn of the $21^{st}$ Century

The transition of technologies based on non-renewable resources to those based on renewable resources, without sacrificing the quality of life enjoyed by the populous, is one of the grand challenges of the $21^{\text{st}}$ century. Concomitantly, developing technologies with environmental sustainability as a central dogma, both from the point of raw materials and product production, is paramount in a world of ever growing population. Vital human needs encompassed by these technological issues are potable water availability and contaminated water purification.

As set forth by the United Nations in their Declaration of Human Rights, Section 25, access to potable water is a basic human right.[1] However, the access to potable drinking water is not trivial in many parts of the world, with many communities forced to boil their

water prior to consumption or simply drink contaminated water. 700 million people are currently dealing with issues of water scarcity in over 40 countries and this number has the capacity to increase to 1.8 **billion** people by 2025. [2] The treatment of wastewater to produce potable water and prevent the spread of disease is a non-trivial task which requires a substantial amount of energy. An estimated 2 million tons of sewage and other contaminated water are discharged into the watersheds of the world everyday. [3] Nevertheless, treating contaminated wastewater is a task that is undertaken throughout the world. Mitigating the energy required to treat wastewater represents an opportunity to prevent both contamination of watersheds and human exposure to toxic wastewater, as this task will become more economically viable as costs are decreased.

Of all of the dihydrogen monoxide ($H_2O$) on planet Earth, 97 % is seawater, 2.5 % is frozen freshwater, and **only** 0.5 % is available freshwater! On average, throughout the world, 8 % of water is used for domestic purposes, 22 % is used for industrial purposes, and 70 % is used for agriculture.[4] The problem of water quality and treatment is not just a problem associated with drinking water for people in exceptionally arid climates, the populous needs water to not only clean our clothes, dishes, and homes, but also to provide cooling for industrial processes that drive our economies, and grow the food that feeds our nations.

## 1.1 Microbial Fuel Cells and Microbial Electrochemical Cells

From a simplistic viewpoint, microbial fuel cells (MFCs) are devices which clean water and produce electricity at the same time. Their goal is to use organic matter in wastewater as fuel for both the fuel cell and the bacteria contained inside. The organic

matter found in wastewater can originate from a multitude of sources but almost all of it is anthropogenic and typically a direct form of human waste. The types of bacteria required for successful operation of a MFC will be discussed in detail in a later section and this topic is one of the main concerns of this thesis.

Before a detailed description of MFCs is possible, a brief discussion of fuel cells in general must precede. Fuel cells and batteries operate on the same basic principles and only differ in their physical configuration. A battery is a self contained entity, where all of the necessary chemical reagents are housed in the casing of the battery, thus making it portable and quick to use. The downside to this is that when a battery has converted all of it's chemical potential to electrical potential, it is dead and must be recharged. In a fuel cell, the necessary chemical reagents are not housed in the same casing as the electronics, such that chemical reagents are flowed from another container (usually a tank of some sort) into the electronic circuitry of the fuel cell, allowing for power generation to occur. This allows the fuel tanks of a fuel cell to be refilled as needed, but also makes the entire system more complex and less transportable.

The basic operation that a fuel cell (and battery) performs is to convert a chemical potential to electrical work, this is known as a galvanic cell. However, in some cases (especially microbial bioelectrosynthesis) a fuel cell can be used to convert electrical work into chemical free energy, this is known as a electrolytic cell. We will focus on using fuel cells as galvanic cells here. A typical fuel cell is constructed of two half-cells which are separated by an optional proton selective membrane; the anode half-cell, where fuel is oxidized to give electrons to an electrode, and the cathode half-cell, where electron acceptors receive electrons from an electrode to complete the electrochemical reaction.[5] This process **releases energy**, as the reactants are energy rich, and the process as a whole is spontaneous. The process occurring in each half-cell is known as the half-reaction of the overall electrochemical reaction. There is an energy potential at which each half

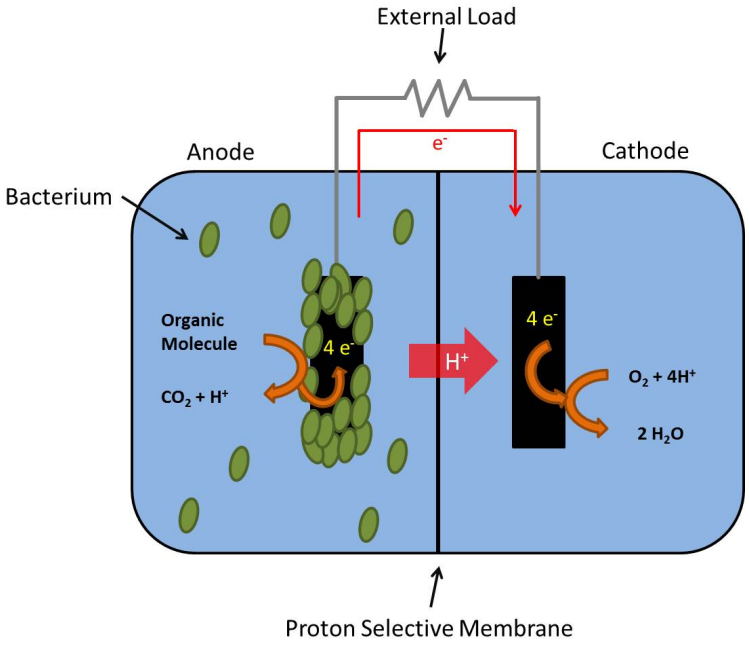


Figure 1.1: Schematic of a MFC showing the bioanode, anode chamber, cathode chamber, and proton selective membrane.

reaction takes place, and the difference in energy between the two half-reactions is the maximum energy that one can obtain from the fuel cell.

In a MFC, the basic principles of operation are exactly the same as in a traditional fuel cell and microbes are introduced to act as *catalysts* in the oxidation of organic matter (which serves as fuel for the fuel cell and food for the bacteria). A diagram of a MFC is shown in 1.1. For most lines of inquiry, especially here, one is mostly concerned with the processes occurring in the anode chamber of the MFC, as this is where bacteria are present to catalyze the oxidation of organic matter. It is necessary that the anode chamber of a MFC be anaerobic because oxygen is typically the terminal electron acceptor for most organisms, humans are a relevant example in this context. The organisms used a MFC are either *facultative* anaerobes or *obligate* anaerobes. Facultative anaerobes are organisms which are capable of respiring on oxygen, but can switch their

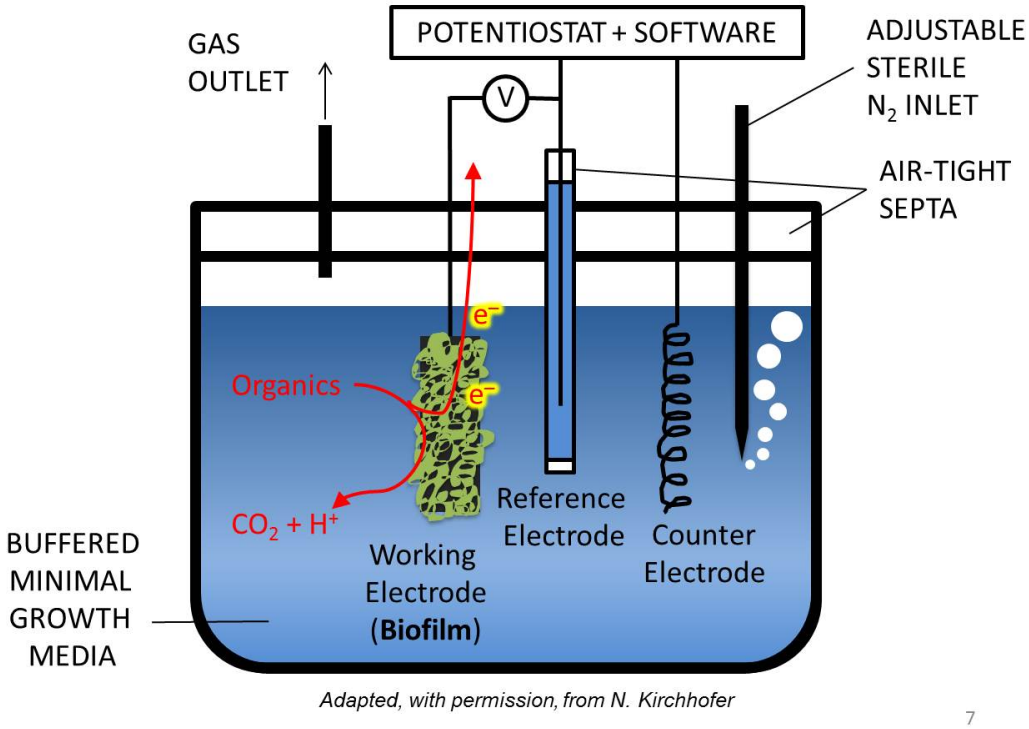


Figure 1.2: Schematic of a typical M3C.

terminal electron acceptor to another species in the absence of oxygen. Facultative anaerobes typically prefer to respire on oxygen, as it can easily diffuse into the cell, offers a larger energy gain (more ATP is produced), and is typically available in adequate concentrations. Obligate anaerobes are organisms which cannot respire on oxygen and will usually die in the presence of oxygen. In either case, the presence of oxygen in the anode of a MFC will cease the production of current in the fuel cell.

Due to the fact that the anode chamber of an MFC is of particular interest, it is possible to construct a device similar to a MFC that affords interrogation of the anode specifically, this is a microbial electrochemical cell (MEC). A MEC, as shown in 1.2, is a single chamber electrochemical cell with working, counter, and reference electrodes (see 1.4- Electrochemistry for more detail on electrochemical cells). In a MFC, one measures

the voltage produced from a fuel cell under a known resistance, where in a M3C on measures current production in the electrochemical cell with a known voltage applied. At a fixed voltage, one measures the current output from a M3C as a function of time, known as chronoamperometry. The reference electrode allows one to choose a voltage applied in the cell, which can be useful in interrogating processes which occur at specific potentials. Additionally, the 3 electrode set-up allows for *in situ* cyclic voltammetry or differential pulse voltammetry (these techniques are discussed in 1.4- Electrochemistry), which can be vital for understanding processes that occur in M3Cs/MECs and determining factors that lead to improved device performance. For these reasons, M3Cs are useful platforms to interrogate the effects of various chemical additives to the performance of biofilms in bioelectrochemical applications. [6]

## 1.2 Electrogenic Organisms

By virtue of existence on a planet whose atmosphere is composed of almost 21% oxygen ($O_2$), most life on Earth has evolved to use oxygen as the terminal electron *acceptor* in their metabolic respiratory process. The main goal of all metabolic processes occurring in heterotrophs is to produce Adenosine triphosphate (ATP), which serves as the energy currency of organisms. There are two main advantages in using oxygen for respiration; oxygen is a gas than can readily diffuse into cells (although in higher organisms this process is mediated by proteins such as hemoglobin) and the reduction potential of oxygen is larger than other candidates in the environment, thus allowing organisms to generate more ATP per unit of food. The second point, although not immediately obvious, is of paramount importance when considering the amount of energy an organism can extract from a food source. This is because the energy gained (or lost) from a redox processes is equal to the difference in energy between the two half potentials

of the total redox process.

In the absence of oxygen, certain organisms have evolved to either tolerate the absence of oxygen or to utilize other electron acceptors. Organisms such as yeast are familiar to many due to their ability to undergo fermentation and afford products such as alcohol that are popular in society. In humans, fermintation occurs commonly during the course of strenuous exercise which causes a buildup of lactic acid and leads to a burning feeling in muscular tissue. The process of fermentation is inherently less efficient than respiration, as the metabolic oxidation process is stopped prior to the Krebs cycle and oxidative phosphorylation, leading to the formation of only 2 equivalents of ATP instead of *38* afforded with the Krebs cycle and oxidative phosphorylation! [7]

Certain organisms have evolved to respire on electron acceptors other than oxygen, which allows them to generate more ATP than fermentation alone, but requires the use of a terminal electron acceptor. Because oxygen is one of the most powerful oxidizers found in nature, the use of alternative electron acceptors affords less energy to the organism. However, for life in the deep sea, in sediments at the bottom of lakes, and other anaerobic environments there is simply no other option. As such, these organisms have evolved to produce special proteins that allow them to reduce other substrates, such as sulfates, nitrates, and even minerals such as iron oxides. The case of minerals is of particular interest for the problem at hand, as minerals are *solid state* acceptors, meaning that they are not solutes in aqueous media and have physical properties reminiscent of electrodes used in electrochemistry. For this reason, organisms capable of respiring on solid state acceptors can be "tricked" into respiring on an electrode and these organisms are deemed "electrogenic". Of the few known electrogenic organisms, the focus of this thesis will reside on *Shewanella oneidensis* MR-1 or simply *Shewanella*.

First isolated in lake Oneida in the state of New York, *Shewanella* resides in sediments at the bottom of lakes where their is insufficient oxygen for respiration. This single celled

organism is a gram-negative bacterium that is capable of respiring on extracellular solid state acceptors such as Fe(III) and Mn(IV) containing minerals in two distinct ways. In the first mechanism, extracellular reduction of solid state acceptors is accomplished *via* mediated electron transfer (MET) where secreted redox mediators, such as flavins and flavinoids, act as redox shuttles to transport electrons from the surface of the cell membrane to the acceptor. In the second mechanism, the outer-membrane proteins of *Shewanella* form a direct contact with the surface of a solid state acceptor and electron transfer is accomplished without the use of a mediator, this mechanism is termed direct electron transfer (DET). In both cases, the machinery responsible for the reduction are found in a set of proteins known as the MTR pathway. In DET the MTR proteins transfer electron directly to an acceptor, while in MET electrons are first transferred to redox mediators which diffuse to an acceptor.[8]

A cartoon representation of the MTR protein ensemble is shown in 1.3. Electron arrive in the form of quinone pool located in the inner membrane and are transferred to the CymA complex which resides on the outer side of the inner membrane. CymA reduces periplasmic cytochromes, which in turn transfer electrons to MtrA, which docks to MtrB in the periplasm. MtrB is a transmembrane barrel protein which serves to allow for docking of both MtrA and MtrC and facilitates electron transfer from MtrA to MtrC.[9, 8] It is then MtrC which performs the final DET mechanisms or can reduce either CymA (which can reduce redox mediators) or directly reduce redox mediators. [10]. The structures of MTrA, MtrB,MtrC, and OmcA are shown in 1.4.

## 1.3 Organic Semiconductors

Semiconductors are the materials responsible for the "digital age". The transition from analog to digital circuitry and the resulting increase in processing power, along

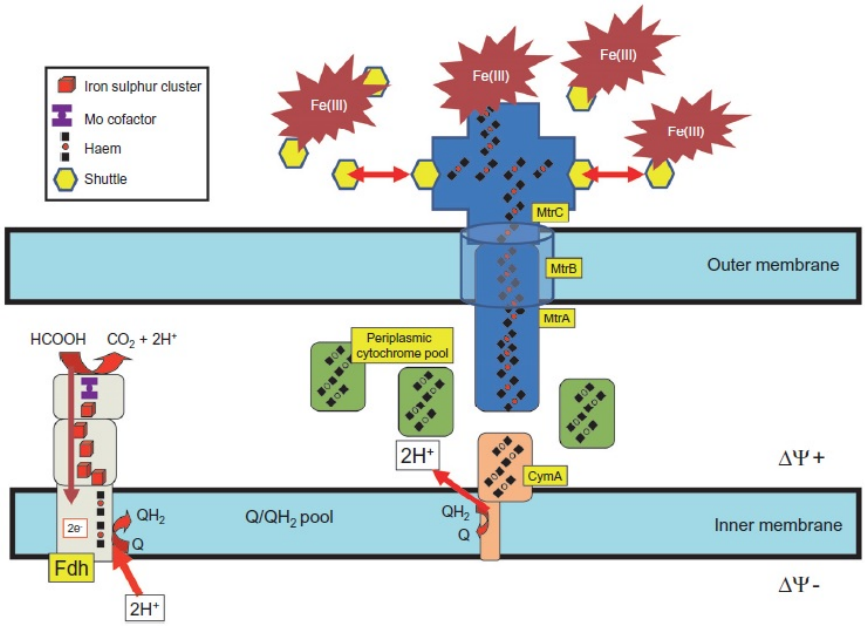


Figure 1.3: Cartoon representation of the MTR protein complexes showing other relevant components. Reproduced with permission, Jon Wiley & sons

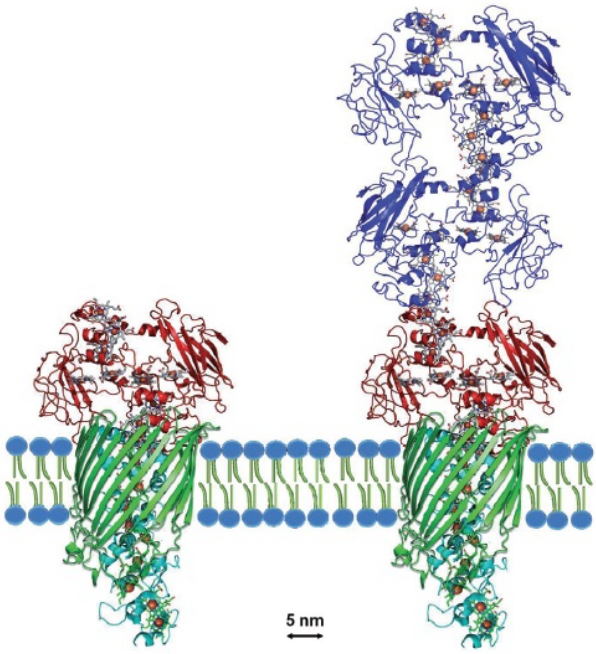


Figure 1.4: Structures of MTR protein complexes and OmcA. MtrA (light blue), MtrB (Green), MtrC (Red), OmcA (blue). Reproduced with permission, Jon Wiley & sons

with a decrease in module size, has changed the world as we know it within as little as fifty years. Indeed, the main application of semiconductors in the context of the "digital age" is their function in the field effect transistor (FET), however the applications of semiconductors is not limited to FETs. Other technologies employing semiconductors are light emitting diodes, solar cells, photodetectors, and microbial fuel cells; just to name a few. In the past 50 or so years, the semiconductor industry has focused almost solely on inorganic semiconductors, such as silicon. The usefulness of inorganic semiconductors is unquestionable in modern applications, however, their production and implementation has some disadvantages. Most inorganic semiconductors require high temperature processing, are composed of toxic or rare elements, and are relatively fragile materials not capable of large stresses or strains. Due to their hard physical properties, there is an inherent challenge in interfacing inorganic semiconductors with biological components, which themselves are composed of soft materials.

In contrast, organic semiconductors (OSCs) are mostly composed of carbon and hydrogen, along with heteroatoms such as nitrogen, oxygen, and sulfur. The abundance, economic availability, and toxicity of the elements composing OSCs are advantageous when comparing them to their inorganic counterparts. Additionally, OSCs can be synthesized using common organic chemistry techniques, processed in lower temperature settings, and incorporated into lightweight, flexible devices. The synthetic approach to the creation of OSCs also makes them highly modular, with many similar structures being obtainable from common starting materials.[11] This allows for the timely creation of a library of OSCs to which one can study structure property relationships. Additionally, compared to inorganic semiconductors, the synthesis of OSCs can be accomplished without needing high temperature reactors, clean rooms, or lithography steps and this greatly reduced the complexity and cost of their manufacturing. [12, 13]

The challenges of OSC research is related to their subtly different properties with

respect to inorganic complexes; in short, they are molecules or polymers. Intermolecular interactions, even in the crystalline form state, are quite different than inorganic crystals as the forces holding OSC solids together originate from Van Der Waals interactions instead of ionic bonds in inorganic semiconductors.[14] Van Der Waals interactions, being much weaker than ionic bonding, change the electronic interactions in solids of OSCs dramatically and this manifests in poor figures of merit in OSCs, such as charge carrier mobility, dielectric constant, and charge carrier densities. These lower figures of merit are due to OSCs having less charge delocalization, higher coulomb binding energies for charges, and overall poorer intermolecular electronic communication. The valence and conduction bands in inorganic solids can be described as a completely delocalized "sea" of electrons, whereby an electron or hole can be effectively delocalized along large length scales.

In OSCs, the valence and conduction bands originate from the highest occupied molecular orbital (HOMO) and the lowest unoccupied molecular orbital (LUMO), respectively. [15] The HOMO and LUMO are molecular properties that can be attributed to single molecules in the gas state or in dilute solution. As molecules start to interact to form a solid, the intermolecular interactions in OSC solids cause both the HOMO and LUMO to delocalize and the extent of this delocalization is highly depending on the motif of molecular packing in the solid. The properties that afford OSCs to be semiconductors at the single molecule level are delocalization of of electrons across the molecular framework of the molecule. This is readily accomplished through $\pi$-bond overlap, such as seen in aromatic compounds and other unsaturated hydrocarbons, which leads to resonance delocalization of electrons. Resonance delocalization is paramount in OSCs and is what allows for intramolecular electronic communication across molecules and polymers.[16] $\pi$-bonding in organic molecules occurs orthogonal to single bonds and as a result OSCs tend to be composed of planar units, typically in the form of aromatic rings. [17] The

overall coplanarity of substituents in OSCs leads to electron delocalization over the entire $\pi$-system of the molecule. These themes in OSC design are apparent throughout the content of these thesis, where aromatic $\pi$-conjugated units are connected together to afford OSCs with properties tailored to a specific application.

## 1.4 Introduction to Experimental Techniques

The interrogation of OSCs, both in their fundamental properties and their applications in material science, requires the use of a multitude of experimental techniques. Throughout the course of this thesis, these techniques will be used as needed to interrogate the relevant phenomenon pertaining to the problem at hand and they will be discussed here in relevant detail to afford the reader with a basic understanding of these techniques. Although not comprehensive, the coverage that will follow will be sufficient to understand the results and conclusions of each section of this thesis. Therefore, mention of the principles of each technique will not be brought up after the conclusion of this section.

**A brief introduction to the electronic processes occurring in molecules**

The interactions of molecules (or atoms) with electromagnetic radiation (*e.g.* light) is dictated by the tenants of quantum mechanics.[18] From an electronic standpoint, the absorption of a photon of light by a molecule will promote an electron from the ground state ($S_0$) to an electronically excited state ($S_{\geq 1}$), the ground state of a molecule is usually a singlet (denoted at S) per the Pauli exclusion principle, but in some cases can be a triplet (denoted as T). The difference in energy between $S_0$ and an excited state, that an electron is promoted to, is equal to the energy of the photon absorbed. The movement of electrons is instantaneous with respect to the nuclear motion of the

atoms in a molecule, known as the Born-Oppenheimer approximation.[19] Thus, when a photon is absorbed and an electron is promoted to a higher lying electronic level, the atoms in a molecule do not have sufficient time to move in the time-scale that electron promotion occurs. Additionally, the electron density surrounding the nuclear framework of a molecule differs from state to state and the promotion of an electron to a higher energy state is concomitant with a redistribution of electron density around the molecule. This new electron density distribution causes the nuclear framework to rearrange to lower the energy of the system around the new electron density, this is known as vibrational relaxation and occurs on time scales longer than that of excitation of an electron. This series of events is encompassed by the Frank-Condon principle, which says, among others things, that excitation of electrons to higher lying electronic states occurs in a "vertical" fashion, followed by vibrational relaxation of an electron to the lowest vibrational level of that electronic state.[20, 21, 22] Excitation of an electron to a higher lying electronic state requires that the vibrational states in each of the two electronic states (or manifolds) have wavefunction overlap. This wavefunction overlap is a function of the symmetry of the molecule and is what causes the excitation of an electron from $S_0$ to $S_{\geq 1}$ to initially reside in a higher vibrational level in the $S_{\geq 1}$ manifold. When vibrational states of an singlet excited state are equienergetic to that of vibrational levels in a triplet state, intersystem crossing may occur, which is the process by witch singlets may be converted to triplets. Direct promotion of an electron from a singlet ground state to a triplet excited state is "spin forbidden" and highly unlikely to occur.[23]

When an electron in an excited state relaxes down to the lowest excited state of the molecule ($S_1$), there are two possible paths the electron can "take" to return to the ground state. In a non-radiative relaxation process, the electron decays to the ground state via vibrational processes and the energy released in this process is given off in the form of heat. In a radiative process, the electron decays to the ground state *via* the

emission of a photon of light, known as fluorescence.[23] This photon is always lower in energy than the the photon which was absorbed to initially excite the electron, due to vibrational relaxation in the excited state, and this phenomenon is known as the "Stokes shift". Additionally, the relaxation back to the ground state always occurs *via* $S_1$, known as "Kasha's Rule".[24] If an excited single is converted to a triplet, the electron has the same two options: to decay radiatively or non-radiatively. Radiative decay from the triplet, known as phosphorescence, occurs on longer time scales than fluorescence due to the fact that the spin must flip to return to the singlet ground state.

**Ultraviolet-Visible Spectroscopy (UV-Vis)**

The ability of a molecule to absorb light is a fundamental molecular property which depends on the electronic structure of the molecule and the environment that the molecule is in. When in dilute solution, analytes follow the Beer-Lambert law, which describes how much light a solution will absorb, as shown in 1.1, where A is the amount of light absrobed by the solution, $\epsilon$ is the molar absorbtivity of the molecule (in $M^{-1}cm^{-1}$), b is the path length of light that travels through the solution (in cm), and c is the concentration of the analyte in solution (in M).[25, 26]

$$A = \epsilon bc \tag{1.1}$$

The molar absorbtivity of a molecule is a fundamental property which is wavelength dependent and also sensitive to the solvent the molecule is dissolved in. As can be seen in 1.1, there is a linear relationship between the absorbance of the solution and the concentration or path length of light. Typically, the path length of light is fixed to 1 cm, and if the concentration of the analyte is known, it is possible to determine the molar absorbtivity of a solution from the measured absorbance spectrum. In order for Beer-Lambert Law to hold true, the solution must be homogeneous and the concentration of the

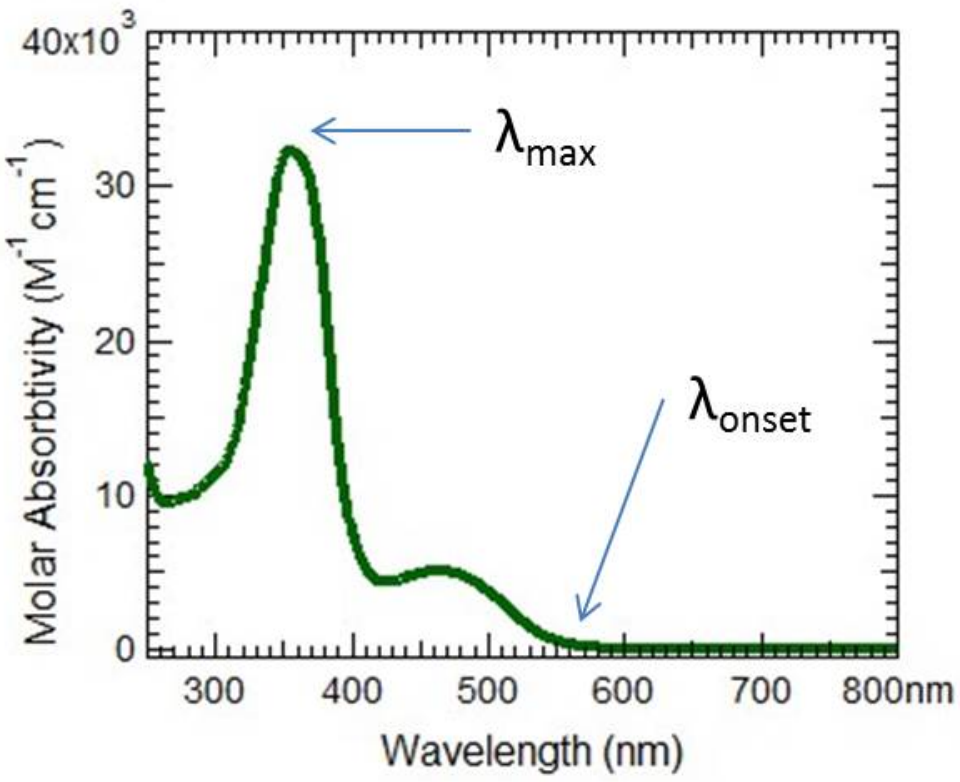


Figure 1.5: Typical Absorbance Spectrum of an Analyte in Dilute Solution.

solution must be low, in the $\mu$M to low mM range (this is dependent on the magnitude of $\epsilon$). At higher concentrations, Beer-Lambert Law deviates from linearity and a saturation in light absorbed is observed as the concentration of the analyte is increased, this can be a result of instrumental deviations, chemical deviations, and theoretical deviations from the Beer-Lambert Law.[27] When reporting an absorbance spectrum, it is typical to plot the molar absorbtivity as a function of wavelength of light.

The use of UV-Vis spectroscopy is a valuable tool in the interrogation of organic semiconductors, as one can determine the wavelength of maximum absorbance ($\lambda_{max}$), $\epsilon$, onset of absorbance ($\lambda_{onset}$), and absorbance spectrum of a material. For example, by knowing $\epsilon$ and the path length of light traveling through the solution *a priori*, one

can determine the concentration of an analyte in an unknown solution by measuring the absorbance of the solution at a wavelength of interest, or more commonly, the absorbance spectrum of the solution. Knowledge of the absorbance spectrum of a molecule will allow one to determine a suitable application of the material, such as use in a solar cell or other optoelectronic application. 1.5 shows a typical absorbance spectrum, which is labeled with $\lambda_{max}$ and $\lambda_{onset}$.

**Electrochemistry**

Electrochemistry provides a tool to probe the oxidation or reduction of a molecule, determine the energies at which these processes occur, and how reversible they are. In organic molecules, the first oxidation and reduction waves are correlated to the HOMO and LUMO orbitals, respectively. The energy difference between the HOMO and LUMO levels determined electrochemically are typically slightly larger than the those determined from optical experiments, as there are Coulumbic interactions in electron-hole pairs produced from optical excitation. One electron reduction of the LUMO produces a radical anion, while one electron oxidation of the HOMO produces a radical cation, both of which do not possess the Cuolumbic attractions of electron-hole pairs.

In the field of electrochemistry, there are a multitude of various electrochemical analyses that can be performed to probe a property if interest, all with their own advantages and disadvantages. Cyclic Voltammetry (CV) and differential pulse voltammetry (DPV) are two such experimental techniques that find use in the interrogation of organic semiconductors. Both of these techniques share identical experimental set-ups, with only the method of data acquisition being variant. As shown in 1.6, an analyte of interest is dissolved in a solvent which is electrochemically inert, along with an eletrochemically inert supporting electrolyte. The purpose of supporting electrolyte is to provide a large ionic background to screen the charges formed from the oxidation/reduction of the analyte, thus allowing assumptions that simply the mathematical models used to analyze the

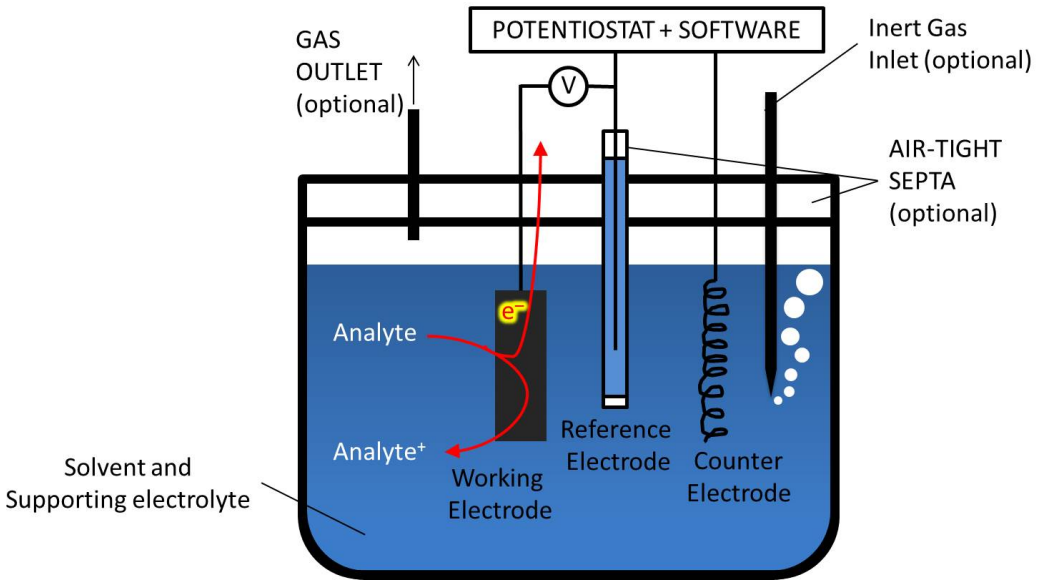


Figure 1.6: Experimental Set-Up for Electrochemical Analysis.

data. The solution of interest is exposed to 3 electrodes which are connected to a potentiostat; the working electrode, counter electrode, and reference electrode. The working electrode, as the name implies, is where redox process between the analyte and electronic circuit occur, and the counter electrode completes the circuit. The reference electrode serves as a way to control the potential applied to the solution, so that electrochemical occurrences can be correlated to the energies they occur at. Thus, a potential is applied between the reference and working electrode and the current between the working and counter electrode is recorded.[25, 28]

In the case of CV, the potential applied to the solution is ramped linearly as a function of time until the maximum desired potential is applied, at which time the voltage is linearly ramped down to the initial starting voltage, as shown in 1.7. In the diffusion-limited regime, where the sane rate (V/s) is sufficiently high, one observes a peak in current as the voltage is increased. This peak occurs because there is insufficient time for fresh substrate to be supplied to the electrode surface as the voltage is being swept

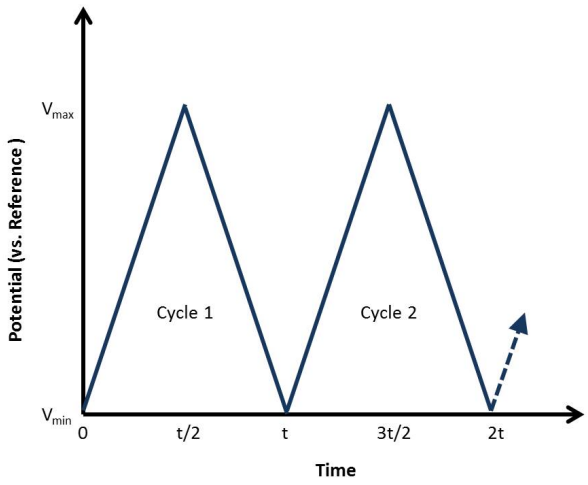


Figure 1.7: Voltage Ramping in a CV experiment.

and the result is a buildup of product at the electrode surface , thus the situation is termed "diffusion limited". In the situation where the scan rate is sufficiently slow, one observes a voltammogram with a sigmoidal shape, in this case there is sufficient time for substrate to be replenished to the electrode and this is termed the "steady state" regime. A typical CV voltammogram in the diffusion limited regime is shown in 1.8, where there are important features to note. Initially, as a positive voltage is swept in the electrochemical cell there is no change in the measured current, until at a certain point, a current increase is observed , followed by a peak in current. This peak occurs due to oxidation of the analyte, because the potential applied is of positive magnitude. Once $V_{max}$ is reached, the potential is swept back to lower values and one notices another peak at a lower potential than what was observed for the oxidation of the analyte, this peak originates from the re-reduction of the analyte that was initially oxidized. The separation between the oxidation peak and reduction peak is proportional to the square root of the scan rate. The half-potential of the red-ox event of interest, $E_{1/2}$, is a useful figure of merit for a red-ox process and is a signature of a specific analyte. As can be seen form

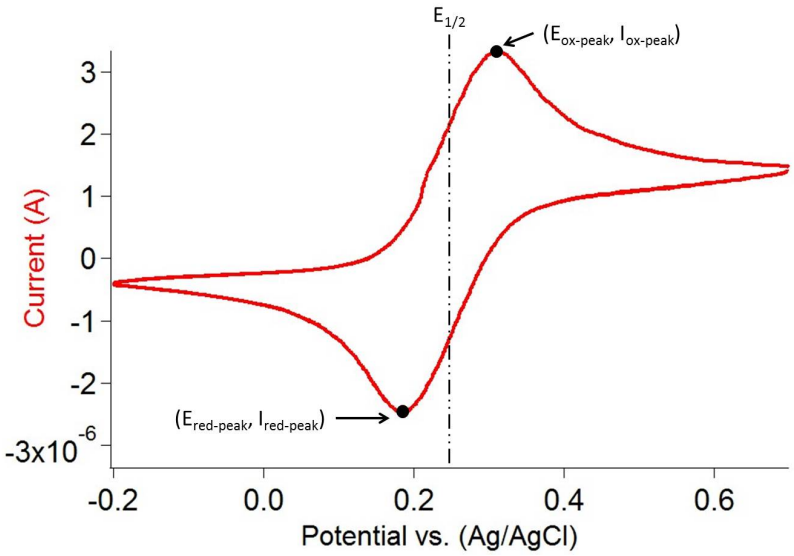


Figure 1.8: A typical CV voltammogram in the diffusion limited regime.

1.8, there is a peak voltage ($V_{ox-peak}$) and peak current ($I_{ox-peak}$) for the oxidation wave and a similar peak voltage ($V_{red-peak}$) and peak current ($I_{red-peak}$) for the reduction wave. The determination of $E_{1/2}$ is given by the average between ($V_{ox-peak}$) and ($V_{red-peak}$).

Differential pulse voltammetry (DPV) is a technique similar to CV that uses a pulse based approach to improve sensitivity by mitigating capacitive current. In DPV, the acquisition of data follows a pulsed based technique shown in 1.9, whereby the current is sampled before and after a potential pulse and the difference in current before and after the pulse is reported. This approach in data aquisition eliminates the capacitive current associated with solvent and electrochemical cell, thus leading to an increase in sensitivity. The information one can gather form a DPV trace is similar to that of a CV trace, but one only records a potential sweep in one direction. $E_{1/2}$ determined from a DPV trace is equal to $V_{peak}$-$V_{step}/2$. A typical DPV trace is shown in 1.10, which has been corrected such that the peak in the plot represents $E_{1/2}$. When comparing1.10 to 1.8, one can easily see the increase in resolution with respect to the x-axis and in the

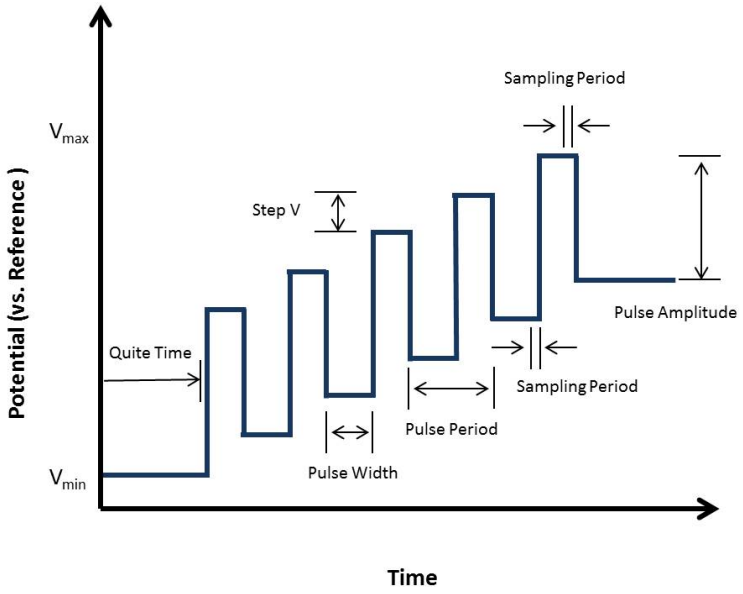


Figure 1.9: Voltage Ramping in a DPV experiment.

case of a complex voltammogram which contains multiple peaks, a DPV voltammogram offers superior ability to deconvolute electrochemical signals.

**Dynamic Light Scattering and Zeta Potential**

Dynamic Light Scattering (DLS) is a technique which probes particles in a solution, in an effort to determine their size and size distribution.[29] This technique uses Rayleigh scattering from particles in solution and measures the scattered light as a function of time. Typically, a laser light source is sent into the sample and the diffracted light is measured by a photomultiplier tube. The intensity of light received by the detector fluctuates as a function of time, as scattered photons will constructively or deconstructively interfere as particles in solution are moving in Brownian motion. The timescale that these particles move is related to their diffusion coefficient, which itself is related to their hydrodynamic diameter via the Stokes-Einstein relation. If one measures the coherence of light as a function of time, the decay in coherence will be faster for smaller particles than larger

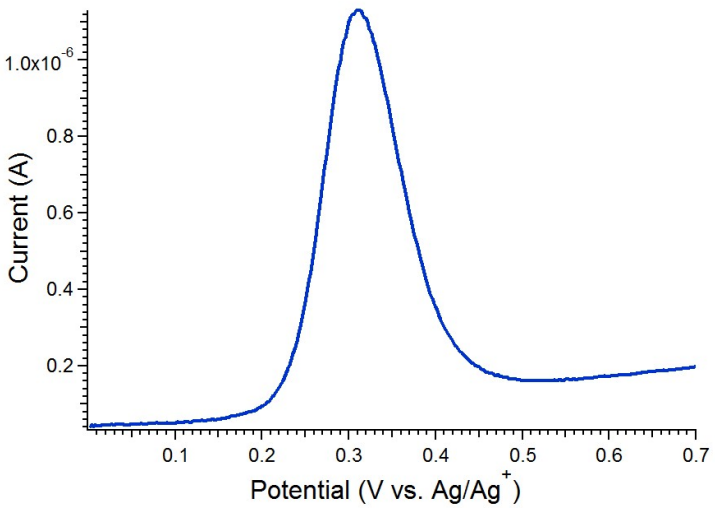


Figure 1.10: A typical DPV voltammogram.

particles because smaller particles, with their larger diffusion coefficients, will move in space more per unit of time.

The hydrodynamic diameter of the particle is related to the ionic strength of the medium due to the fact that the Deybe length of the particle is dependent on the screening of charges in solution. Higher ionic strengths reduce the Debye length and, thus, the hydrodynamic diameter of the particle. It is important to take this effect into consideration when comparing DLS measurements from different data sets. Additionally, DLS measures scattering from all particles which are in solution and measuring samples contaminated with other particulates, especially dust, can drastically change the results obtained. It is important that all samples are filtered to remove any other possible contributions form contaminates, but that this filtration step does not concomitantly remove particles of interest. Lastly, DLS uses the principle of elastic scattering, so samples must not be able to absorb the wavelengths of light used to measure scattering. For monodisperse samples, one can use DLS to interrogate the size distribution of particles from their mean value. This information can prove to be very useful when determining

the quality or properties of particles in solution. Additionally, it is possible to measure samples which have multiple components using a distribution analysis. In this case, it is necessary to know the refractive index of the particles in order to make statements about the abundance of populations.

The Zeta Potential (ZP) is a measure of the charge on the surface of a particle.[30] More specifically, this is a measure of the electric potential of the interfacial double layer at the slipping plane of a particle. The Debye length is a measure of the double layer thickness, which contains the slipping plane. The slipping plane is the plane in the double layer in which tangential motion of liquid is restricted and intimately associated with the particle. In colloid science, the ZP is an important metric used to define the stability of a suspension and understand phenomenon such as coagulation and sedimentation. ZP uses electrophoretic light scattering and is related to he principles discussed in DLS. Electrophoretic light scattering allows one to determine the electrophoretic mobility of a particle by measuring the particle's velocity under a known electric field strength. The electrophoretic mobility of a particle is related to the ZP of a particle using the Henry equation and in polar media, the Smoluchowski approximation is a convenient way to simplify ZP calculations. Laser light is introduced into a sample containing electrodes poising a known alternating potential. The scattering from those particles allows for the determination of the electrophoretic mobility of a particle and by knowing the dielectric constant of the medium and the viscosity, one can calculate the ZP. In my work, changes in ZP have been used to determine how additives effect the ZP of a particle and correlations of these changes to other quantities have allowed for determination of mechanisms of action.

# Chapter 2

# Devolpment and Implementation of a Redox-Active COE

*Let's add some ferrocene!*

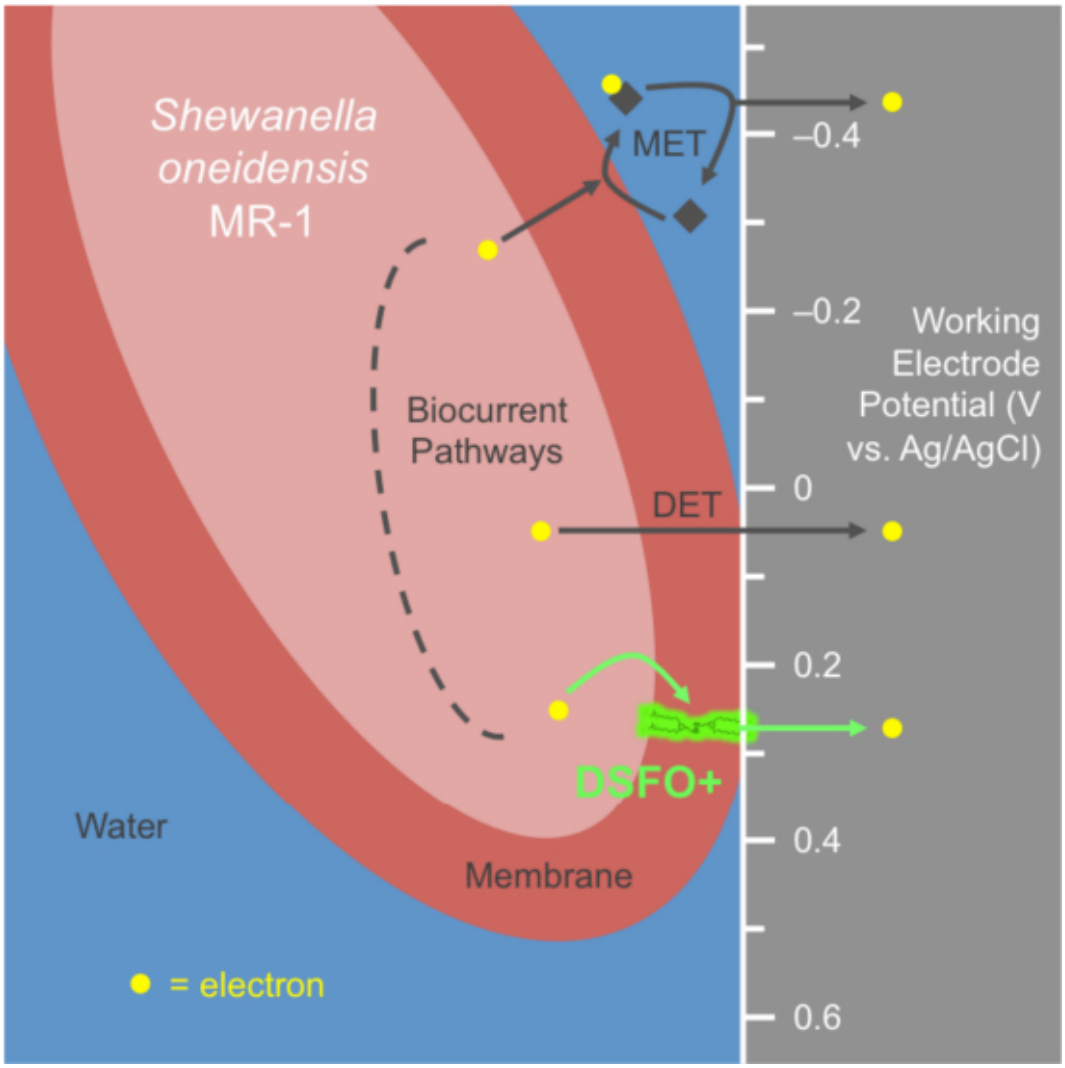


## 2.1 Abstract

For emerging bioelectronic technologies, charge transfer processes remain rate-limited by energy level mismatching and poor contacts at biotic-abiotic interfaces. Direct chemical modification of these interfaces represents an under-developed approach for amplifying biocatalyzed current production. We present the synthesis and application of DSFO+, a redox-active molecule designed for membrane affinity that catalytically couples to biological respiratory transmembrane electron transport, similar to a heme-containing protein.

DSFO+ is employed with three strains of Shewanella oneidensis MR-1 (electrogenic wild type and two non-electrogenic knockout mutants) and amplifies anodic biocurrent in all strains without toxicity at a physiologically-relevant redox potential. Of particular interest, DSFO+ increases metabolic efficiency and biological electron production, thus stimulating respiratory biocurrent production in non-electrogenic bacterial phenotypes. The overall effect is akin to a protein prosthetic electron transfer agent.

## 2.2 Introduction

Microbial bioenergy technologies take advantage of so-called electrogenic microorganisms[31, 32, 33, 34, 35, 8] to catalyze the anaerobic conversion of organic fuels into usable electrical current. Geobacter and Shewanella represent key electrogenic genera,[36] but most microorganisms are ineffective electrocatalysts because they lack the native capacity to exchange electrons with extracellular solid-state conductors.[35] Genetic engineering provides one effective workaround [37, 38] that is challenged by the lack of genetic manipulation tools for many species. [39] Overcoming the scarcity of electrogenic microorganisms is conceivable, however, by using synthetic materials that improve the electrical communication between biological entities and electronic components. Developing effective methods to modify living biotic/abiotic interfaces therefore provides a key materials challenge for advancing bioelectronic and bioelectrochemical technologies.[40, 41] From this perspective, biocompatible organic conjugated and redox-active molecules or polymers are attractive, based on their previous applications ranging in bioelectrochemical and optoelectronic technologies.[42, 43, 44]

As a relevant example, membrane-intercalating p-phenylenevinyelene-based conjugated oligoelectrolytes (PPV-COEs) have been demonstrated to enhance voltage, dark current, photocurrent, power, electrode colonization, coulombic efficiency, and electrical

contacts in (photo)bioelectrochemical systems with limited toxic side-effects.[45, 46, 47, 48, 49, 50, 51, 52, 53] One might initially surmise that PPV-COEs assist in transmembrane electron tunnelling[54, 55] or hopping, but this appears unlikely after accounting for PPV-COEs frontier orbital mismatch with the electrode workfunction[56] and difficulties in achieving direct contacts.[57] Emerging experimental evidence and considerations of charge neutralitywhich require cations to traverse a membrane to balance electronssupport the notion that PPV-COEs may instead facilitate transmembrane ion conductance.[58, 59] Such a mechanism remains consistent with observations of PPV-COEs enhancing the native direct electron transfer (DET) component of microbial electrode respiration[53] by alleviating a rate-limiting cation transfer bottleneck. The challenge of creating membrane-specific molecules that mimic the function of electron transport proteins therefore remains an area of opportunity.

Shewanella oneidensis MR-1 is a well-characterized model electrogenic microorganism used in bioelectrochemical studies. S. oneidensis MR-1 will partially oxidize one equivalent of lactate to theoretically yield one equivalent of acetate and four equivalents of electrons[60] for collection at an electrode:

$$\mathrm{Lactate^- + 2\,H_2O \longrightarrow Acetate^- + HCO_3{}^- + 5\,H^+ + 4\,e^-} \tag{2.1}$$

For S. oneidensis MR-1, these electrons ultimately depart the cell during electrode respiration (biocurrent production) by direct and mediated electron transfer (DET and MET) mechanisms.[53, 61, 62, 63] For DET, physical contact of the terminal membrane-bound MtrCAB-OmcA protein complex with the electrode surface enables electrons to directly pass from inside to outside the cell by hopping through a sequence of iron atoms. For MET, riboflavin and flavin mononucleotide are produced by the cells and act as both bound cofactors for the MtrCAB-OmcA complex and freely diffusing redox agents[64] en-

abling longer-range electronic communication with the electrode. Because of their structural interdependences[9, 65, 66], genetic deletion of any of these proteins either partially inhibits (ΔmtrC and ΔomcA) or almost completely disables (ΔmtrA and ΔmtrB) respiratory current production on solid acceptors.[67] Access to these mutants has enabled a wide range of basic science studies geared toward understanding the mechanistic basis of microbial transmembrane electron transfer. Changes in the rate of electron transfer may be probed, for example, by using bioanodic, single-chamber microbial three-electrode electrochemical cells (M3Cs).[68, 69, 70, 71, 72] M3Cs mimic the anode chamber of a microbial fuel cell while also allowing precise control of the potential of the anode. This enables mechanistic studies of the potential dependence of electron transfer at the anode that are unavailable in microbial fuel cells. Because the cell metabolism is electrochemically coupled to the anode in M3Cs, quantitative bioelectrochemical conversion with environmental control and potentiometric interrogation of electrode-associated microorganisms is afforded. M3Cs thus represent an attractive reactor platform for measuring biocurrent perturbations from modification with COEs.

In this contribution we report on the synthesis of E,E-1,1-bis(2-(3,5-bis(6-trimethylammoniumhexyloxy)phenyl)ethenyl)ferrocene tetraiodide (DSFO+), shown in 2.1, and its impact on S. oneidensis MR-1. This molecule was designed to increase the scope of function that transmembrane agents with conjugated structures may achieve beyond the possibilities afforded by PPV-COEs. DSFO+ is amphiphilic, has a molecular length that can match the lipid bilayer membrane thickness ( 4 nm), and has a biocompatible iron redox centerfeatures mimetic of a membrane-spanning mono-heme cytochrome. DSFO+ was further predicted to intercalate into a membrane from aqueous media because of its structural similarity to the membrane-intercalating PPV-COEs known as DSBN+ and COE2-3C.[45, 48] Therefore, we first describe the synthesis of DSFO+. Cyclic voltammetry (CV) is then used to characterize redox activity in a variety of solvents with

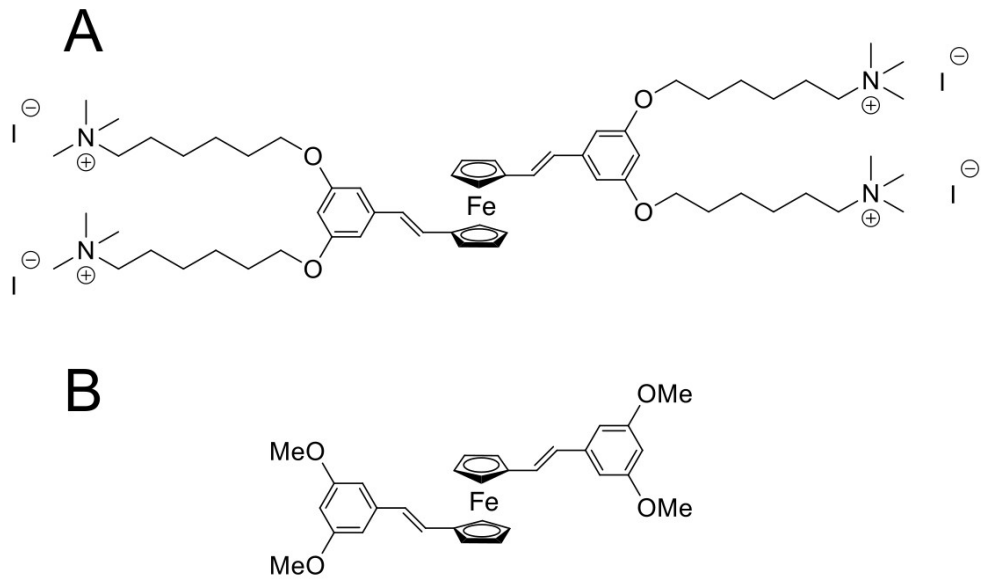


Figure 2.1: Chemical structures of $DSFO^{+}$ (A) and $DSFO(Me)_4$ (B).

different dielectric constants, $\epsilon$. Then, S. oneidensis MR-1 growth inhibition by DSFO+ is measured with minimum inhibitory concentration (MIC) assays. Chronoamperometry (CA) in M3Cs is used as a final calibration experiment to determine the optimal in operando concentration of DSFO+. With these data in hand, M3Cs are employed with WT, ΔmtrA, and ΔmtrB strains of S. oneidensis MR-1. Bacteria are modified in M3Cs in operando with additions of DSFO+ in order to explore biocurrent amplification in WT and rescue of biocurrent in the mutants. Using electrochemical measurements, coulombic efficiency (CE) analysis via high performance liquid chromatography (HPLC), live/dead confocal fluorescence microscopy, and scanning electron microscopy (SEM), the bioelectrochemical effect of DSFO+ is characterized in these M3Cs. The overall study is consistent with DSFO+ directly catalyzing transmembrane respiratory biocurrent.

## 2.3 Molecular Design Considerations

After considering several redox-active molecular substituents for this study, we settled on ferrocene because of its biocompatibility, high stability, well understood synthetic techniques, and the literature surrounding its applications.[73, 74, 75] The redox potential of the ferrocene moiety ( 0.21 V vs. Ag/AgCl)[76] is physiologically relevant because it falls between the pH = 7 redox potentials of organic fuels (E  0.44 V vs. Ag/AgCl) and oxygen reduction to water (E = 0.62 V vs. Ag/AgCl).[77, 78, 79] This unlocks the possibility of using DSFO+ as a transmembrane redox intermediate to amplify electron transfer and to help rescue respiratory biocurrent in non-electrogenic mutantseffects not achievable with PPV-COEs. By density functional theory calculations (2.2), it is apparent that the highest occupied and lowest unoccupied molecular orbital (HOMO and LUMO) wavefunctions of DSFO+ are fully delocalized, which should aid in such transmembrane electron motion. Successful respiratory biocurrent amplification or rescue via DSFO+ should therefore be detectable as increased faradaic current via a catalytic electron transfer wave[68] centered at the redox potential of the ferrocene moiety in a lipid bilayer (i.e. nonpolar organic media).

## 2.4 Synthesis of DSFO

The synthetic route chosen for DSFO+ was a result of some trial and error, with respect to creating the internal alkene of the semiconducting backbone. Initial attemps forcused on the use of Horner-Wadsworth-Emmons (HWE) reactions, by coupling an aldehyde and diethylphosphonate to generate the internal alkene with *trans* slectivity. The synthesis of the desired coupling partners, either tetraethyl (1,1'-ferrocenylbis(methylene)) bis(phosphonate) to couple with 3,5-dialkyloxybenzaldehyde or 1,1'-diformylferrocene to

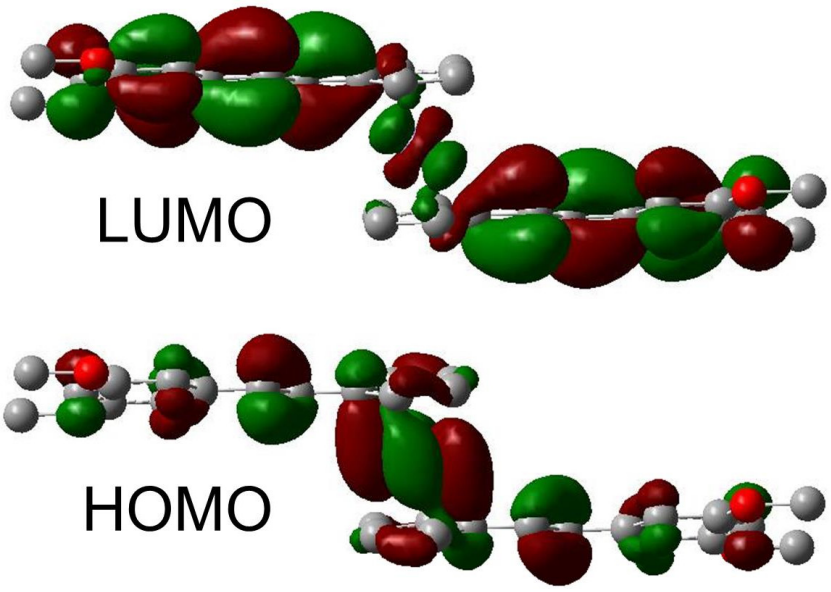


Figure 2.2: HOMO and LUMO orbitals of DSFO$(Me)_4$.

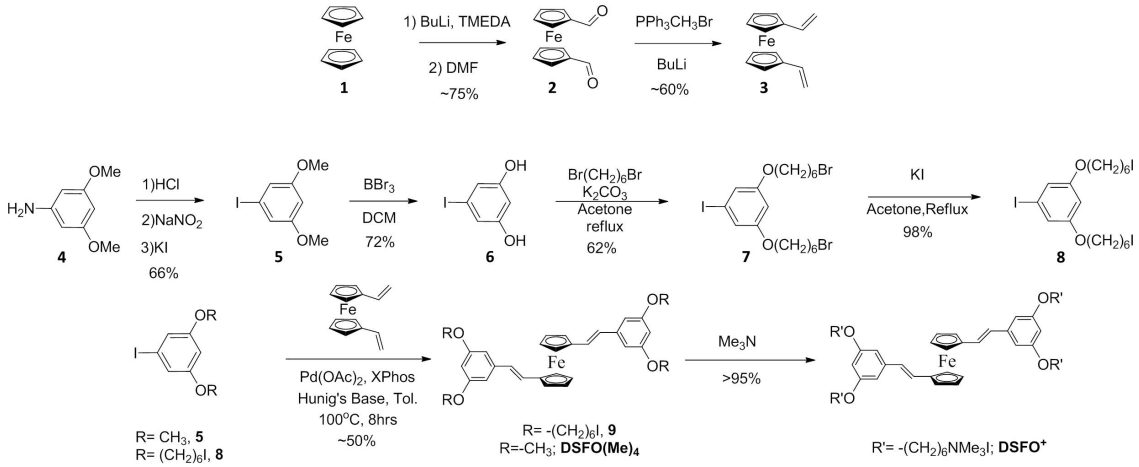


Figure 2.3: Synthetic Route for $DSFO^+$ and DSFO$(Me)_4$.

couple with diethyl 3,5-dialkyloxybenzylphosphonate, was readily accomplished. Hwoever, attempts to accomplish the desired HWE transformation, with the use of either of the two pairs of coupling partners, was unsucessful, returning only starting materials or complex mixtures of products without signs of significant formation of the desired product. The inefficency of these transformations is rationalized by looking closely at the electronics of both coupling partners. Due to the electron rich nature of the cyclopentadienyl ligands on ferrocene, the $pK_a$ of the methylene protons is quite high and delocalization of the resulting anion, due to both the cyclopentadientyl ring and bis-diethylphosophonate located geminal to one another, seemingly makes this substrate a poor nucleophile or possibly an unstable intermediate. In the case of the other coupling partners, the electron rich nature of 1,1'-diformylferrocene makes it a poor electrophile for coupling with a diethyl 3,5-dialkyloxybenzylphosphonate. After a lack of sucess using these coupling partners, it seemed necissary to install the internal alkene with the use of other chemical transformations. When considering possible reactions that would fit in with the synthetic scheme, multiple reactons were considered: such as alkene metathesis, Wittig reactons, eleimation reactions, and palladium catalyzed coupling reactions. Of the choices considered, palladium catalysis was the most attractive, due to its functional group tolerability, high reaction yields, minimal side products, and accesability fo coupling partners. Moreover, the use of Heck couplings would afford the desired *trans* alkene from starting materials which are readily accesable.

The synthesis of DSFO+ is convergent and starts from two commercially available starting materials, ferrocene (**1**) and 3,5-dimethoxyaniline (**4**), as seen in 3.1. Lithiation of **1** with butyl lithium, in the presence of TMEDA, and quenching with dimethylformamide affords 1,1'-diformylferrocene **2** in 75% yield. Compund **3** was affording in 60% yield under classical Wittig conditions and be purified by quickly passing the crude mixture through a silica plug, although it is ***unstable*** on silica for a prolonged period of time

(*e.g.* the length of time it takes for normal column chromatography). Next, compound **5** is afforded in 68% yield from the acid catalyzed diazotization of **4**, followed by release of molecular nitrogen, after treatment with a nucleophilic source of iodide. Demethylation of **5** is accomplished with the use of borontribromide as a lewis acid, followed by quencing with water, in 72% yield, to afford diol **6**. Diol **6** was then used as a nucleophile in the presence of potassium carbinatre and 1,6-dibromohexane to afford alkylated intermediate **7** in 62%, followed by a Finkelstein reaction to swap bromie for iodine, to yield **8** in 98% yield.The key transformation involved a palladium-catalyzed Heck coupling employing **3** and **8**[80, 81, 82, 83] that selectively gave the desired *trans* olefin in 49% yield. After ionization of neutral compound **10** with trimethylamine, DSFO+ was afforded in quantitative yield. $DSFO(Me)_4$, shown in 2.1 and 3.1, was prepared in a similar mannor, except compound **5** was employed in the Heck rection with **3**. $DSFO(Me)_4$ was prepared to examine the redox properties of the ferrocene containing conjugated framework in nonpolar media.

## 2.5 Redox Properties of $DSFO^+$

CV experiments were undertaken with DSFO+ and $DSFO(Me)_4$ in solvents with dielectric constants in the range $5 \leq \epsilon \leq 80$. As can be seen in the resulting CV traces in Figure 2, $DSFO(Me)_4$ in chloroform ($\epsilon \approx 5$) exhibits a reversible oxidation wave with an onset at E = 0.21 V vs. $Ag/Ag^+$ (0.16 V vs. Ag/AgCl), while DSFO+ in water ($\epsilon \approx 80$) exhibits an oxidation wave with an onset at E = 0.68 V vs. $Ag/Ag^+$ (0.62 V vs. Ag/AgCl). In Figure 2, the redox potential in organic media is centered at 0.27 V vs. Ag/AgCl, so this is the potential poised for all CA experiments in this study, as DSFO+ will only exhibit redox current at that potential if it resides in the nonpolar lipid membrane. CV traces of these compounds in solvents of intermediate polarity may

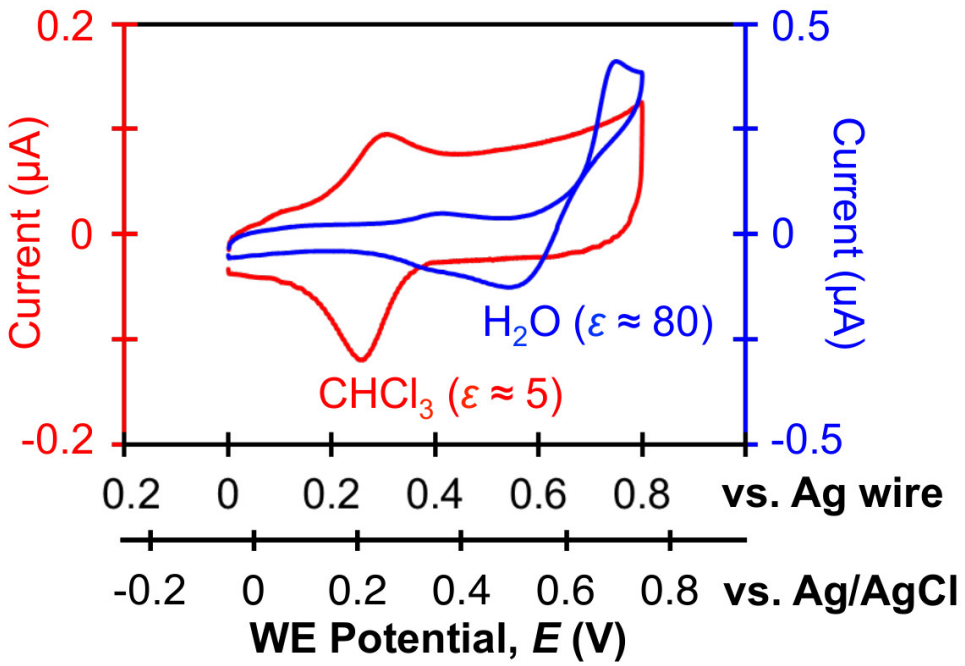


Figure 2.4: Electrochemical features of $DSFO^+$ in water and $DSFO(Me)_4$ in Chloroform.

be found in 2.5, where a linear regression yields an empirical relationship between the oxidation onset potential, $E_{ox-onset}$, and $\epsilon$ given by

$$E_{Ox-onset} = 0.007 + 0.162 \qquad (R^2 = 0.915) \tag{2.2}$$

This positive proportionality of $E_{ox-onset}$ to $\epsilon$ is counterintuitive, as one typically expects a decrease in oxidation potential with increasing dielectric constant [84, 85] because higher-polarity solvents are usually more effective at stabilizing a charged oxidized state. Crucially, one may use 4.2 to deduce the polarity of the medium wherein the molecules have accumulated from the measured oxidation potential of the ferrocene moiety.

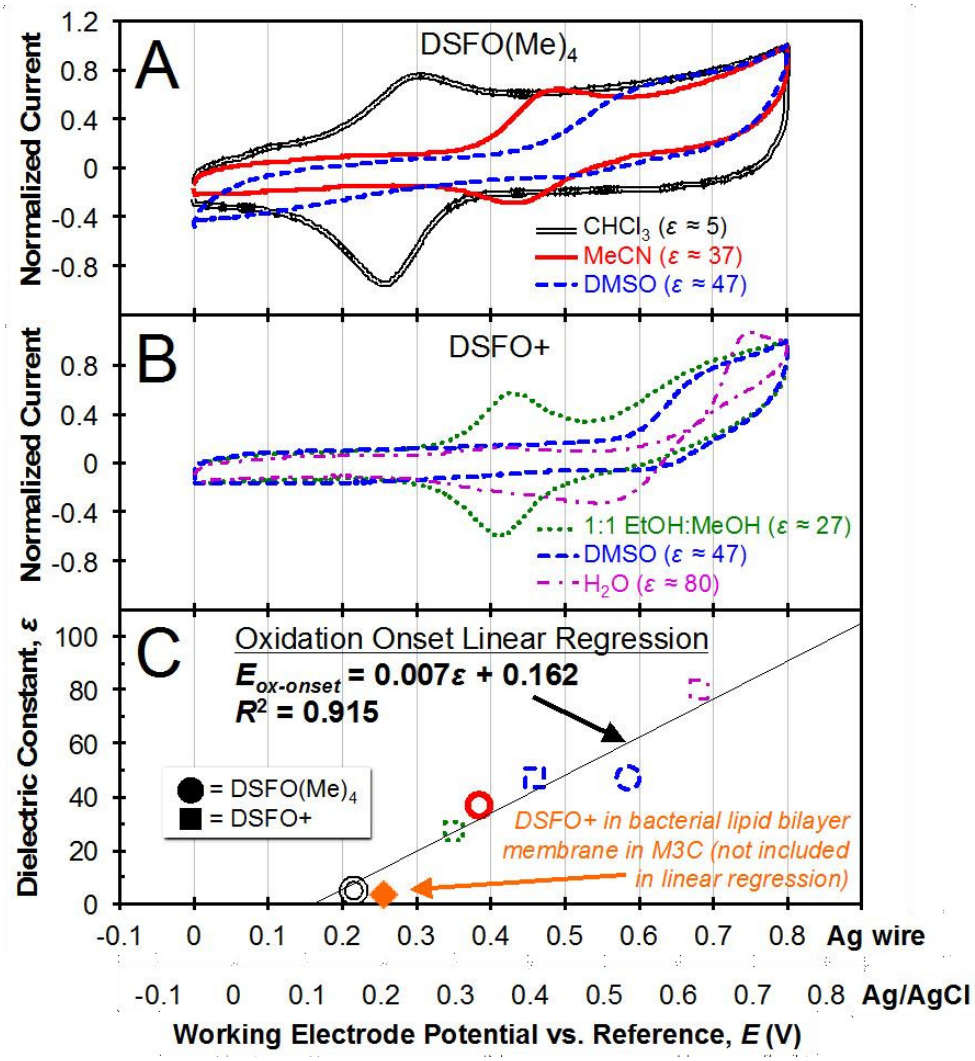


Figure 2.5: Electrochemical features of $DSFO^+$ and $DSFO(Me)_4$ as a function of the solvent's dielectric constant.

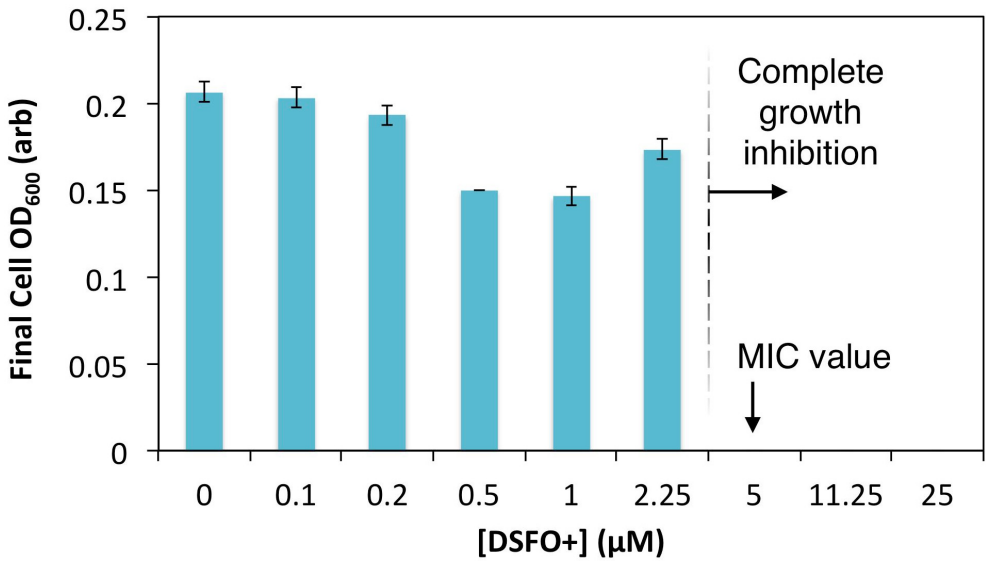


Figure 2.6: Determination of the MIC of DSFO+ for S. oneidensis MR-1. Triplicate average cell culture optical density at t = 72 h was measured at 600 nm as a function of logarithmic $DSFO^+$ concentrations. The MIC is read as the lowest concentration that completely inhibits growth1 of the target organism (here detected as 5 $\mu$M).

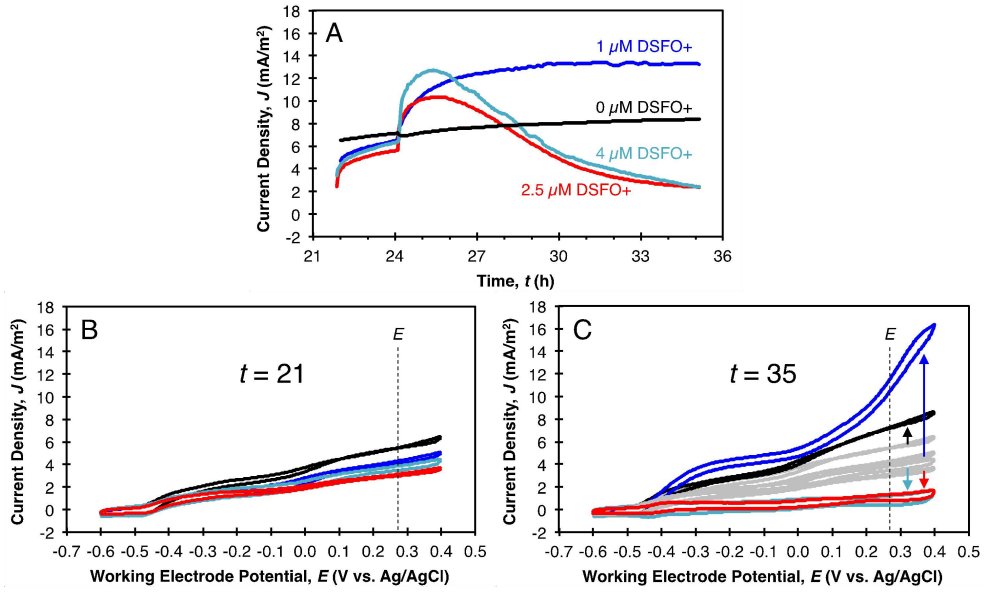


Figure 2.7: Determination of the MIC of DSFO+ for S. oneidensis MR-1. Triplicate average cell culture optical density at t = 72 h was measured at 600 nm as a function of logarithmic $DSFO^+$ concentrations. The MIC is read as the lowest concentration that completely inhibits growth of the target organism (here detected as 5 $\mu$M).

## 2.6 $DSFO^{+}$ catalyzes biocurrent production

An aqueous 100 $\mu$M stock solution of DSFO+ was prepared in growth medium. S. oneidensis MR-1 cultures were exposed in triplicate to a logarithmic series of DSFO+ concentrations by adding appropriate volumes of the stock solution to culture tubes containing growth medium prior to inoculation, and the MIC of DSFO+ was determined to be 5 $\mu$M (see 2.6). This value agrees with inhibitory values measured for PPV-COEs[45, 46, 47, 48, 49, 50, 51, 52, 53] and represents a fairly high degree of toxicity likely caused by DSFO+ accumulation in cells that creates localized higher concentrations. Next, CA in M3Cs was used to establish biofilms at E = 0.27 V vs. Ag/AgCl for determination of $[\text{DSFO+}]_{optimal}$, the highest *in operando* concentration of DSFO+ without long-term negative effects on biocurrent. Representative CA traces for these experiments with the WT reactors may be found in 2.7 and show that $[\text{DSFO+}]_{optimal}$ = 1 $\mu$. Therefore, all remaining experiments were conducted at this concentration.

Representative CA traces for WT, ΔmtrA, and ΔmtrB biofilms that were exposed to either 0 $\mu$M or 1 $\mu$M DSFO+ are presented in 2.8. These data illustrate a key point: biofilms of all three strains exhibit an immediate, sustained amplification in respiratory biocurrent at E = 0.27 V vs. Ag/AgCl when DSFO+ is injected into the reactors (t = 2 h). Control reactors injected with DSFO+ in the absence of bacteria produce negligible current at the same poised potential (see 2.9), suggesting the increase in current is biologically derived. Moreover, when current was collected for multiple days (>90 h) with WT biofilms, the devices modified with 1 $\mu$M DSFO+ show continuous enhancement relative to controls without DSFO+ (see 2.10), suggesting the effect of DSFO+ is sustained and not related to respiratory uncoupling or a loss of cell viability. In order to quantitatively explore DSFO+ current amplification, eight biological replicate[86] biofilms of each of the three S. oneidensis MR-1 strains were established by identical methods, and similar

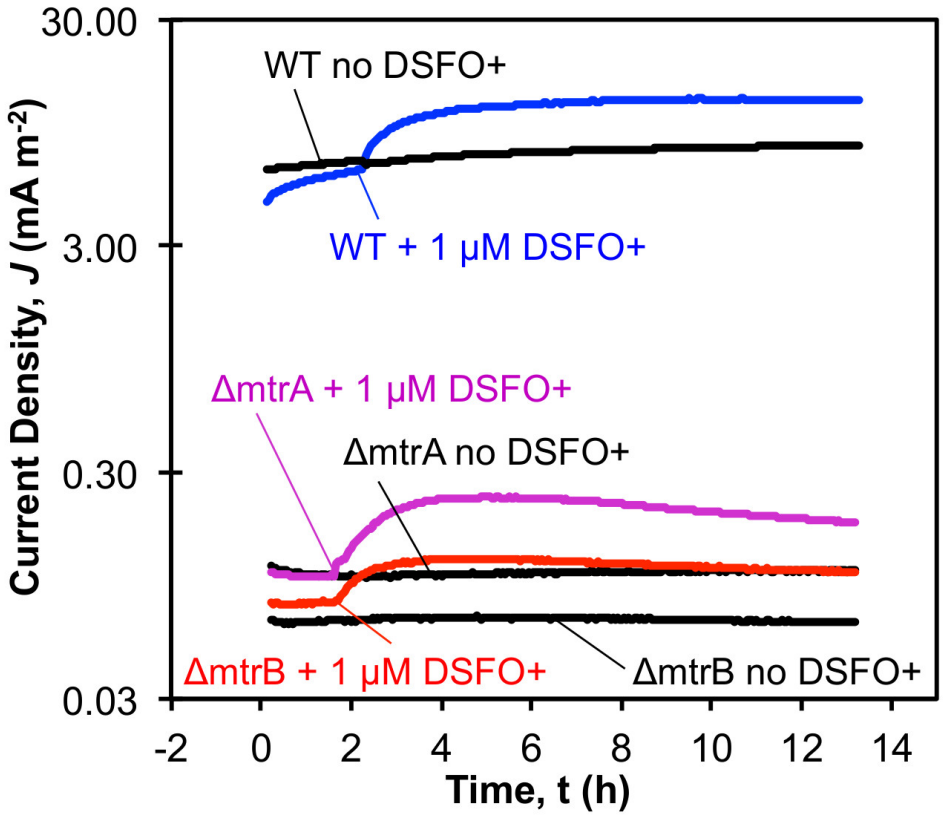


Figure 2.8: CA traces from representative M3C replicates operated at E = 0.27 V vs. Ag/AgCl with WT, ΔmtrA, and ΔmtrB strains. At t = 2 h, M3Cs were injected with (colored traces) 1 $\mu$M DSFO+ or (black traces) no DSFO+. Note that DSFO+ was added as a concentrated solution made from the same media as used in reactors.

CA experiments were then repeated. This time, four WT-M3Cs, four ΔmtrA-M3Cs, and four ΔmtrB-M3Cs received no modification (controls), while four of each type received a 1 $\mu$M dosage of DSFO+ at t = 1 h (test cases). Replicate CA measurements were averaged for each of the six conditions, and these are presented in 2.11. Electrochemical analyses were performed during the course of these experiments, with key timepoints as follows. At t = 1 h (i.e., one hour before initiation of CA measurements), CV was conducted. At t = 0 h, HPLC samples were extracted and CA was initiated. At t = 1 h, DSFO+ was added into reactors. At t = 2 h, CA was paused for CV analyses that interrogated the bioelectrochemical effect of DSFO+ on the biofilms. At t = 4 h, CA was resumed and proceeded until termination, when CV, HPLC sample extractions, live/dead confocal fluorescence microscopy, and chemical fixation (for SEM) of bioanodes were undertaken.

In 2.11, comparing the control and test WT-M3Cs at t = 2 h (i.e. 1 h after DSFO+ addition), one immediately observes a catalytic electron transfer wave centered at E = 0.27 V vs. Ag/AgCl (onset at 0.20 V) as the primary source of increased current in test reactors (2.11 A). For ΔmtrA-M3Cs (2.11 B) and ΔmtrB-M3Cs (2.11 C), a similar and smaller-magnitude catalytic current feature also arises in test M3Cs at t = 2 h at an identical potential of E = 0.27 V vs. Ag/AgCl (onset at 0.20 V). By 4.2 and 2.5, this consistent oxidation onset at 0.20 V implies a dielectric constant of $\epsilon = 5.4$, suggesting that DSFO+ has incorporated into a nonpolar environmentmost reasonably, in analogy to other COEs, the membrane. This value argues against the possibility of aqueous or periplasmic diffusion of redox-active DSFO+ as the governing mechanism, as these would require a poised potential more than 0.4 V higher by 2.5. We note that a pure lipid bilayer membrane has a dielectric constant of $\epsilon \approx$ 2-3,[87, 88] while living lipid bilayers have $\epsilon \approx 5$,[89] similar to our measurement. For concentrations of DSFO+ in the range $0 - 50\mu$M, molecules of DSFO+ fully associate with cells in cultures of S. oneidensis

MR-1, as measured by absorbance spectroscopy of the supernatant after cell removal by centrifugation (2.12). This association provides additional evidence that DSFO+ accumulates in the cell membranes, and likely occurs first by electrostatic attraction to the negatively charged bacterial surface[90] followed by membrane insertion.

Because the current enhancement is catalytic in nature and occurs at a redox potential suggestive of membrane incorporation for all three bacterial strains, we conclude that we are directly measuring the bacterial utilization of DSFO+ redox activity for respiratory transmembrane electron transfer. This mechanistically distinguishes DSFO+ from other PPV-COEs that boost native S. oneidensis DET at E $\approx$ 0.05 V in M3C devices.[53]

## 2.7 DSFO$^+$ increases the efficiency of substrate conversion

As described by Equations 2.4−2.7 in the Experimental Procedures section, CE is a measure of the current collected at the electrode during consumption of the organic fuel (lactate) by bacteria in M3Cs.[53, 91, 92, 5] Lactate is the sole source of carbon and energy for S. oneidensis MR-1 in these devices (4.1), so the quantity of lactate molecules consumed from solution, $\Delta$[lac], sets an upper bound on both the number of electrons that can be extracted from the bacteria by the electrode (4 e per consumed lactate molecule) and the number of acetate molecules that may be produced from the reaction (1 per consumed lactate molecule). The number of lactate-derived electrons collected by the electrode, $Q_{coll}$ (2.4), must be less than 100% of the above described theoretical upper bound on lactate-derived charge, $Q_{lac}$ (2.5), and this is quantitatively represented by the value of $CE_{lac}$ (2.7). Higher $CE_{lac}$ values thus indicate that the cells more efficiently use lactate to generate current. Note also that because some acetate equivalents will be

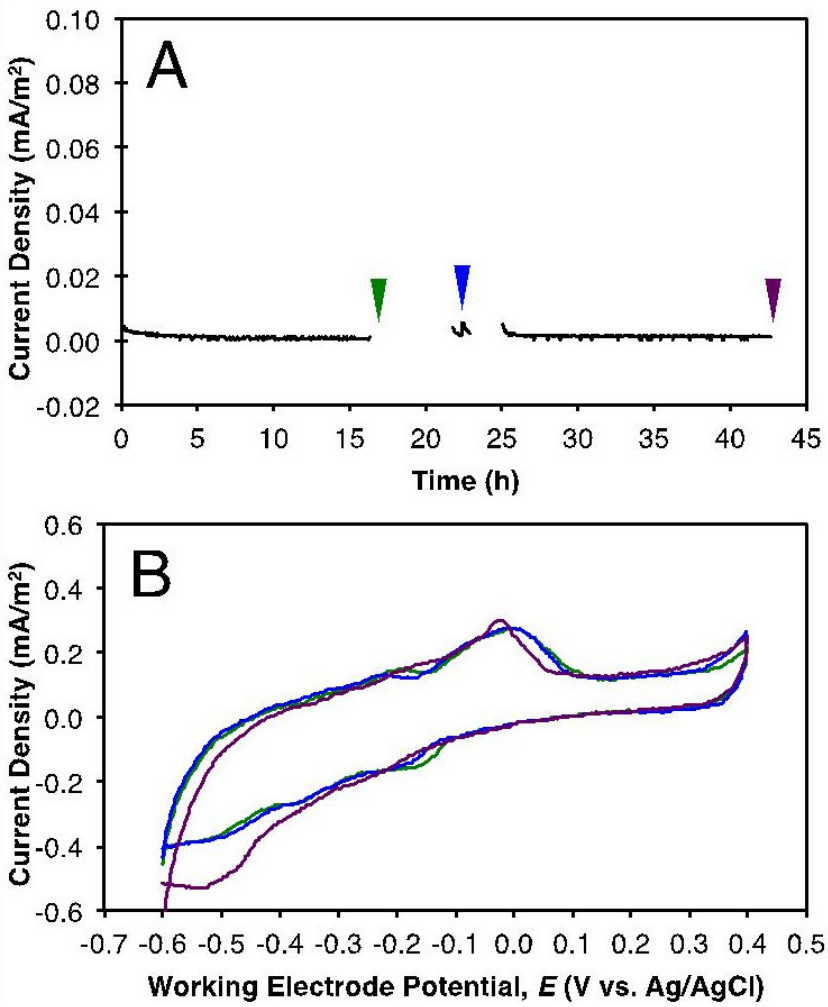


Figure 2.9: Abiotic (negative control) M3C CA and CV traces. The M3Cs contain only buffered growth media and DSFO+. The experiments were conducted as single replicates concomitant with the M3Cs in Fig. 2 in the main text. (A) CA trace collected at E = 0.27 V showing current density over time. Salient timepoints during M3C operation are as follows. At t = 0 h, current collection begins. At t = 17 h (green arrow), current collection is paused for CV analysis, causing a break in the current collection. At t = 22, current collection is resumed so that 5 $\mu$M DSFO+ may be spiked in during current collection at t = 22.5 h (blue arrow). At t = 23 h, current collection is again paused for CV analysis to discern the effects of DSFO+ addition, again causing a break in current collection. At t = 25 h, current collection is resumed. At t = 43 h (purple arrow), current collection is terminated and CV analysis is undertaken. (B) CV traces corresponding to the timepoints in (A) where CA was paused at t = 17 h (green trace), t = 23 h (blue trace), and t = 43 h (purple trace).

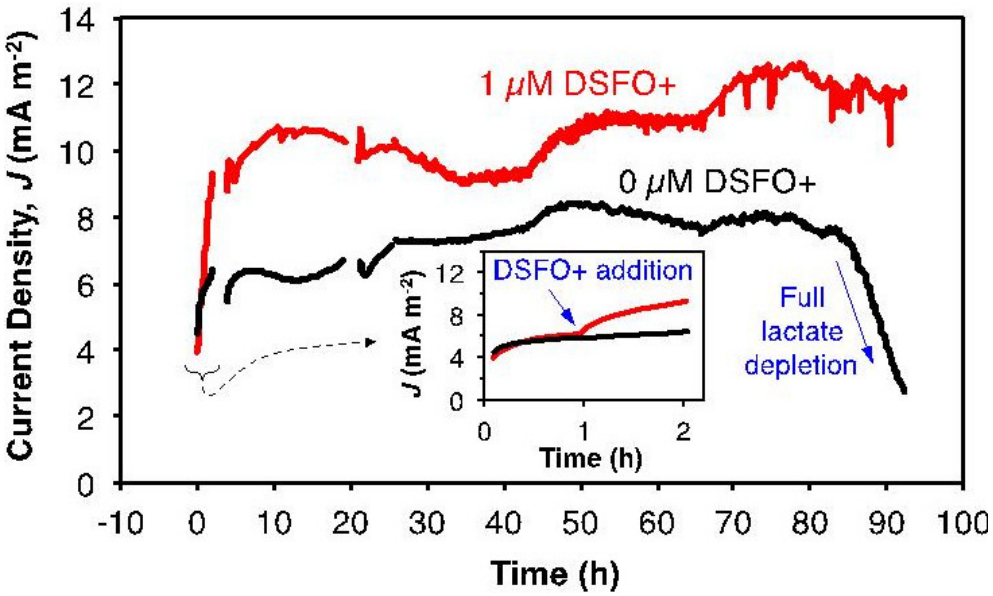


Figure 2.10: Long-term CA of representative M3Cs showing the sustained enhancement from $DSFO^+$ over time. Breaks in the traces correspond to timepoints when CV was undertaken (data not shown). Inset: zoom view of the first two hours of operation to show the immediate effect of addition of 1 $\mu$M DSFO+ compared to the control.

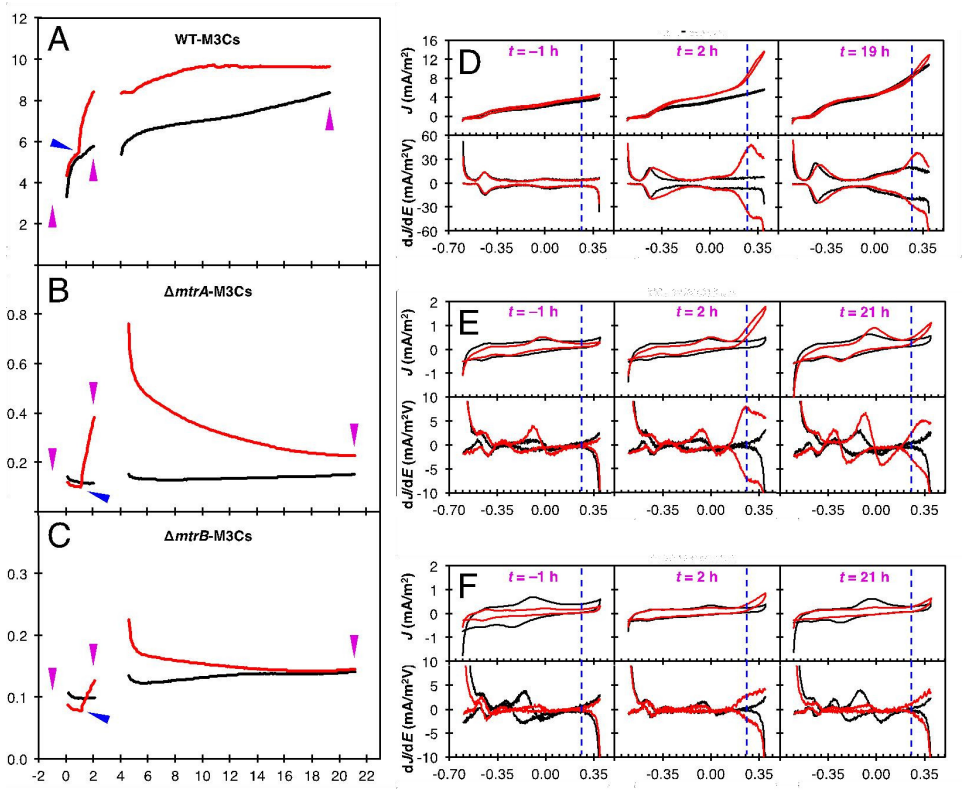


Figure 2.11: Average CA and CV data for M3Cs containing the three S. oneidensis MR-1 strains, with and without DSFO$^{+}$. Note that part of this data is presented in the main text and presented in full here for clarity. The timepoint t = 2 h corresponds to the end of 16 h biofilm establishment. Black traces represent reactors containing no DSFO+, while red traces represent reactors modified with 1 $\mu$M DSFO+. Magenta arrows and times indicate timepoints when CA current collection was paused for CV analysis (this creates the breaks in the data). Blue arrows indicate when DSFO+ was spiked in at t = 1 h. Vertical blue dashed lines in the CV and derivative data indicate the poised potential of E = 0.27 V used to collect the CA traces (this potential was chosen to match the expected formal potential of DSFO+ in lipid). (A) CA traces for WT-M3Cs. (B) CA traces forΔmtrA-M3Cs. (C) CA traces for ΔmtrB-M3Cs. (D) CV and derivative traces for WT-M3Cs at the timepoints indicated. (E) CV and derivative traces for ΔmtrA-M3Cs at the timepoints indicated. (F) CV and derivative traces for ΔmtrB-M3Cs at the timepoints indicated.

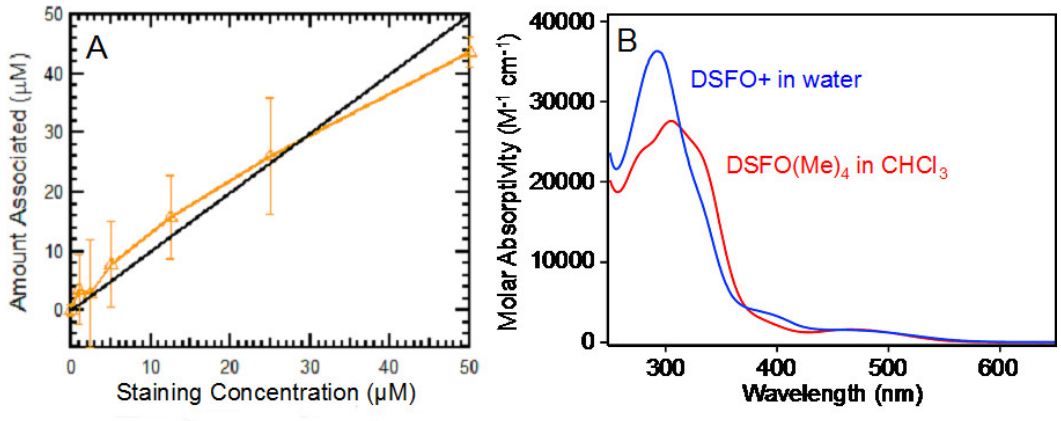


Figure 2.12: (A) Association of DSFO+ with cells of S. oneidensis MR-1. Data points falling on the solid black line indicate 100% association of DSFO+ with cells for a given staining concentration. Concentrations were measured by taking the absorbance spectra of growth medium (water) solutions containing varying concentrations of DSFO+, resuspending the bacteria for 2 h at constant OD = 0.44 in these solutions to enable association, centrifugation, and re-measuring the absorbance spectra of the supernatant to calculate the difference in concentration. (B) Molar absorptivity of $DSFO^+$ in water (as well as $DSFO(Me)_4$ in $CHCl_3$) used to calculate the concentration of $DSFO^+$ by optical absorption.

assimilated for biosynthesis purposes, the actual acetate released to solution, $\Delta$[ac], must be less than the 1:4 production level implicated in 4.1. It is therefore also informative to compare the electron equivalents of the actual amount of acetate produced, $Q_{ac}$ (2.6), to the actual amount of current collected ($Q_{coll}$). This is represented by the value of $CE_{ac}$ (2.7) which provides a measure of the bacterias ability to catalytically channel electrons towards current production: a higher $CE_{ac}$ indicates a higher rate of current production relative to biosynthesis. The values of $CE_{lac}$ and $CE_{ac}$ are useful because they represent conversion as a measure of output per unit input, rather than the raw magnitudes of lactate, acetate, and current changes.

As can be seen in 2.13, in M3Cs with DSFO+ added, $Q_{coll}$ increases during operation for all three strains, while the quantities of lactate consumed and acetate produced decrease for all three strains. This broadly indicates that efficiency is increased by

| | | WT-M3Cs | | *ΔmtrA*-M3Cs | | *ΔmtrB*-M3Cs | |
|---|---|---|---|---|---|---|---|
| Measured Parameter | Expression | No DSFO+ | 1 μM DSFO+ | No DSFO+ | 1 μM DSFO+ | No DSFO+ | 1 μM DSFO+ |
| Charge collected (C)[b] | $Q_{cell} = A\int J(t)dt$ | 9.9 ± 1.7 | 12.8 ± 1.2 | 0.21 ± 0.08 | 0.48 ± 0.07 | 0.20 ± 0.11 | 0.22 ± 0.08 |
| Lactate consumed (mM)[c] | $\Delta[lac] = [lac]_f - [lac]_i$ | −5.5 ± 1.7 | −4.0 ± 0.9 | −1.3 ± 0.3 | −0.4 ± 0.2 | −1.1 ± 0.8 | −0.2 ± 0.1 |
| Lactate charge equivalent (C)[d] | $Q_{lac} = -\Delta[lac]VFn$ | 32 ± 10 | 23 ± 5 | 7.5 ± 2.0 | 2.3 ± 1.0 | 6.1 ± 4.7 | 1.3 ± 0.7 |
| Lactate coulombic efficiency (%) | $CE_{lac} = 100 \times Q_{cell}/Q_{lac}$ | 31 ± 11 | 56 ± 14 | 3 ± 1 | 21 ± 10 | 3 ± 3 | 17 ± 11 |
| Acetate produced (mM)[c] | $\Delta[ac] = [ac]_f - [ac]_i$ | 3.4 ± 0.6 | 2.6 ± 0.5 | 1.0 ± 0.3 | 0.5 ± 0.3 | 0.6 ± 0.4 | 0.2 ± 0.1 |
| Acetate charge equivalent (C)[d] | $Q_{ac} = \Delta[ac]VFn$ | 20 ± 4 | 15 ± 3 | 5.8 ± 1.6 | 2.6 ± 1.8 | 3.5 ± 2.1 | 0.9 ± 0.3 |
| Acetate coulombic efficiency (%) | $CE_{ac} = 100 \times Q_{cell}/Q_{ac}$ | 50 ± 12 | 85 ± 16 | 4 ± 1 | 18 ± 13 | 6 ± 5 | 26 ± 13 |
| Electrode cell density ($10^9$/m$^2$)[e] | $\rho = (1/K)\Sigma_k(2N_k/\pi d_k h_k)$ | 107 ± 39 | 113 ± 46 | 63 ± 32 | 58 ± 21 | 67 ± 40 | 28 ± 13 |
| Current density at $t$ = 2 h (mA/m$^2$) | $J(2)$ | 5.8 ± 1.0 | 8.4 ± 0.8 | 0.11 ± 0.06 | 0.38 ± 0.14 | 0.10 ± 0.05 | 0.13 ± 0.04 |
| Current per cell (fA/cell) | $I_{cell} = J(2)/\rho$ | 54 ± 22 | 75 ± 31 | 1.8 ± 1.3 | 6.6 ± 3.3 | 1.5 ± 1.1 | 4.5 ± 2.5 |

[a] Quoted uncertainties represent ± 1 standard deviation (for measured values) or are propagated errors by addition of standard deviations in quadrature (for calculated values). [b] The surface area of working electrodes (average of 24 replicates) is $A = 0.0226 \pm 0.0012$ m$^2$ after Ref. 24. [c] Note that $\Delta[lac] < 0$ and $\Delta[ac] > 0$ because the bacterial electrode reaction (Equation 1) converts lactate to acetate and electrons; this is why values for $Q_{lac}$ and $Q_{ac}$ have different signs. [d] Reactor volume is $V$ = 15 mL. Faraday's constant is $F = eN_A \approx 96485$ C mol$^{-1}$, where $e = 1.602 \times 10^{-19}$ C and $N_A = 6.02 \times 10^{23}$ mol$^{-1}$. The electron equivalents produced per equivalent of substrate is $n$ = 4 (Equation 1). [e] After M3C operation, $\rho$ is determined from SEM images of the chemically fixed graphite electrode fibers by averaging counts per area of fiber-associated cells. For this, fibers are approximated as cylindrical and divided into $K$ sections with diameters $d_k$ and heights $h_k$ (surface area is $\pi d_k h_k$). $N_k$ is the number of cells counted on the $k$th cylindrical section; $2N_k$ is therefore used in the calculation of $\rho$ to account for the fact that only half of any fiber cylinder may be imaged for cell counting. $K \geq 12$ in all cases.

Figure 2.13: Quadruplicate average measured M3C device parameters[a].

DSFO+ because while less substrate (lactate) is consumed, the lactate that is consumed is converted to electrons at a much higher rate. For lactate consumption, unmodified WT-M3Cs had a $CE_{lac}$ of 31 ± 11%, which increased to 56 ± 14% with DSFO+ modification. For acetate production, the $CE_{ac}$ of WT-M3Cs increased from 50 ± 12% to 85 ± 16% upon DSFO+ addition. Because lactate consumption not only yields current but also provides electron and carbon equivalents for biosynthesis, it inherently has a lower CE. Acetate is produced during respiration (biocurrent production), so the greater percent increase in CE with respect to acetate production is consistent with ability of DSFO+ to improve electron transfer in S. oneidensis MR-1. As shown in 2.13, increases in CE for both acetate and lactate also occur when DSFO+ is added to ΔmtrA-M3Cs and ΔmtrB-M3Cs. These global increases in CE suggest that incorporation of DSFO+ causes bacteria to produce more current per unit of consumed lactate, making it a better electrocatalyst. This feature has positive implications for DSFO+ in bioelectrochemical conversion: greater biocurrent production and more-efficient organic content removal are simultaneously allowed.

## 2.8 Biofilm characterization reveals more current per cell with DSFO$^+$

Once measurements were terminated, live/dead confocal fluorescence microscopy was immediately performed to assess the toxicity of 1 $\mu$M DSFO+. The resulting images (2.14) display sparse emission from propidium iodide (dead stain) relative to emission from DAPI (live stain), and there is no readily discernable difference in control and test reactors. This suggests low toxicity due to either DSFO+ or reactor conditions, consistent with the [DSFO+] = 1 $\mu$M < MIC determined earlier. Accordingly, the data in 2.8 and

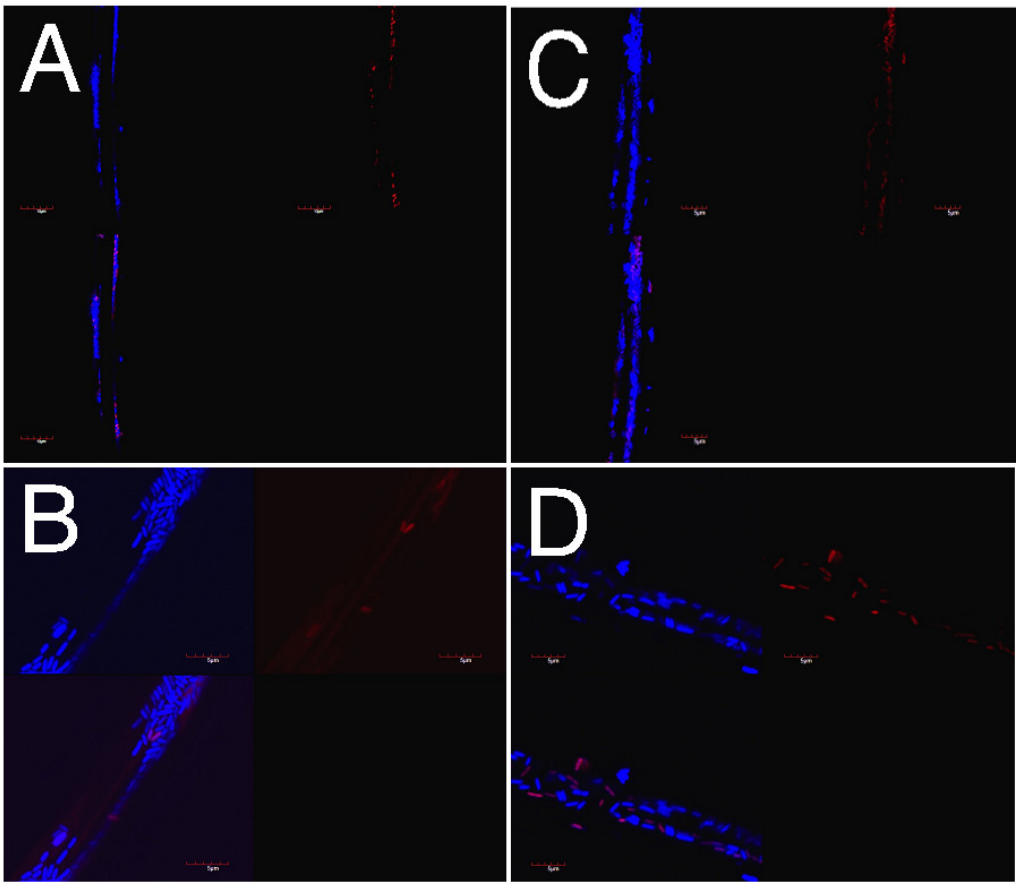


Figure 2.14: Representative CFM images of M3C working electrodes immediately after CA measurements to assess for in operando toxicity of 1 $\mu$M DSFO+. Electrodes were simultaneously stained with 4',6-diamidino-2-phenylindole (DAPI, live stain) and propidium iodide (PI, dead stain). Note that images are false-color. Each panel is divided into four quadrants as follows: upper left, emission from DAPI (blue); upper right, emission from PI (red); lower left, overlay of DAPI emission (blue) and PI emission (red); lower right, bright field transmittance showing complete occlusion due to the graphite electrode. In all images, scale bars are 5 $\mu$m. (A) WT-M3C electrode with 0$\mu$M DSFO+. (B) WT-M3C electrode with 1 $\mu$M DSFO+. (C) $\Delta$mtrA-M3C electrode with 1 $\mu$M DSFO+. (D) $\Delta$mtrB-M3C electrode with 1 $\mu$M DSFO+.

2.11 and 2.13 represent measurements of biologically-derived current.

After confocal fluorescence microscopy characterization, electrodes were chemically fixed and dehydrated for imaging with SEM. Representative images obtained for each type of device are presented in 2.15 A-F, and serve to quantify the number of cells on the electrode surface, but not necessarily locate DSFO+ molecules. Electrode surface cell density, $\rho$, is estimated from cell counts in such images. Values for  are summarized in 2.13. For each strain, there is no statistically significant measured difference in $\rho$ with and without DSFO+, so we conclude that biocurrent output per bacterial cell, $I_{cell}$, increases upon addition of DSFO+. One illustrative measure of Icell is given by dividing the current density at t = 2 h, J(2), by the value of $\rho$ for the same reactor conditions, given by

$$I_{cell} = \frac{J(2)}{\rho} \tag{2.3}$$

Note that $\rho$ is measured at t $\geq$ 19 h, at which time it must be larger than it would have been at t = 2 h for any reactor conditions; $I_{cell}$ may therefore be considered a lower bound on the amperage produced by each cell. These data are summarized in 2.13, and as can be seen, addition of DSFO+ to test reactors causes $I_{cell}$ to increase 1.4-fold, 3.7-fold, and 3.0-fold for WT, ΔmtrA, and ΔmtrB, respectively. This contrasts with previously observed PPV-COE enhancements to S. oneidensis MR-1 M3Cs that show increased total current but decreased current on a per-cell basis.[53] These data therefore agree with the conclusion that the mechanism of enhancement from adding DSFO+ (respiratory redox coupling) is different than that from additions of PPV-COEs (native DET enhancement). The systematically lower values of $\rho$ forΔmtrA-M3Cs and ΔmtrB-M3Cs as compared to the WT-M3Cs are consistent with their lower current output (non-electrogenic phenotype) seen in 2.8 and 2.11 because electrode respiration

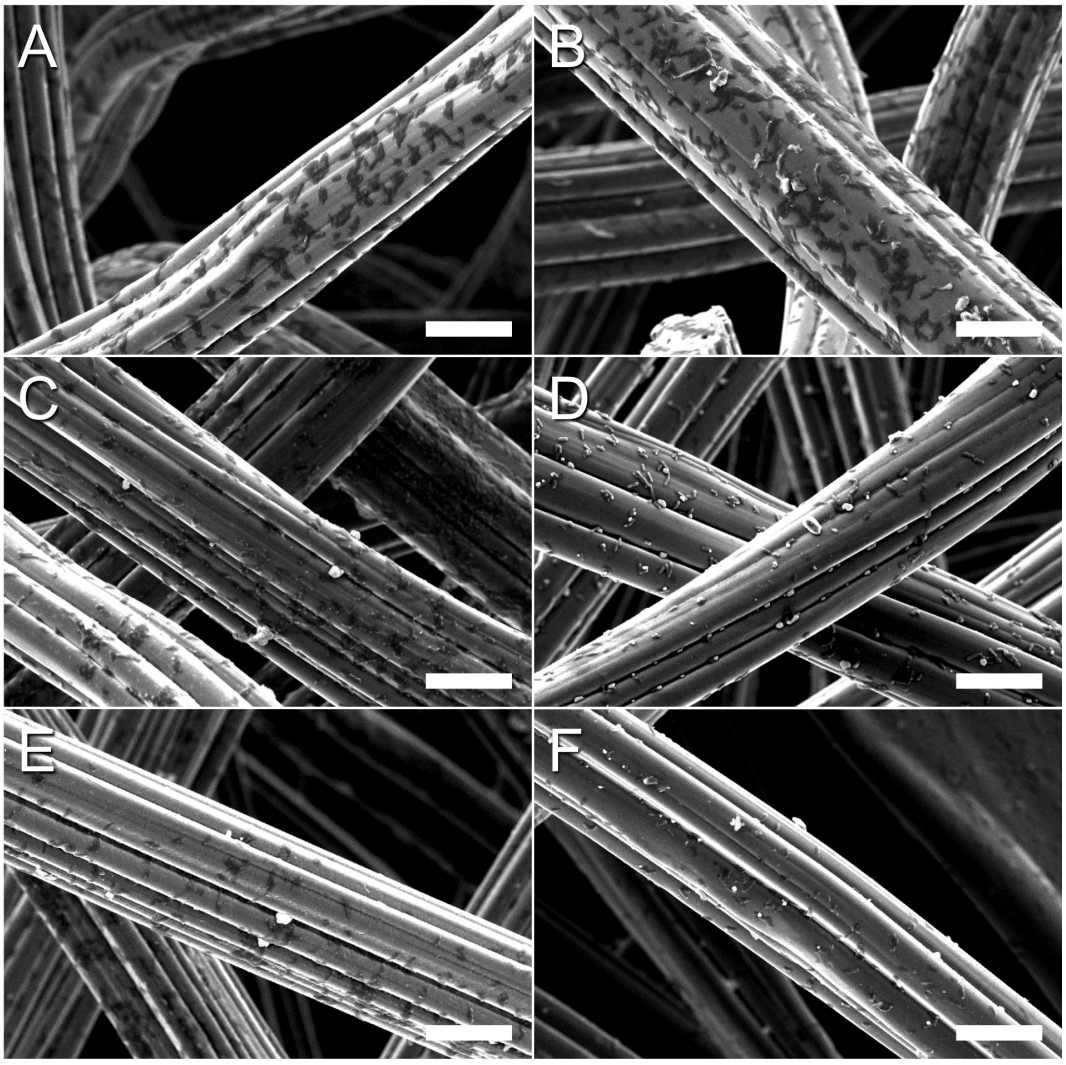


Figure 2.15: Representative SEM images of graphite electrode fibers from all M3C conditions showing bacterial adhesion to the surfaces. Scale bars are 10 $\mu$m. (A) WT-M3Cs with 0 $\mu$M DSFO+. (B) WT-M3Cs with 1 $\mu$M DSFO+. (C) $\Delta$mtrA-M3Cs with 0 $\mu$M DSFO+. (D) $\Delta$mtrA-M3Cs with 1 $\mu$M DSFO+. (E) $\Delta$mtrB-M3Cs with 0 $\mu$M DSFO+. (F) $\Delta$mtrB-M3Cs with 1 $\mu$M DSFO+.

(biocurrent production) is a driving force for electrode cell adhesion. Lower values of $\rho$ are therefore also consistent with the accepted function of MtrB as the exposed docking site for the MtrC-OmcA proteins that are implicated in surface adhesion.[93, 94] Reduced electrode-associated cells limits the total M3C current output, so this additionally agrees well with the CV traces in 2.11 E and F that reveal smaller-amplitude biocatalytic current outputs from the DSFO+ modified mutant strains despite constant additions of 1 $\mu$M DSFO+. These consistencies further support the conclusion that current amplifications are biologically-derived.

## 2.9 Controls implicate bacterial current enhancement from DSFO$^+$

The possibilities that direct DSFO+ or lactate oxidation accounts for the current amplification or that DSFO+ directly catalyzes lactate-to-current conversion in the absence of bacteria are ruled out by three experiments. First, abiotic (negative control) M3Cs containing growth media and DSFO+ produce negligible current by CA under conditions identical to those in 2.8 and 2.11, indicating that neither DSFO+ nor lactate oxidation is the source of current (see 2.9 A). Moreover, a one-electron oxidation of 1 $\mu$M DSFO+ in these reactors (15 mL volume) could provide at most Q = [DSFO+]VFn = (1 $\mu$M)(15 mL)(96485 C/mol e)(1 e) = 0.0014 C of electrons to the working electrode. DSFO+ oxidation therefore cannot account for the increase in charge collected by >100-fold in even the lowest-current M3Cs in this work, which produce 0.20 $\pm$ 0.11 C. Second, the lactate concentration does not decrease for the same abiotic M3Cs during the CA experiments, confirming that lactate is not being oxidized in the absence of bacteria. Third, CV conducted in the potential range 0.6 V < E < 0.4 V in the abiotic M3Cs (2.9 B) lacks

a faradaic current signal associated with DSFO+, further ruling out DSFO+ oxidation and remaining consistent with the E = 0.62 V onset of oxidation of aqueous DSFO+ determined in 2.4 and 2.5. These control experiments provide additional supporting evidence that the amplified current observed upon addition of DSFO+ must be of biological origin.

We have presented the design and synthesis of DSFO+, a redox-active COE. The redox potential of DSFO+ is sensitive to the dielectric constant of the surrounding medium, thereby allowing voltammetric differentiation of the polarity of the medium wherein the molecule accumulates. The amplified current signal in M3Cs modified with DSFO+ is centered at a redox potential that suggests that DSFO+ incorporates into the nonpolar cell membrane of S. oneidensis MR-1, while the catalytic current-voltage dependence at that potential is indicative of the coupling of cell metabolism to DSFO+ redox cycles. In this way, DSFO+ improves electrode respiration and partially rescues electrogenic character in the non-electrogenic ΔmtrA and ΔmtrB mutant strains. The knockout mutants each lack one of the key outer-membrane-bound proteins for the MtrCAB-OmcA electron transfer complex. DSFO+ provides the means to incorporate redox active units throughout the cell membrane and outer wall. Their locations are unlikely to be specifically determined. Thus, DSFO+ enables the cell to significantly increase the options for redox transfer of e and to what degree this increases the function of existing redox proteins or coupling between them has yet to be determined. Our experimental results suggest that the observed current amplification from DSFO+ in all three S. oneidensis MR-1 strains arises from an increase in both the efficiency of biological electron production and the quantity of electrons collected from each cell, rather than from direct electrochemical oxidation of substrates, increased cell accumulation at the electrode surface, or negative impacts on cell vitality. DSFO+ exhibits complete growth inhibition at concentrations $\geq 5$ $\mu$M, with 1 $\mu$M being the optimal device concentration used. These values generally

suggest toxicity, which must in part be due to DSFO+ membrane accumulation creating a high local concentration; however, the low functional concentration of 1 $\mu$M is also notably advantageous in practical settings where utilizing less material is desirable by cost considerations. It is known that the length of COE molecules impacts the distortions of lipid bilayers and that the resulting pinching effect is the most reliable structural parameter to predict toxicity.[95, 96] Therefore, a clear opportunity exists for development of DSFO+ analogs with more extended dimensions-for example by introducing more than one ferrocene structural unit-that would be anticipated to be less toxic. Overall, the successful biocurrent amplification by direct biotic-abiotic interfacial modification provides a new strategy in the field of bioelectronics. It now seems apparent that incorporation of an appropriately designed synthetic redox-active transmembrane molecular protein prosthetic is a valid approach for amplifying and rescuing catalytic biocurrent.

## 2.10 Preliminary Work using *E. coli*

To test the ability of DSFO+ to catalyze biocurrent production in non-electrogenic bacteria, we chose to investigate the performance of a MEC containing a biofilm of *Escherichia coli* K-12 (*E. coli*). We performed the MEC experiments identically to those done with *Shewanella*, except for using glycerol as the electron donor,as we found that *E. coli* cannot be cultured using lactate as the electron donor. As shown in 2.16, DSFO+ is able to increase current producing compared to the control in a 22 hr period. The magnitude of current produced is the control reactors is similar to those using mutant strains of *Shewanella* and the current increase is also similar. This result leads one to believe that the current increase in *Shewanella* from the use of DSFO+ may have very little interaction with the native proteins in *Shewanella* (*i.e.* the set of Mtr proteins that still reside in the membrane in the mutant strains or the entire complex in wild

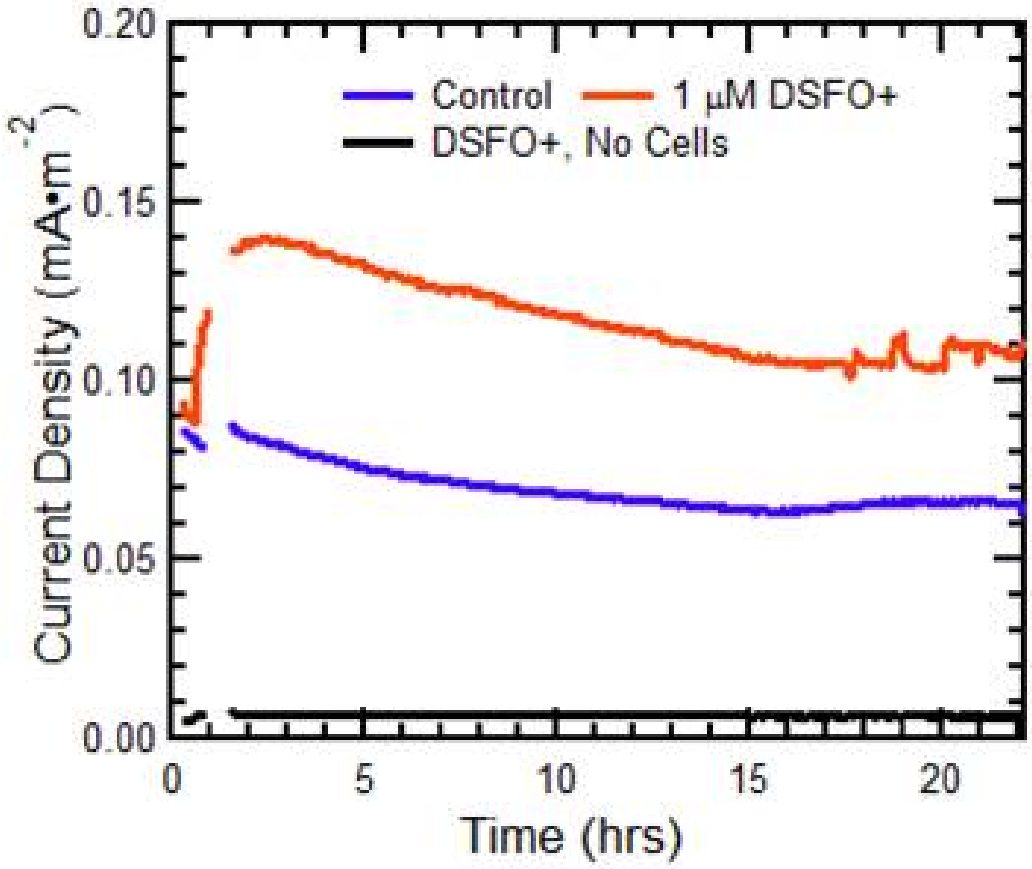


Figure 2.16: Chronoamperometry of MECs containing *E. coli*.

type strains), as on would expect less of an increase in current for *E. coli* compared to mutant strains of *Shewanella* if DSFO+ was electrochemically interacting with the Mtr proteins. In order for this hypothesis to be determine, more rigorous experimentation must be completed, especially with respect to understanding the biofilm of unmodified *E. coli* reactors. This study is outside the scope if this thesis and will be left for future research. At any rate, the ability for DSFO+ to catalyze current production in *E. coli* MECs is a promising result for imparting electrogenic phenotypes in non-electrogenic bacteria using redo active COEs.

## 2.11 Experimental Procedures

**Density Functional Theory (DFT) Calculations**

All DFT calculations were performed using Gaussian09 software suite with GuassView5. The geometry optimizations and frontier orbital visualizations utilized the B3LYP/6-311G** functional/basis set.

**Cell Culture and Inoculation**

Strains of Shewanella oneidensis MR-1 were struck out on LB agar plates from frozen bacterial stock and incubated at 30 °C for ∼24 hours to isolate single colonies. Biological replicate cultures were grown by selecting morphologically similar colonies with a sterile loop to inoculate anaerobic ($N_2$ atmosphere) modified M1 medium[97, 98] containing 20 mM Na-(L)-lactate as donor and 20 mM Na-fumarate as acceptor. After 24 hours of incubation with shaking at 30 °C, such cultures consistently reach a maximum $OD_{600}$ of ∼0.16 (or 1.6  108 cfu/mL, as determined from previous calibrations[53]). These stationary phase cultures (fumarate completely consumed) may then be used to inoculate separate replicate M3Cs or MIC assay tubes as described.

**Cell Association**

Shewanella oneidensis MR-1 cells at an $OD_{600}$ nm= 0.44 were stained with DSFO+ (0-50 $\mu$M) in clear 96-well plates (BD Biosciences, San Jose, CA) at 30 °C for 2 hours in the dark with shaking. The total volume for each sample was 200 $\mu$L and the samples were measured in triplicate. After centrifugation of the 96-well plate (4,500 rpm, 5 min), 100 $\mu$L of supernatant was transferred to a clean 96-well plate for absorbance measurements with a Tecan M220 Infinite Pro plate reader (Tecan, Mnnedorf, Switzerland). Absorbance was recorded at 310 nm and control samples containing no cells were treated in the same manner and used to create a calibration curve. The calibration curve was used to determine the concentration of DSFO+ in the supernatant, allowing for calculation of

cell association.

**Bioreactors**

The 3-electrode, batch-type, membraneless bioelectrochemical reactors used herein (M3Cs) were similar to those previously reported[53]; key components are described here. Glass M3C vials had a 15 mL working volume and were sealed with rubber septa. Electrode specifications were as follows. Reference electrode: Ag/AgCl (saturated KCl) with 3.2 mm Vycor frit (Gamry). Counter electrode: coiled 0.25 mm Ti wire (Aldrich), 10 turns. Working electrode: 1 cm x 1 cm x 0.2 cm graphite felt (Alfa Aesar), interwoven with Ti wire as the electrical lead. Anaerobic conditions were maintained via degassing with humidified, deoxygenated $N_2$. Temperature was maintained at 30 °C by housing the M3Cs in a temperature-regulated incubator.

**Cyclic Voltammetry (CV)**

For characterization of DSFO$(Me)_4$, the working electrode potential was swept twice from $E_{initial} = E_{final} = 0$ V to $E_{vertex} = 0.8$ V and back at a scan rate of 0.01 V/s, and the second trace was used for analysis. The concentration of DSFO$(Me)_4$ was kept constant at 10 $\mu$M and the supporting electrolyte, tetrabutylammonium hexafluorophosphate, was also invariant at 100 mM. DSFO$(Me)_4$ was investigated in chloroform, acetonitrile, and dimethyl sulfoxide as solvents (2.5 A). For characterization of DSFO+, the potential was also swept twice from $E_{initial} = E_{final} = 0$ V to $E_{vertex} = 0.8$ V and back at a scan rate of 0.01 V/s, and the second trace was kept for analysis. The concentration of DSFO+ remained constant at 10 $\mu$M and the supporting electrolyte was invariant at 100 mM. DSFO+ was investigated in water with 100 mM phosphate buffer (pH = 7.2) as electrolyte, in Ethanol/methanol (1:1 volume/volume) with 100 mM sodium perchlorate as electrolyte, and dimethyl sulfoxide with 100 mM tetrabutylammonium hexafluorophosphate as electrolyte (2.5 B). The different supporting electrolytes used were chosen for their electrochemical inertness and their solubility in the desired solvent, as it was not

possible to find a single electrolyte soluble in all of the desired solvents. At various timepoints during CA measurements, current monitoring was paused for CV analyses of the electrode-respiring biofilms. For such experiments, CV parameters were as follows: $E_{initial} = E_{final} = 0.6$ V; $E_{vertex} = 0.4$ V; scan rate = 0.005 V/s.

**DSFO+ Minimum Inhibitory Concentration (MIC) Determination**

A filter-sterile 1 mM stock solution of DSFO+ was prepared in M1 medium. M1 was used so that upon additions of varying volumes of this stock to test conditions, the basal composition of the growth medium was invariant. Triplicate 10 mL volumes of M1 medium containing 20 mM Na-(L)-lactate as donor and 20 mM Na-fumarate as acceptor were then prepared in capped anaerobic test tubes with the following concentrations of DSFO+ (volume of 1 mM stock added to 10 mL provided in parenthesis): 0 $\mu$M (0 $\mu$L), 0.1 $\mu$M (1 $\mu$L), 0.2 $\mu$M (2 $\mu$L), 0.5 $\mu$M (5 $\mu$L), 1 $\mu$M (10 $\mu$L), 2.25 $\mu$M (22.5 $\mu$L), 5 $\mu$M (50 $\mu$L), 11.25 $\mu$M (112.5 $\mu$L), 25 $\mu$M (250 $\mu$L). These concentrations were selected because they are consistent with previously tested PPV-COE concentrations of 1.0 $\mu$M, 5.0 $\mu$M, and 25.0 $\mu$M, and the remaining values fall between those on a base-5 logarithmic scale in approximately half-order of magnitude increments. Finally, 0.5% additions (50 $\mu$L per 10 mL test volume) of triplicate S. oneidensis MR-1 cultures were inoculated into corresponding triplicate test replicates for starting cell loadings of $\sim 8\ \ 10^6$ cfu/mL (this has an undetectable $OD_{600}$ with the spectrometer and by eye). Test tubes were incubated at 30 °C for 72 hours without stirring, and the MIC was read as the lowest concentration that completely inhibited growth.[99] Results are summarized in 2.6.

**Chronoamperometry (CA)**

Using a Gamry potentiostat (Reference 600, Series G 300 or Series G 750 models) and multiplexer (model ECM8), M3C graphite felt working electrodes were poised at E = 0.27 V vs. Ag/AgCl (the central redox potential of $DSFO(Me)_4$ in $CHCl_3$) to serve as the sole terminal electron acceptor for the organisms. Freshly inoculated M3Cs were

incubated in the dark[100] with 100 rpm magnetic stirring for 16 hours to promote growth of an electroactive biofilm. Then a full media change was undertaken to replenish the lactate donor to 20 mM and deconvolute[53] the biofilm from planktonic cell signals. Electrochemical characterization with CV was then immediately used to characterize the biofilm. Steps following this CV are different depending on the nature of the ensuing experiment, as follows. For determination of the optimal in operando concentration of DSFO+, $[\text{DSFO+}]_{optimal}$, in 2.7, CA was then resumed at E = 0.27 V and DSFO+ was injected ∼2 hours later at a series of DSFO+ concentrations in the range $0 \leq [\text{DSFO+}] \leq 4$ $\mu$M. These M3Cs then operated for an additional 11 hours and were terminated. For mechanistic experiments (2.11), CA was then resumed at E = 0.27 V and DSFO+ was injected ∼1 hour later at 1 $\mu$M. The system was allowed to operate for an additional ∼1 hour, and then CA was paused for CV analyses. Then CA was resumed and current was continuously monitored until the end of M3C operation. The current response was measured, recorded, and averaged for 20-second blocks (at 160 second intervals) with Gamry software (Framework Version 6.11, Build 2227, 2013). Time integration of the resulting current response determined the amount of charge transferred by the bacteria, $Q_{coll}$ (2.13).

**Preparation of Confocal Microscopy Samples**

Immediately after the completion of M3C operation, the anode containing the biofilm was blotted dry using a Kimwipe. Then, the electrode was immersed in a water solution containing 10 $\mu$M 4',6-diamidino-2-phenylindole (DAPI, live stain) and 5 $\mu$M propidium iodide (PI, dead stain) for 30 minutes. The electrode was next blotted dry, briefly immersed in deionized water to remove excess dye, and blotted dry again in two consecutive cycles. Next, a small portion of the electrode was cut off, placed on a microscope cover slip, covered in Type B immersion oil, and immobilized with tape. These samples were imaged within 1 hour of sample preparation.

**Confocal Microscope Images of M3C Electrodes**

Fluorescence emission images and concomitant co-localized bright field images were acquired on an inverted Olympus IX81 instrument equipped with a 60x objective. In order to separately image the emission from each chromophore, the instrument was set to the proper excitation wavelength maxima for DAPI (abs. max. = 358 nm) and PI (abs. max. = 535 nm), and separate emission spectra were collected for DAPI (em. max = 461 nm) and PI (em. max = 617 nm). The confocal images are presented as a 4x4 set of images for each condition, as shown in 2.14.

**High Performance Liquid Chromatography (HPLC)**

HPLC analysis of M3C effluent was performed with a Shimadzu LC20AB instrument equipped with an organic acid compatible Aminex HPX-87H column (Bio-Rad). Samples from M3Cs were filtered through 0.22 $\mu$m PVDF filters (GSTek) to remove cells, and diluted 10-fold into mobile phase prior to analysis. The mobile phase was 0.004 M (0.008 N) aqueous $H_2SO_4$ flowing at 0.6 mL/min, and UV detection was set at 210 nm.

**Coulombic Efficiency (CE) Determination**

The efficiency of converting lactate to electricity was calculated by first integrating the current density response (see 2.11) to obtain the total charge collected, $Q_{coll}$ (in Coulombs):

$$Q_{coll} = A \int_0^{21} J(t)\,\mathrm{d}x \tag{2.4}$$

where A is the surface area of the electrode, previously determined[53] to be A = $0.0226 \pm 0.0012$ m$^2$. For the same time period, the concentrations of lactate and acetate were monitored in the M3Cs with HPLC to determine the decrease in lactate concentration, $\Delta$[lac], and increase in acetate concentration, $\Delta$[ac]. By 4.1 each consumed lactate molecule should yield n = 4 e$^-$, representing 100% CE.[60] The charge equivalents (in

Coulombs) of the consumed lactate or produced acetate are given by the expressions

$$Q_{lac} = -\Delta[lac]VFn \tag{2.5}$$

$$Q_{ac} = \Delta[ac]VFn \tag{2.6}$$

where V is the volume of the M3C (15 mL), F is the Faraday constant (equal to $e\mathrm{N}_A$ = 9.64853 $10^4$ C/mol), and the negative sign on $\mathrm{Q}_{lac}$ accounts for the fact that lactate molecules are being consumed. Finally, CE is the ratio of $\mathrm{Q}_{coll}$ to either $\mathrm{Q}_{lac}$ or $\mathrm{Q}_{ac}$ in percent form:

$$CE_{lac/ac} = 100\frac{Q_{coll}}{Q_{lac/ac}} \tag{2.7}$$

**Chemical Fixation of Electrodes**

After all bioelectrochemical and confocal microscopy experiments, M3C working electrodes were submerged for 24 h in 100 mM PBS, pH = 7 containing 2% (v/v) formaldehyde to fix electrode-associated cells. After fixation, electrodes were sequentially rinsed twice each with: 100 mM PBS, pH = 7 (10 min), deionized water (10 min), 70% ethanol in deionized water (10 min), 100% ethanol (30 min). Electrodes were then allowed to air dry for 24 hours and stored in glass scintillation vials for future study.

**Scanning Electron Microscopy and Cell Counting**

Images of chemically fixed graphite felt electrodes were obtained with an FEI XL40 SEM at an accelerating voltage of 5 kV, working distance of ∼5 mm, and a spot size of 3. The brightness and/or contrast of the images were increased post-acquisition by up to 40% in order to better visualize cells. The expression for the number average cell density for each electrode, $\rho$, is given in 2.8. An example of this method using K different sections

of the electrodes has been previously reported.[53]

$$\rho = \frac{1}{K}\sum_{k=1}^{K}(\rho_k) = \frac{1}{K}\sum_{i=1}^{K}(\frac{N_k}{\pi d_k h_k}) \tag{2.8}$$

**Acknowledgments**

Funding was provided by the Institute for Collaborative Biotechnologies (ICB) under grant W911F-09-D-0001 from the U.S. Army Research Office. Z. D. R. is grateful for funding from the National Science Foundation Graduate Research Fellowships Program (NSF GRFP). The three strains of Shewanella oneidensis MR-1 presented in this manuscript (WT, ΔmtrA, and ΔmtrB) were provided by the group of D. R. Lovley (UMass Amherst). Spectroscopy and electron microscopy were conducted in MRL Shared Experimental Facilities at UCSB, which are supported by the MRSEC Program, a member of the NSF-funded Materials Research Facilities Network, under grant NSF DMR 1121053. We acknowledge the use of the NRI-MCDB Microscopy Facility and the Spectral Laser Scanning Confocal supported by the Office of The Director, National Institutes of Health, under Award #S10OD010610. For the DFT work, we also acknowledge the Center for Scientific Computing at UCSB under NSF Grant CNS-0960316.

**Supplemental Experimental Procedures**

**General information for the synthesis of DSFO(Me)4 and DSFO+**

The full synthetic route to the compounds of interest is provided in Scheme S1, and preparations of intermediate compounds are provided below. Unless otherwise noted, materials were purchased from suppliers (Sigma Aldrich, Acros, Strem, and TCI) and were used without further purification. $^{1}$H and $^{13}$C NMR spectra were recorded on either a Bruker DMX 500 MHz or Varian VNMRS 600 MHz spectrometer and all chemical shifts are reported in ppm values (Δ) versus tetramethylsilane. Dry toluene and dry, inhibitor-free THF were taken from a solvent purification system, using packed alumina

columns under Argon. Silica gel column chromatography was purchased from Dynamic Adsorbents Inc. and had particle size of 32-64 $\mu$m. Compounds **2** - **6** were synthesized according to literature procedures.[80, 81, 82, 83]

**Preparation of 1-iodo-3,5-bis((6-bromohexan-1-yl)oxy)benzene (7)**

1 g of 1-iodo-3,5-dihydroxybenzene (6) (1 eq., 4.24 mmol), 6.5 mL of 1,6-dibromohexane (10 eq., 42.4 mmol), and 1.758 g of $K_2CO_3$ (3 eq., 12.72 mmol) were charged into a 50 mL round bottom flask. Then, 10 mL of dry acetone was added and the flask equipped with a reflux condenser and an argon line was attached. The solution was allowed to reflux for 18 hours and cooled to room temperature. The resulting solution was diluted with dichloromethane and filtered through a celite plug. The solvent was removed in vacuo and the resulting yellow oil was purified using silica gel chromatography with 20% (v/v) dichloromethane in hexane to give a clear oil, which was the desired product contaminated with excess 1,6-dibromohexane. The oil was triturated with methanol ( 10 mL) three times to give 1.471 (62% yield) of a white powder. $^1$H NMR (500 MHz, $CDCl_3$) $\Delta$ = 6.86 (d, J=2.5, 2H), 6.41 (t, J=2.7, 1H), 3.93 (t, J=6.4, 4H), 3.45 (t, J=6.8, 4H), 1.92 (p, J=6.7, 4H), 1.79 (p, J=6.8, 4H), 1.51 (m, J=10.8, 5.5, 8H). $^{13}$C NMR (600 MHz, $CDCl_3$) $\Delta$ 160.49, 116.24, 101.42, 94.05, 67.95, 33.74, 32.63, 28.93, 27.85, 25.22. HRMS m/z (ESI) calcd for C18H27O2Br2I $[M]^+$ 559.9427, found: 559.9423

**Preparation of 1-iodo-3,5-bis((6-iodohexan-1-yl)oxy)benzene (8)**

500 mg (1 eq., 0.89 mmol) of 1-iodo-3,5-bis((6-bromohexan-1-yl)oxy)benzene (7), 738 mg of sodium iodide (5 eq., 4.45 mmol) and 20 mL of dry acetone were charged into a 50 mL 3-neck round bottom flask. The solution was heated to reflux under an inert atmosphere for 6 hours. The solution was cooled to room temperature, diluted with dichloromethane, and filtered through a silica plug. After the removal of solvent, the product was purified

using a short silica gel column with 20% (v/v) dichloromethane in hexane to give 581 mg (98% yield) of a light yellow oil that solidifies to a white powder. $^{1}$H NMR (500 MHz, $CDCl_3$) $\Delta$ = 6.86 (d, J=2.2, 2H), 6.41 (t, J=2.2, 1H), 3.92 (t, J=6.3, 4H), 3.23 (t, J=6.9, 4H), 1.88 (m, J=7.7, 3.9, 3.4, 4H), 1.79 (m, J=10.0, 8.3, 5.2, 4H), 1.50 (p, J=3.6, 8H). $^{13}$C NMR (600 MHz, $CDCl_3$) $\Delta$ 160.53, 116.30, 101.50, 94.07, 67.99, 33.37, 30.20, 28.91, 25.02, 6.88. HRMS m/z (ESI) calcd for C18H27O2I3 $[M]^+$ 655.9156, found: 655.9145

**Preparation of E,E-1,1-bis(2-(3,5-bis-((6-iodohexan-1-yl)oxy)phenyl)ethenyl)ferrocene (9)**

In a nitrogen filled glovebox, 317 mg of 1-iodo-3,5-bis((6-iodohexan-1-yl)oxy)benzene (2.3 eq., 0.48 mmol), 50 mg of 1,1-divinylferrocene (1 eq., 0.21 mmol), 3 mg palladium acetate (5 mol %, 0.011 mmol), 10 mg XPhos (10 mol %, 0.021 mmol), 0.15 mL diisopropylethylamine (4 eq., 0.84 mmol), and 1.5 mL of toluene were charged into a 0.5-2 mL microwave tube. This tube was sealed and heated at 100 °C in a pre-heated oil bath for 8 hours. The solution was allowed to cool to room temperature and was directly loaded onto a silica gel column using 19% (v/v) toluene and 1% (v/v) ethyl acetate in hexane to give 130 mg (48% yield) of a deep red oil. $^{1}$H NMR (500 MHz, $CDCl_3$) $\Delta$ = 6.76 (d, J=16.1, 2H), 6.58 (d, J=16.1, 2H), 6.49 (d, J=2.1, 4H), 6.34 (t, J=2.1, 2H), 4.42 (t, J=1.7, 4H), 4.28 (t, J=1.8, 4H), 3.91 (t, J=6.4, 8H), 3.25 (t, J=7.0, 0.7, 8H), 1.96  1.85 (m, 8H), 1.81 (m, 8H), 1.55  1.43 (m, 16H). $^{13}$C NMR (600 MHz, $CD_2Cl_2$) $\Delta$ 160.35, 139.61, 126.49, 126.40, 104.05, 100.15, 83.95, 70.21, 67.96, 67.70, 33.52, 30.28, 29.12, 25.05, 7.21. FD-MS: m/z Calculated 1294.05, Found 1293.97. Due to the molecular weight of the product (>1000 amu) it was not possible to obtain AMM data for this compound. Additionally, due to the nature of the synthetic procedure, there are no perceived impurities with similar molecular weights.

**Preparation of E,E-1,1-bis(2-(3,5-dimethoxyphenyl)ethenyl)ferrocene (DSFO(Me)$_4$)**

In a nitrogen filled glovebox, 238 mg of 1-iodo-3,5-dimethypxy)benzene (2) (2.3 eq., 0.97 mmol), 100 mg of 1,1-divinylferrocene (1 eq., 0.42 mmol), 5 mg palladium acetate (5 mol %, 0.021 mmol), 20 mg XPhos (10 mol %, 0.042 mmol), 0.44 mL diisopropylethylamine (6 eq., 0.84 mmol), and 1.5 mL of toluene were charged into a 0.5-2 mL microwave tube. This tube was sealed and heated at 100 oC in a pre-heated oil bath for 8 hours. The solution was allowed to cool to room temperature and was directly loaded onto a silica gel column using 5% (v/v) dichloromethane and 10% (v/v) ethyl acetate in hexane. After completion of the column, the desired product crystallized out of solution in the collection test tubes and was collected by filtration to give 104 mg (49% yield) of a deep red crystalline solid. $^1$H NMR (500 MHz, $CDCl_3$) $\Delta$ = 6.73 (d, J=16.1, 1H), 6.57 (d, J=16.1, 1H), 6.48 (d, J=2.2, 2H), 6.34 (t, J=2.2, 1H), 4.43 (t, J=2.0, 2H), 4.29 (t, J=1.9, 2H), 3.78 (s, 6H). $^{13}$C NMR (600 MHz, $CDCl_3$) $\Delta$ 160.49, 116.24, 101.45, 94.04, 68.02, 67.95, 33.73, 32.63, 29.03, 28.93, 27.85, 25.22. HRMS m/z (ESI) calcd for C130H30O4Fe $[M]^+$ 510.1494, found: 510.1493

**Preparation of E,E-1,1'-bis(2-(3,5-bis((6-N,N,N-trimethylammoniumhexan-1-yl)oxy)phenyl)ethenyl)ferrocene tetraiodide (DSFO+)**

50 mg (1 eq., 38.6 $\mu$mol) of E-1,1-bis(2-(3,5-bis-((6-iodohexan-1-yl)oxy)phenyl)ethenyl)ferrocene was weighed into a 10 mL round bottom flask and 5 mL of dry, inhibitor-free THF was added via syringe and the flask sealed with a septum. Then, 0.3 mL (20 eq., 0.772 mmol) of 3.2 M trimethylamine solution in methanol was added via syringe. The solution was allowed to stir for 24 hours, at which time a red semi-solid precipitate remains. The THF was removed in vacuo and the resulting semi-solid was dissolved in methanol and another 0.3 mL of trimethylamine solution was added. After stirring for another 24 hours,

the solvent was removed in vacuo and the resulting semi-solid was dissolved in deionized water and lyophilized to give a deep red, fluffy solid of mass 59 mg (quantitative yield). $^{1}$H NMR (500 MHz, $D_2O$, 340K) $\Delta$ = 7.04 (d, J=16.2, 2H), 6.86 (d, J=16.1, 2H), 6.78 (d, J=2.2, 4H), 6.73 (t, J=2.1, 2H), 4.84 (t, J= 1.3, 4H), 4.63 (t, J= 1.3, 4H), 4.22 (t, J=6.5, 8H), 3.61  3.57 (m, 8H), 3.41 (s, 36H), 2.11  2.02 (m, 16H), 1.85  1.77 (m, 8H), 1.73 (m, 8H). $^{13}$C NMR (600 MHz, $D_2O$, 313K) $\Delta$ 160.20, 139.64, 127.09, 126.14, 104.77, 100.49, 68.41, 67.56, 66.69, 53.50, 32.88, 29.03, 25.87, 25.45, 23.09, 22.81. MS: (M-4I)/4Z: Calcualted= 255.68, Found= 255.68; (M-2I)/2Z: Calculated= 638.26, Found= 638.28 Due to the molecular weight (>1000 amu) and ionic nature of the product it was not possible to obtain AMM data for this compound. Additionally, due to the nature of the synthetic procedure, there are no perceived impurities with similar molecular weights.

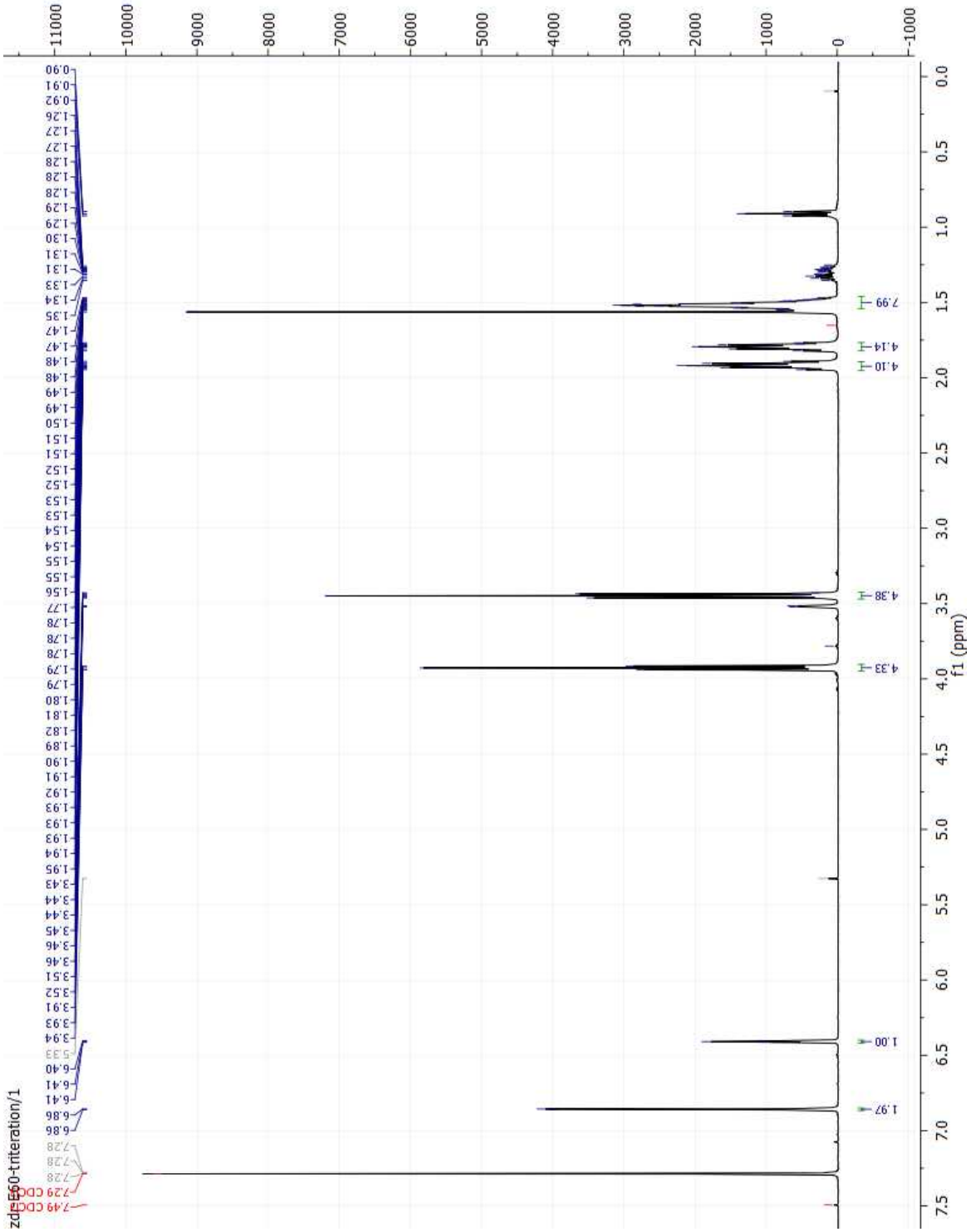


Figure 2.17: $^{1}$H NMR of compound **7**.

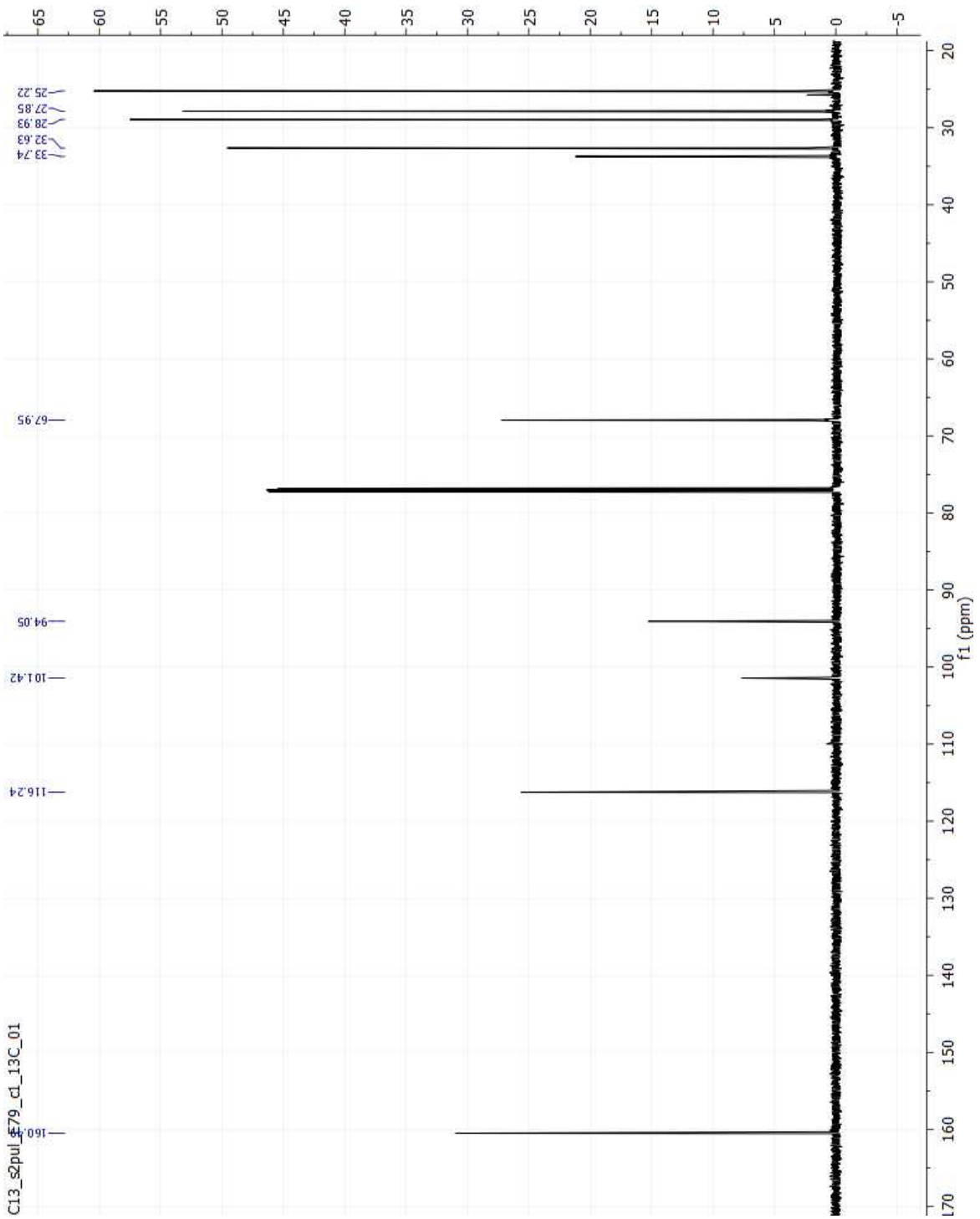


Figure 2.18: $^{13}$C NMR of compound **7**.

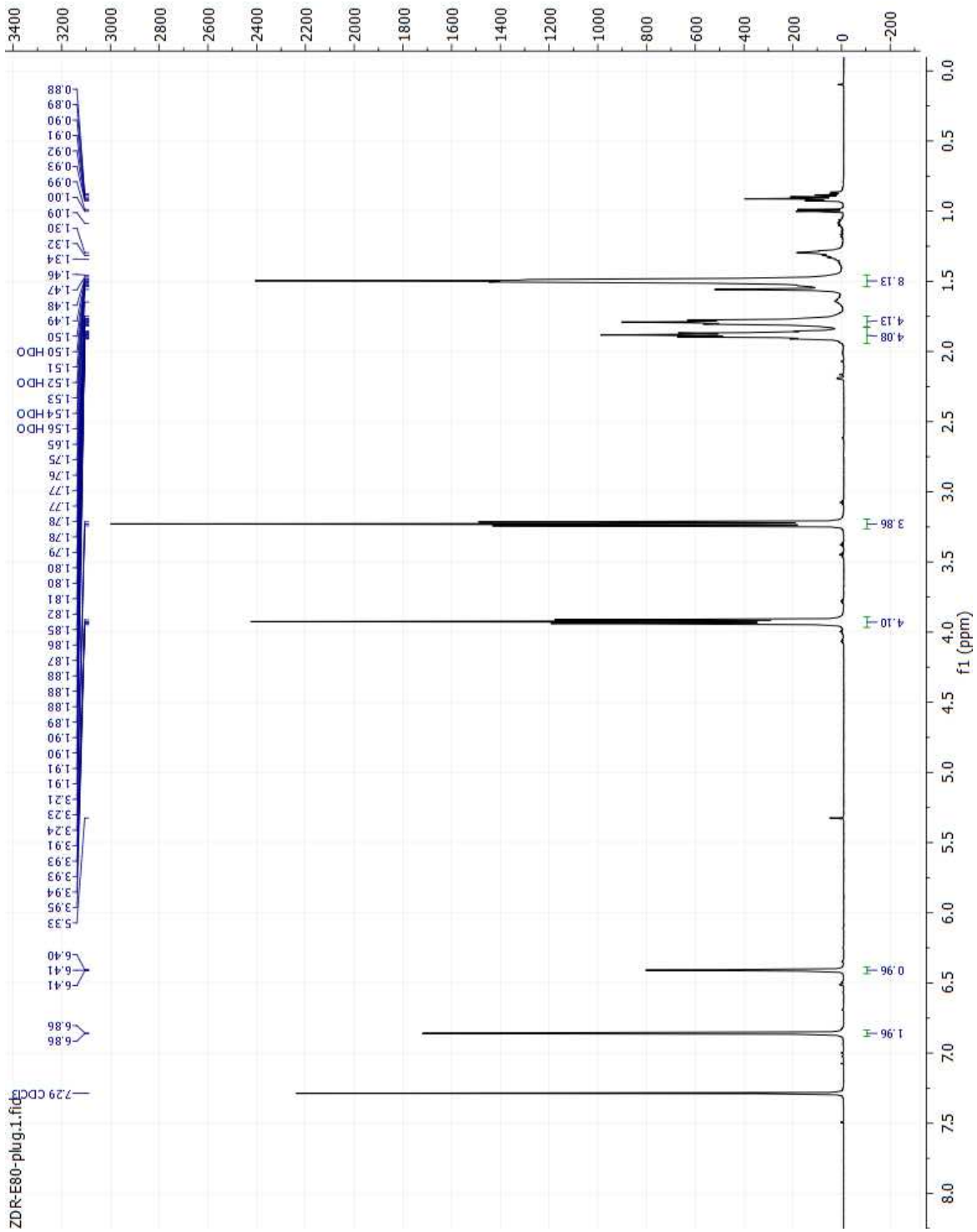


Figure 2.19: $^{1}$H NMR of compound **8**.

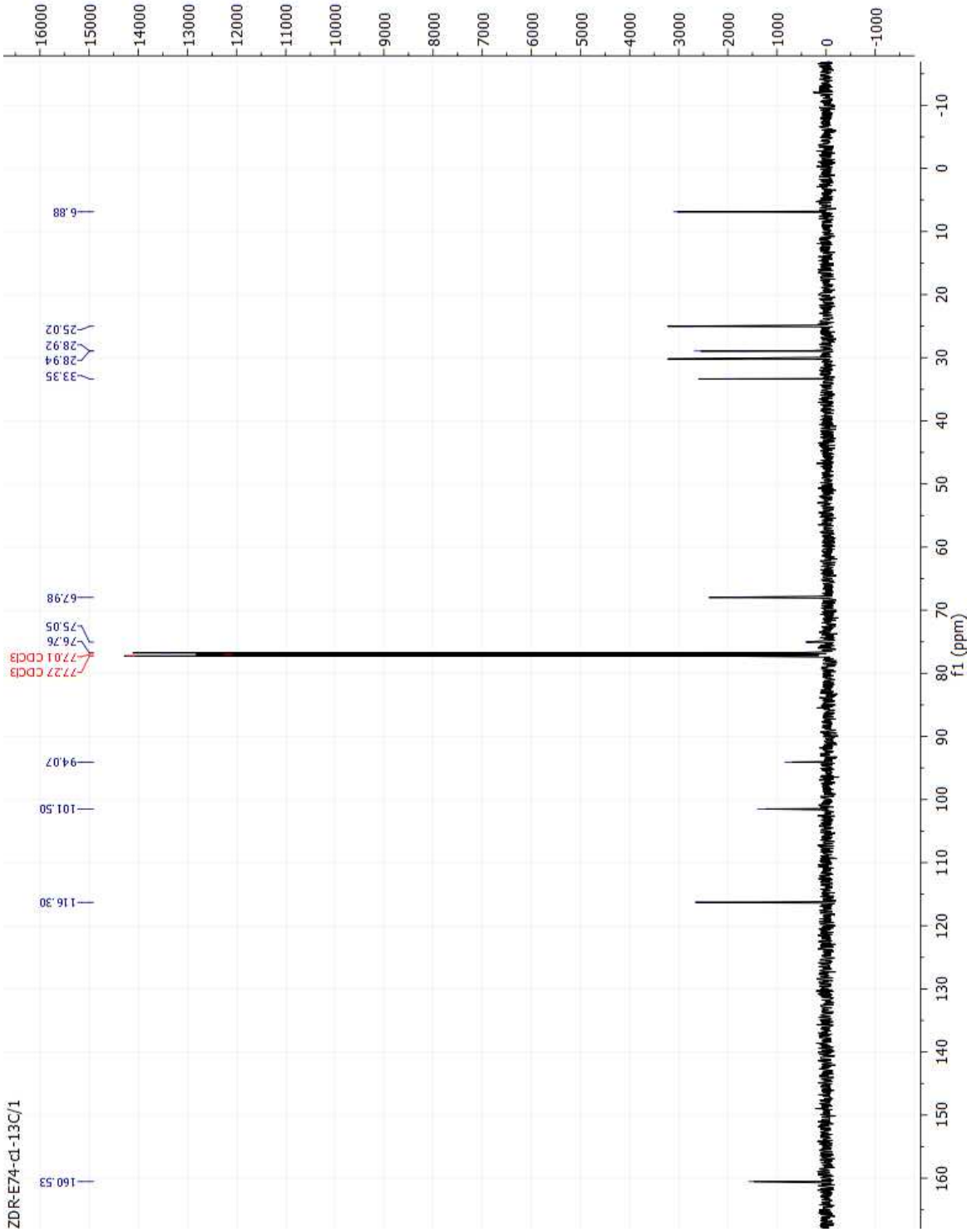


Figure 2.20: $^{13}$C NMR of compound **8**.

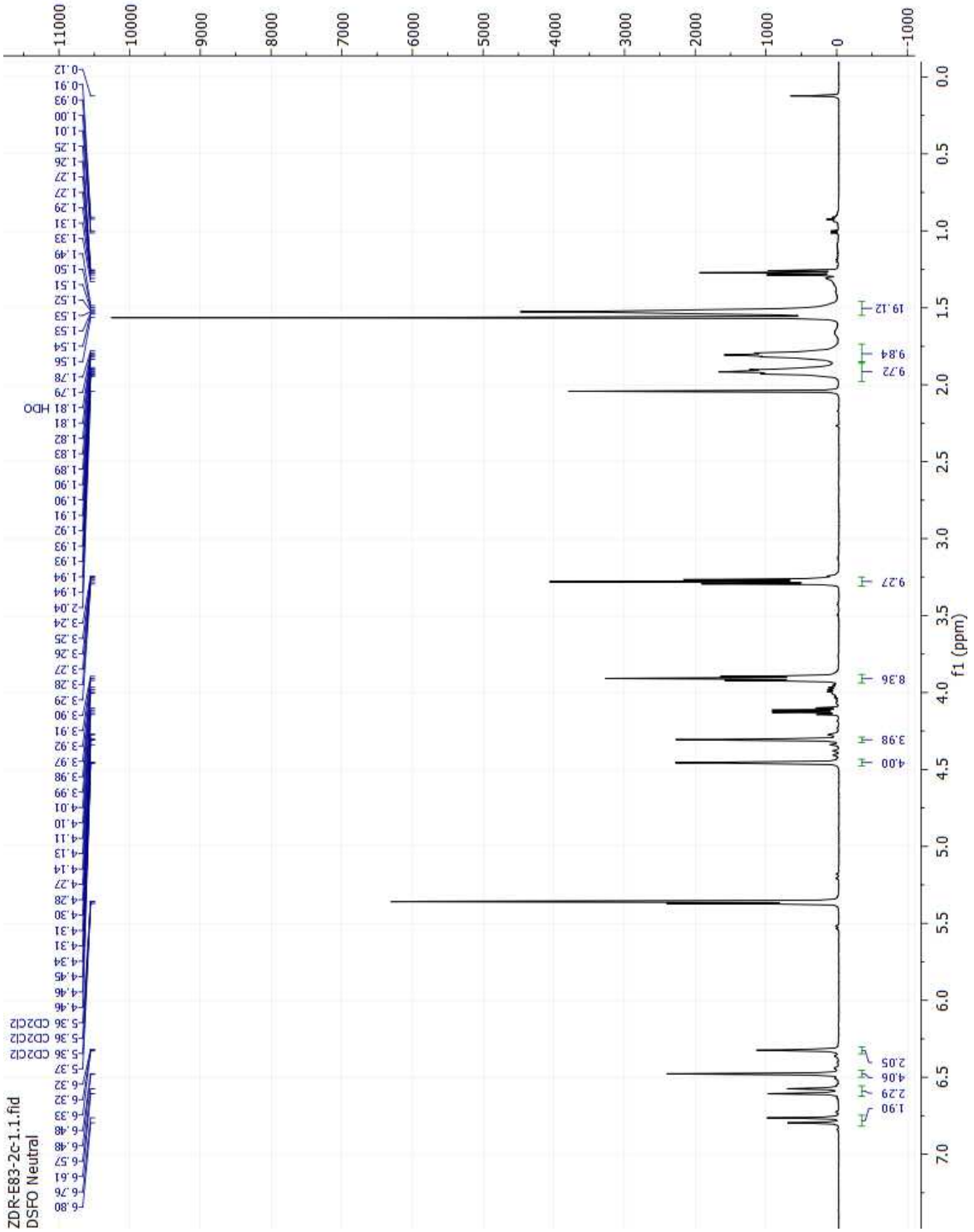


Figure 2.21: $^{1}$H NMR of compound **9**.

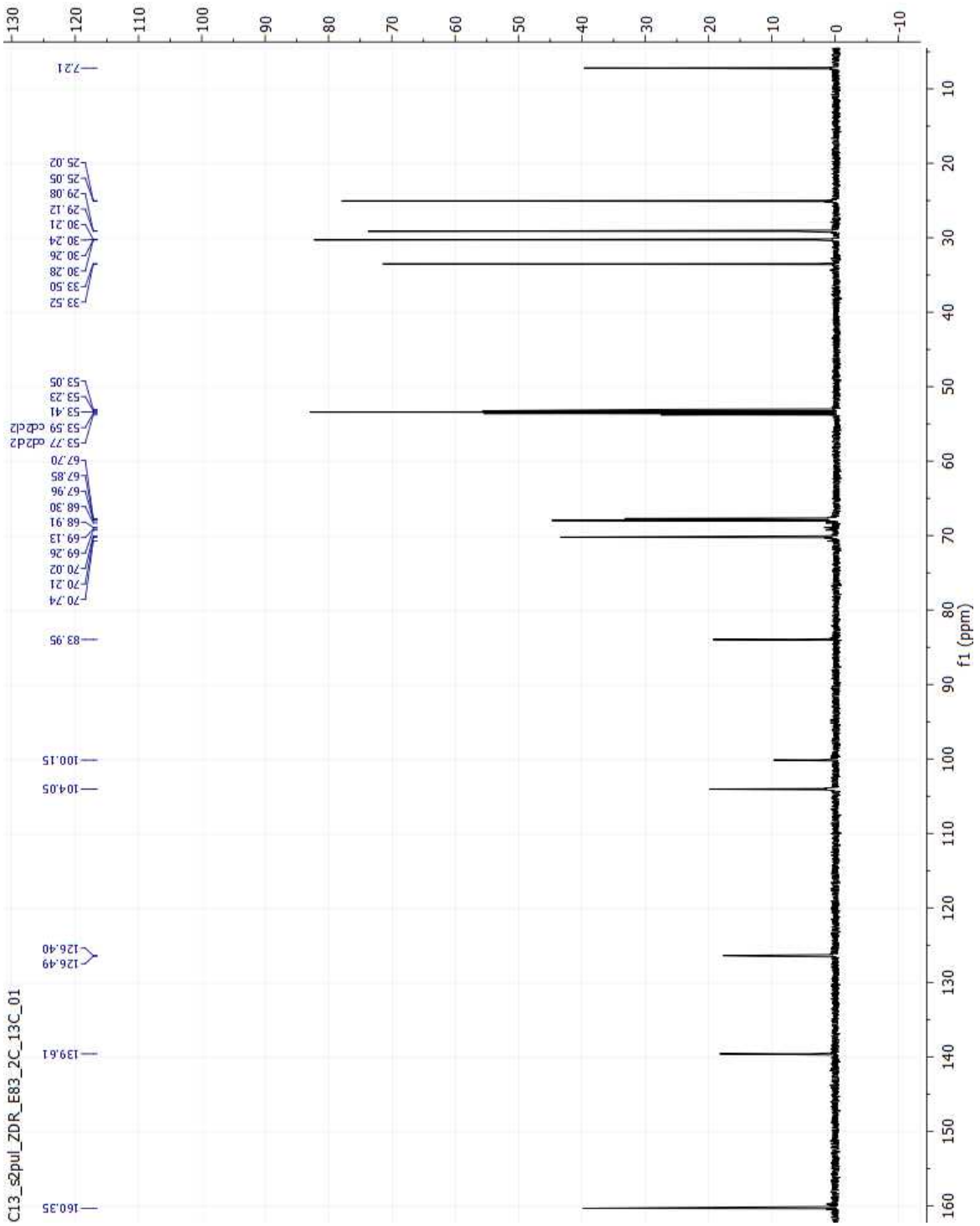


Figure 2.22: $^{13}$C NMR of compound **9**.

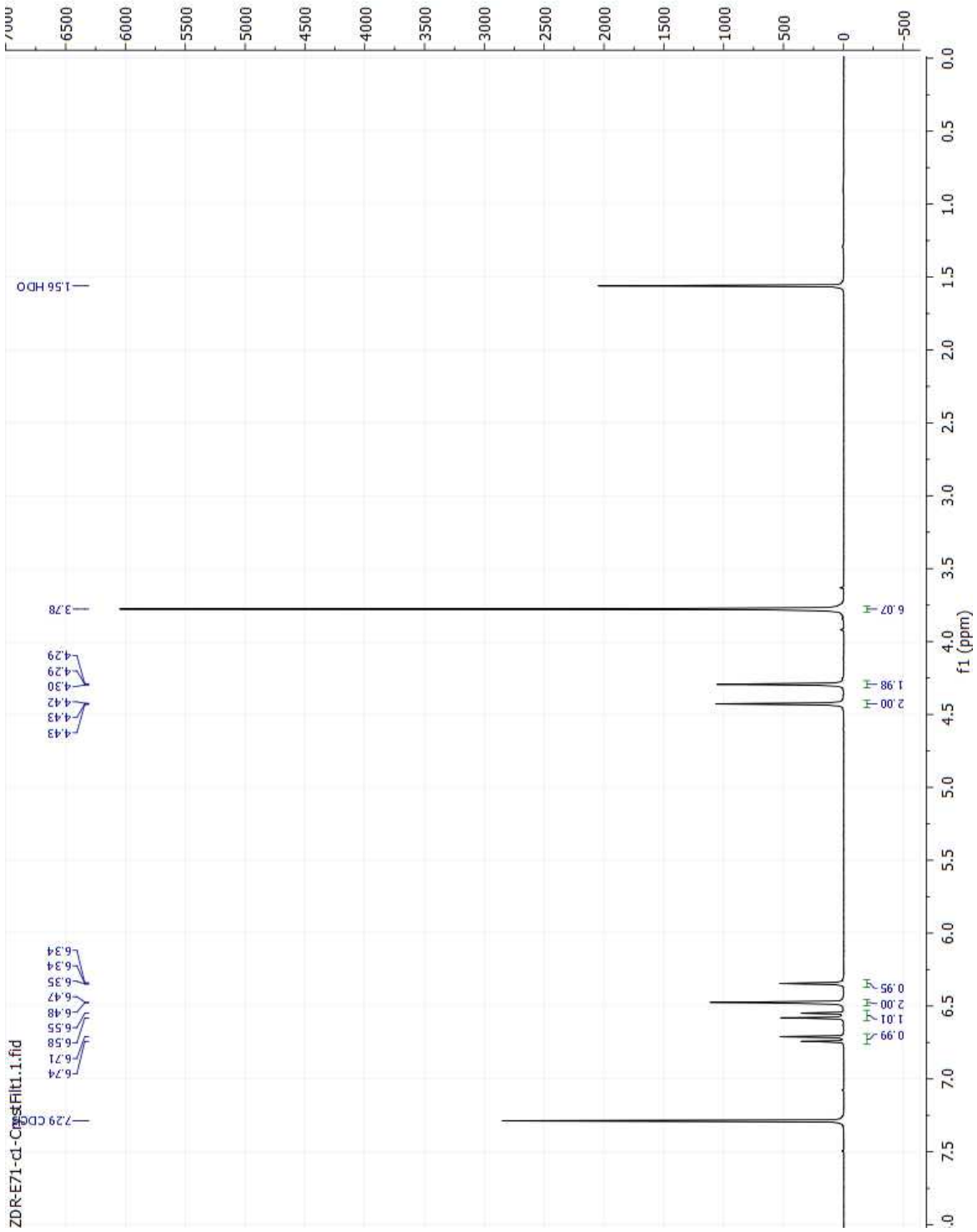


Figure 2.23: $^{1}$H NMR of compound **DSFO(Me)$_4$**.

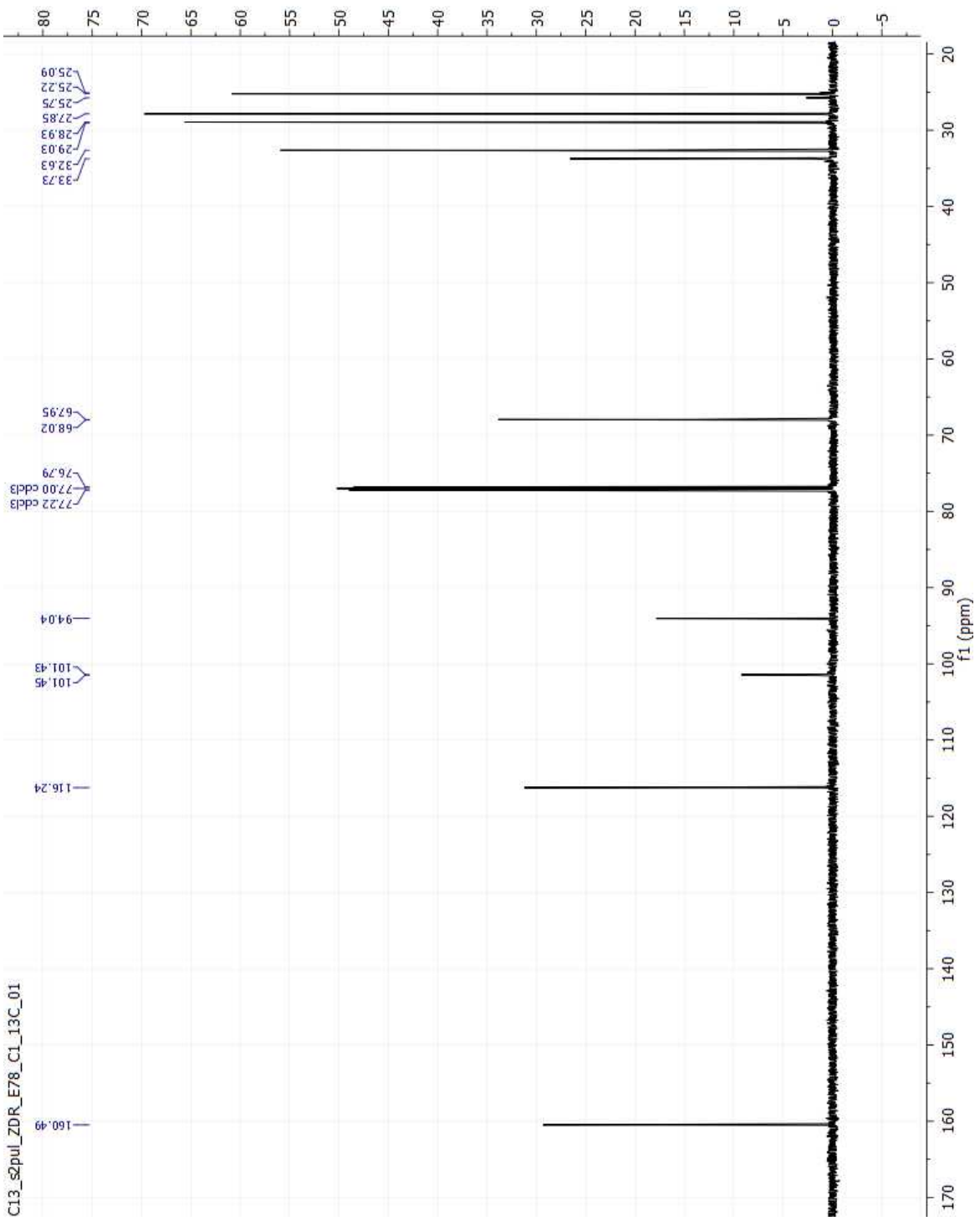


Figure 2.24: $^{13}$C NMR of compound **DSFO(Me)$_4$**.

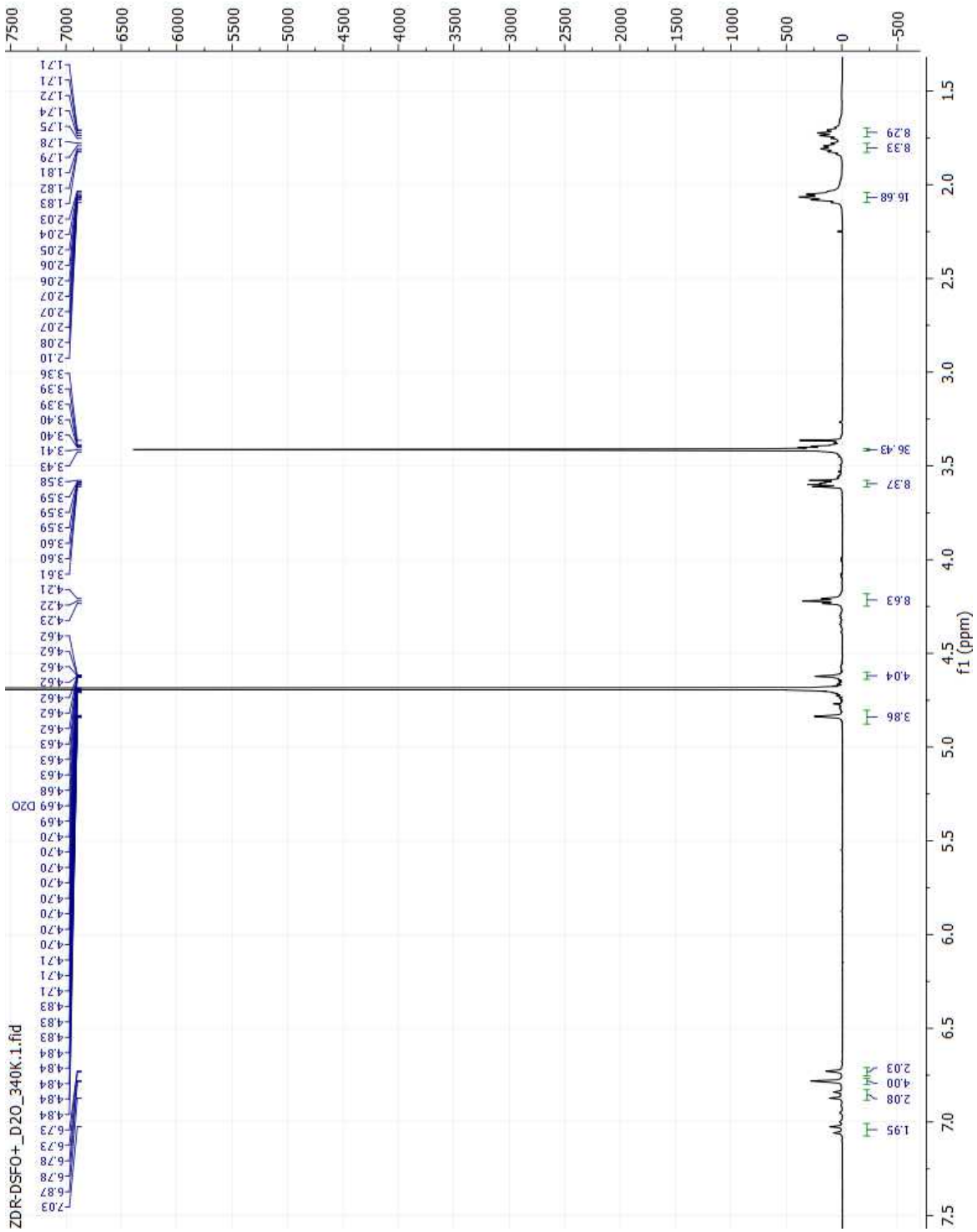


Figure 2.25: $^{1}$H NMR of compound **DSFO+**.

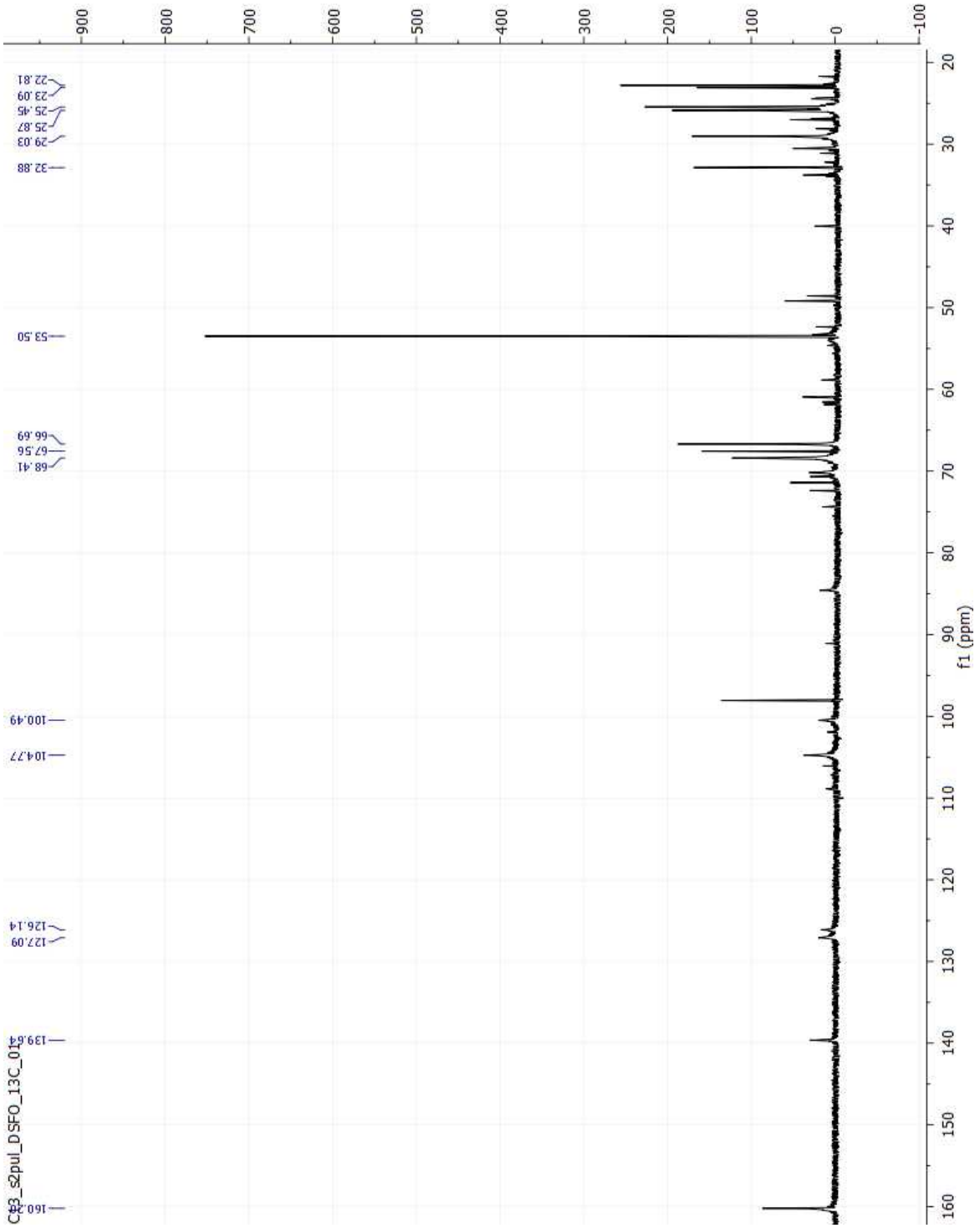


Figure 2.26: $^{13}$C NMR of compound **DSFO+**.

# Chapter 3

# $2^{nd}$ Generation Redox Active COEs Bearing Two Redox Center

*We need more Ferrocene!!*

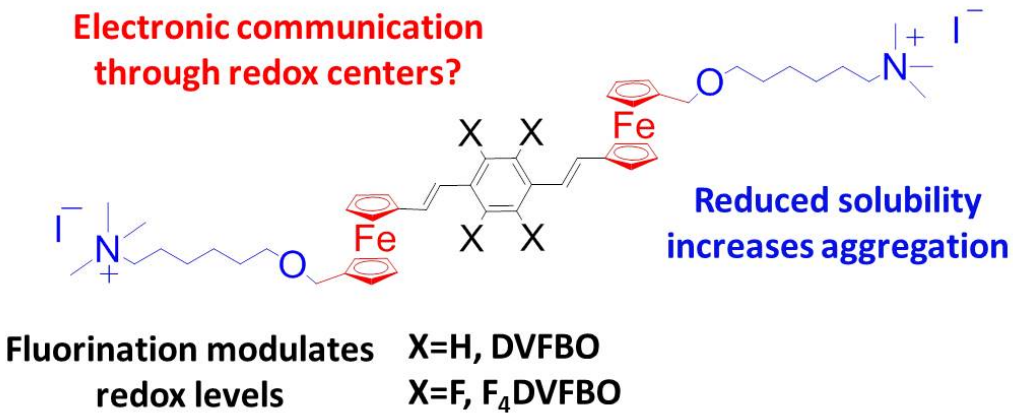

## 3.1 Introduction

Increasing the ability of microorganisms to electronically interact with abiotic components in a facile and controllable way is of great interest in biocatalytic technologies.[101, 102, 103] Applications of biocatalytic electron transfer include microbial fuel cells, biofuel production, commodity chemical production, biosensors, microbial community enrichment, and more.[104, 105, 106] In the absence of oxygen, certain microorganisms are capable of respiring on mineral oxides or, more interestingly, on electrodes of electronic devices. Bacterial genera such as *Shewanella* and *Geobacter* represent microorganisms capable of such tasks.[36] In these organisms there exists transmembrane protein complexes responsible for transporting electrons from the cytosol to the extracellular matrix, and ultimately to a solid-state acceptor, such as a mineral oxide or electrode.[36, 107] Our laboratory is interested in molecular additives that are capable of increasing biocatalytic electron transfer. In the past, the use of conjugated oligoelectrolytes(COEs) has led to improvement of many device parameters associated with biocatalytic electron transfer from organisms such as *E. Coli*, *S. oneidensis*, and *G. sulfurreducens*.[108, 109, 49, 110] In all of these studies the redox states of COEs were outside of the metabolic respiratory window of these organisms, i.e. the oxidation potential of COEs were greater than the poised potential of the device. This scenario is contrasted by the function of the native electron transport mechanism, where heme-containing proteins use multiple redox sites that move electrons from the inside to the outside of the cell during the course of a respiratory process.[107]

In the previous chapter, we drew inspiration from these considerations to design a COE that maintained the membrane intercalating behavior of COEs with the added functionality of a redox active moiety in the conjugation path of the semiconductor.[111] This new redox active COE, named DSFO+, was shown to catalyze electron transfer in

microbial electrochemical cells, even when key electron transfer proteins in *Shewanella oneidensis* were genetically removed. This observation implicated DSFO+ as a protein prosthetic capable of partially recovering the electrogenic phenotype of a biofilm by replacing the function of a redox-active protein with that of a chemical additive. The results of this study also showed that DSFO+ improved current production on a per-cell basis and that the improvement in current production occurred at very short timescales after the addition of DSFO+.

The result of this initial study motivated us to design a second series of redox active COEs, with features that may improve their use in a bioelectrocehmial scenario. DSFO+ contains a redox active unit capped on each side by a $\pi$-delocalized backbone. We were interested if switching this relationship, by using a $\pi$-delocalized backbone capped on each end with a redox center, would allow for improved electron transfer in a bioelectronics situation. Placing the redox center in a location spatially closer to the outside of the membrane should reduce the effective electron tunneling distance from an electron donor inside the cell or to an electron acceptor outside of the cell. Previous work has shown that the ability of ferrocene moieties to communicate through a $\pi$-delocalized bridge is a function of the frontier orbital levels of the $\pi$-delocalized bridge and the Ferrocene units.[112] In other words, as the frontier energy levels of the two moieties become degenerate, communication through the $\pi$-bridge is more facile. We were curious how this situation would translate to a circumstance where the semiconducting moiety was appended with ionic linkers to make a COE and how these properties would manifest in a situation pertinent to a biological system. To look closer at this effect, we decided to closely investigate the electrochemical and optical properties of a redox-active COE in an abiotic situation, in order to ascertain fundamental properties of these systems before implementation into a biologic system.

The main absorption band in most ferrocene derivatives is dominated by a metal-

to-ligand charge transfer band, with very minor contributions from Laporte forbidden, low-intensity d-d transitions.[113] In typical $\pi$-delocalized semiconductors, the major absorption band arises from a $\pi$- $\pi^*$ transition, which typically has a much larger molar absorptivity value when compared to ferro-cene derivatives.[114] For these two reasons, when one combines a $\pi$-delocalized ligand with a ferrocene unit, the most intense absorption band is expected to be a $\pi$- $\pi^*$ transition arising from the semiconducting backbone.[115] Due to the fact that the lowest energy transition in the molecule arises from a metal-to-ligand charge transfer complex, the redox properties are expected to be dictated by this lower strength, red shifted feature. This difference in optical and electronic features represents a synthetic handle in which one can control these two properties independently. It is also known that introducing electron withdrawing/donating groups around the ferrocene core can have a drastic effect on the redox potential of ferrocene derivatives, as they have the ability to destabilize/stabilize the resulting ferrocenium species.[116] Due to the fact that this effect is mostly inductive, we reasoned that we could modulate the redox properties of the ferrocene core without affecting the $\pi$- delocalized bridge by fluorination of the core, thereby increasing the inductive withdrawing effect of the $\pi$-bridge without drastically perturbing the resonance structures in the $\pi$-system.

Therefore, we designed a second class of redox active COEs shown in 3.1. It was important that the synthetic scheme we developed was modular in nature, moderate to high yielding, and required minimal purification in order to allow for a material that was cost effective, had minimal environmental impact, and could be easily derivatized.

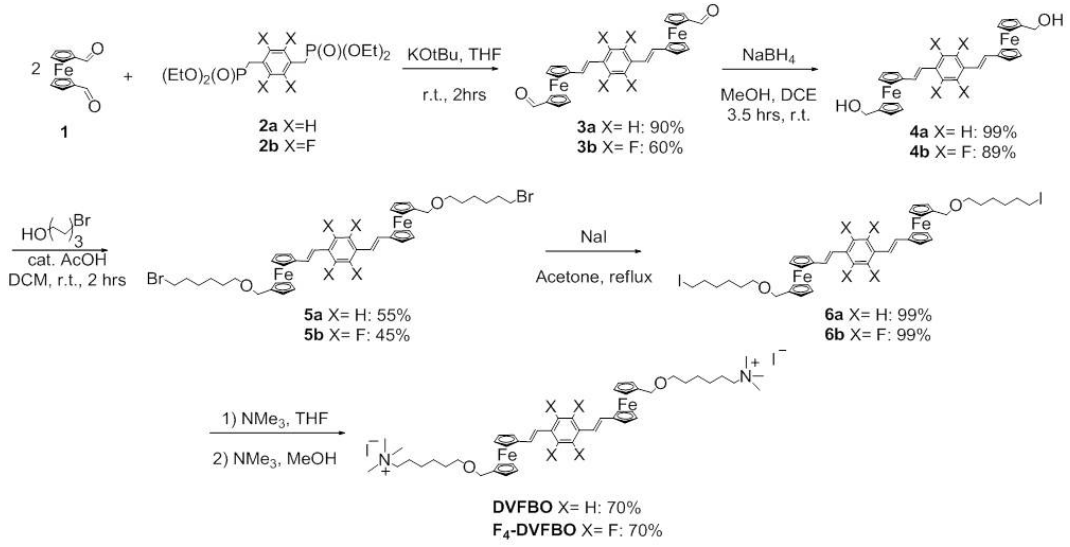


Figure 3.1: Synthetic Approach for **DVFBO** and **$F_4$-DVFBO**.

## 3.2 Synthesis

The synthesis of **DVFBO**) and **$F_4$-DVFBO** starts from building the internal semiconducting core using 1,1-diformylferrocene (**1**) and the appropriate bis(diethylphosphonate) (**2a** or **2b**) affording the aldehyde terminated cores **3a** and **3b** in good yield via a Horner-Wadsworth-Emmons (HWE) reaction. We chose the HWE reaction due to its known high trans selectivity, mild reaction conditions, and good yield. Additionally, building up the semiconducting core before attaching solubilizing chains was intentionally chosen to provide an intermediate of low solubility that could readily be purified by filtration or recrystallization. Indeed, analysis of the crude of **3a** after precipitating the reaction mixture with water and filtration through a Buchner funnel showed only the desired product in 90% yield. The analogous reaction with the fluorinated bis(diethylphosponate) **2b** proceed in a similar manner, except the isolated yield of **3b** was only 60%. We attribute the lower efficiency of this transformation to the stabilization and resulting lower nucleophilicity of the anion of **3b** due to fluorination of the benzene

ring.

Reduction of the aldehydes using sodium borohydride in the presence of methanol afforded the bis-diols **4a** and **4b** in 99% and 89% yield, respectively. Due to the low solubility of intermediates **3a**/**3b**, it was found that 1,2-dichloroethane with 10 mol% methanol allowed the reaction with sodium borohydride to proceed smoothly in under 2 hours, while reaction in dichloromethane or under aprotic conditions returned starting material after reacting for 48 hours. Attempts to use alcohols **4a** and **4b** as nucleophiles to synthesize ethers **5a** and **5b** failed in the presence of potassium carbonate under refluxing conditions, only returning starting materials. The inefficiency of this transformation is attributed to the decrease in acidity of alcohols **4a** and **4b** due to the electron rich nature of the cyclopentadienyl ligand located geminal to the alcohol. In order to exploit the electron rich nature of these alcohols, we reasoned that they could be electrophiles in an acid-catalyzed condensation reaction. Encouraged by reports from literature, we were pleased to find that the reaction of alcohols **4a** and **4b** with 6-bromo-1-hexanol proceeded smoothly in the presence of catalytic acetic acid, to afford both ethers in moderate yield.[117] The purification of **5a** and **5b** is the only step in the synthesis of **DVFBO** and **$F_4$-DVFBO** that requires chromatography, affording **5a** and **5b** in 55% and 45% yield, respectively. After a Finkelstein reaction to exchange the pendant alkyl bromides for iodides, **DVFBO**) and **$F_4$-DVFBO** were generated by reacting alkyl iodides **6a** and **6b** with an excess of trimethylamine. In-depth details of the synthetic procedures used and characterization of compounds **DVFBO**, **$F_4$-DVFBO**, and all intermediates can be found in3.6 .

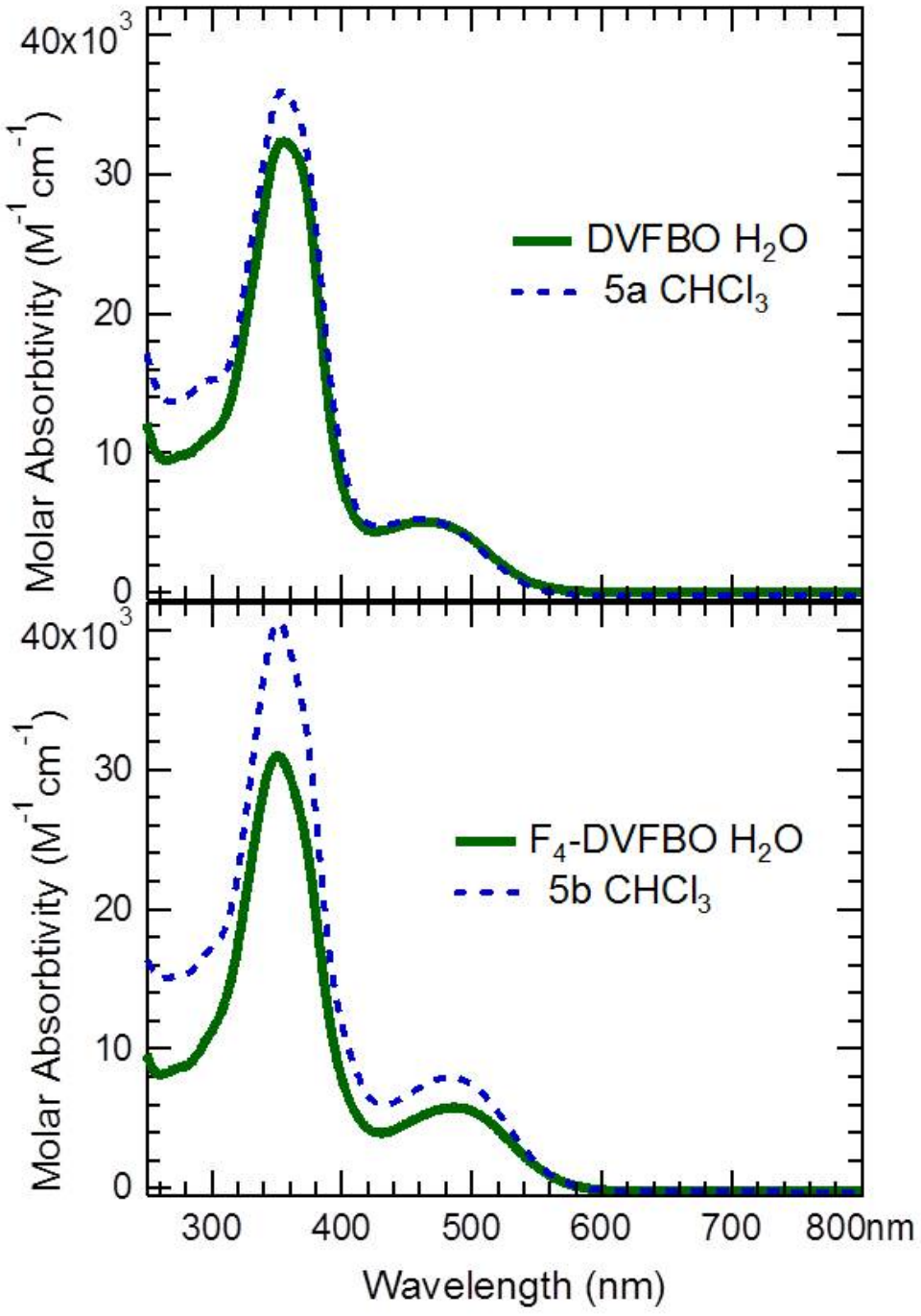


Figure 3.2: UV-Vis Spectrum of **DVFBO** in water and **5a** in $CHCl_3$ (top) and **$F_4$-DVFBO** in water and **5b** in $CHCl_3$ (Bottom).

## 3.3 Characterization

To ascertain the behavior of **DVFBO** and **$F_4$-DVFBO** in a low dielectric constant media, e.g. a biological membrane, we investigated the optical and electrochemical features of compounds **5a** and **5b** in chloroform. We chose compounds **5** over compounds **6** due to the lower stability of alkyl iodides when compared to alkyl bromides and the fact that the alkyl chains have a negligible contribution to optical and electrochemical properties. As mentioned earlier, we expected that the optical properties of compounds **5a** and **5b** to be quite similar due to the fact the fluorination of the internal benzene ring of **5a** results in an inductive withdrawing effect but little resonance delocalization of the semiconducting backbone, both of these effects due to the small, electronegative nature of fluorine atoms. As 3.2 shows, the absorption maximum for **5a** is 352 nm and fluorination of the core causes the maximum absorption of **5b** to hypsochromically shift by only 2 nm. The molar absorptivity of these molecules shifts from 35,960 $M^{-1}cm^{-1}$ in compound **5a** to 40,520 $M^{-1}cm^{-1}$ in **5b**, displaying a weak hyperchromic effect upon fluorination. In both molecules there exists a lower energy, lower intensity peak which is assigned to a metal to ligand charge transfer band. Examination of this lower energy peak reveals a more significant bathochromic shift by 19 nm upon fluorination of the core of **5a** along with a more pronounced hyperchromic effect, which speaks to the fact that fluorination of the internal core does impart a small amount of donor-acceptor character into the semiconducting backbone by creating a more delocalized state in the ligand $\pi^*$ orbital. The optical properties of compounds **DVFBO** and **$F_4$-DVFBO**, when compared to **5a** and **5b** respectively, show a small hypochromic effect when water was used as the solvent, this effect is more pronounced in the case of **$F_4$-DVFBO**. The absorption maxima showed no shifts or solvochromatic effects. All of the compounds were found to lack any fluorescence signal using a standard fluorometer, which is common for ferrocene derivatives. We

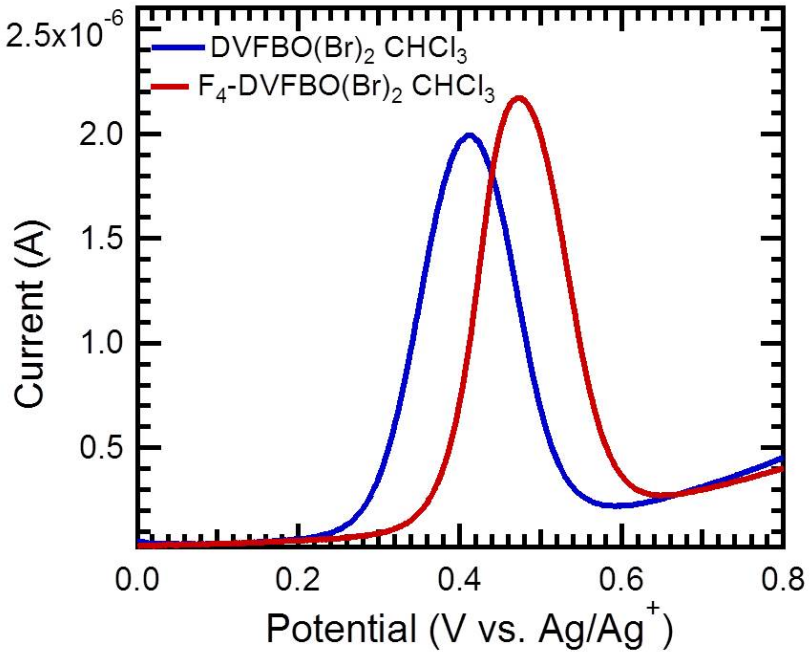


Figure 3.3: DPV Traces of **5a** and **5b** in $CHCl_3$, with 100 mM TBAF supporting electrolyte.

were pleased to find that the optical properties of **DVFBO/F4-DVFBO** and **5a/5b** were a convolution of features found in both ferrocene and COEs. In all spectra there are two absorption bands that vary drastically in their molar absorptivity. The higher energy, hyperchromic peak is assigned to a $\pi$ to $\pi^*$ transition that is highly similar to that of the parent COE in both peak wavelength and molar absorptivity.[118] The lower energy, hypochromic peak is assigned to a metal to ligand charge transfer process typical of ferrocene derivatives, however this peak is bathochromically shifted compared to many ferrocene derivatives due to the electron rich nature of the delocalized $\pi$ framework.

The similarity in the optical properties of **5a** and **5b** is contrasted by their differences in electrochemical features. 3.3 shows the redox potentials of compounds **5a** and **5b** at 100 $\mu$M in chloroform, as measured by differential pulse voltammetry (DPV). We chose to investigate the electrochemical features of these materials using DPV, instead of cyclic

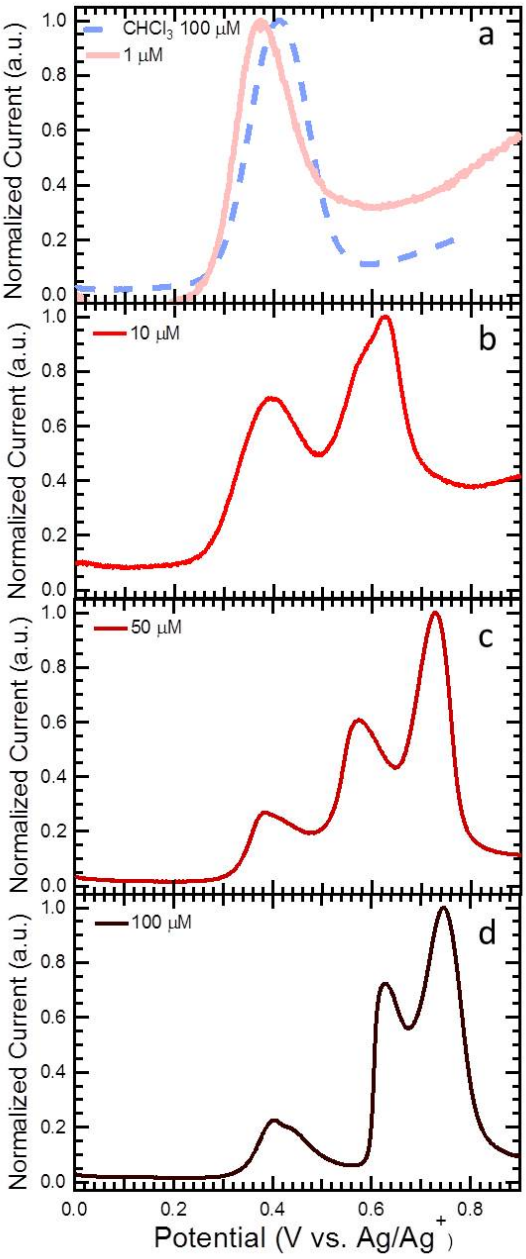


Figure 3.4: DPV Traces of **DVFBO** as a Function of Concentration. **5a** (dotted line) in $CHCl_3$is shown in the top panel.

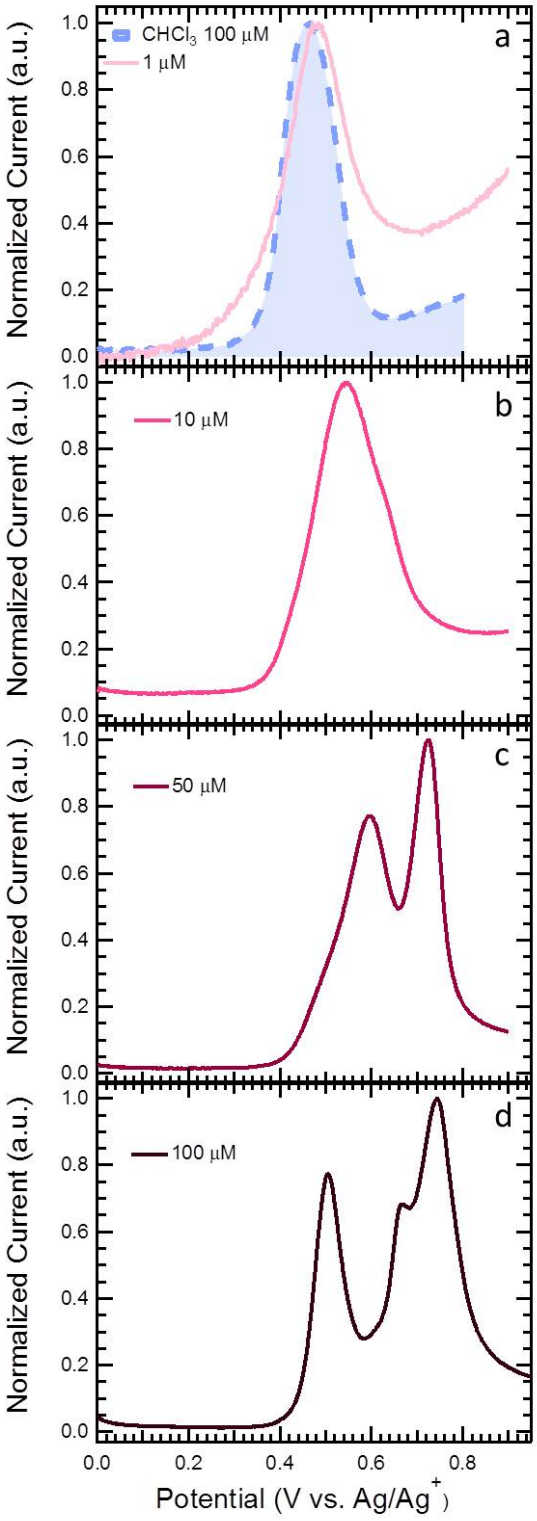


Figure 3.5: DPV Traces of **$F_4$-DVFBO** as a Function of Concentration. **5b** (dotted line) in $CHCl_3$is shown in the top panel.

voltammetry, due to its superior ability to resolve redox features.[28] Fluorination of the core of **5a** causes compound **5b** to have a redox potential that is shifted anodically by 80 mV. 3.3 also shows that both compounds **5a** and **5b** exhibit only one oxidation peak, indicating that both electrons from the iron centers are removed at the same potential. The width at half max of the DPV peaks indicate a one electron process, akin to what one would expect if the redox centers were linked by a saturated linker.[28] This finding is an indication that the delocalized semiconducting backbone of these compounds does not allow for electronic communication of the peripherally located redox centers, likely due to the fact that the frontier orbitals of the semiconducting backbone are too high in energy for interaction with the iron centers. These results are encouraging for the design of redox active COEs that have tunable optical and electronic independent of one another.

Upon dissolution in 100 mM pH 7.2 phosphate buffer (PB), the electrochemical features of compounds **DVFBO** and **$F_4$-DVFBO** display the same trend as their non-ionized counterparts, with a few important differences. Fluorination of the backbone once again shifts the low-energy electrochemical features anodically by 80 mV, however these peaks are accompanied by two new high-energy peaks that were absent from both of the neutral compounds. These two peaks were initially assigned to the oxidation of the two iron centers followed by the oxidation of the semiconducting backbones. If this were true, this would indicate that the redox centers are in electronic communication, however further experiments have proven this to be false, *vide infra*. When the DPV traces of **DVFBO** and **$F_4$-DVFBO** were taken as a function of concentration, it was found that the peak potential of the high-energy features were concentration dependent and that these features converged towards the neutral traces of **5a**/**5b** at 1 $\mu$M in PB, as shown in 3.4 and 3.5. This concentration dependence of redox features is suggestive of an intermolecular process due to aggregation or micelle formation. Moreover, when the DPV

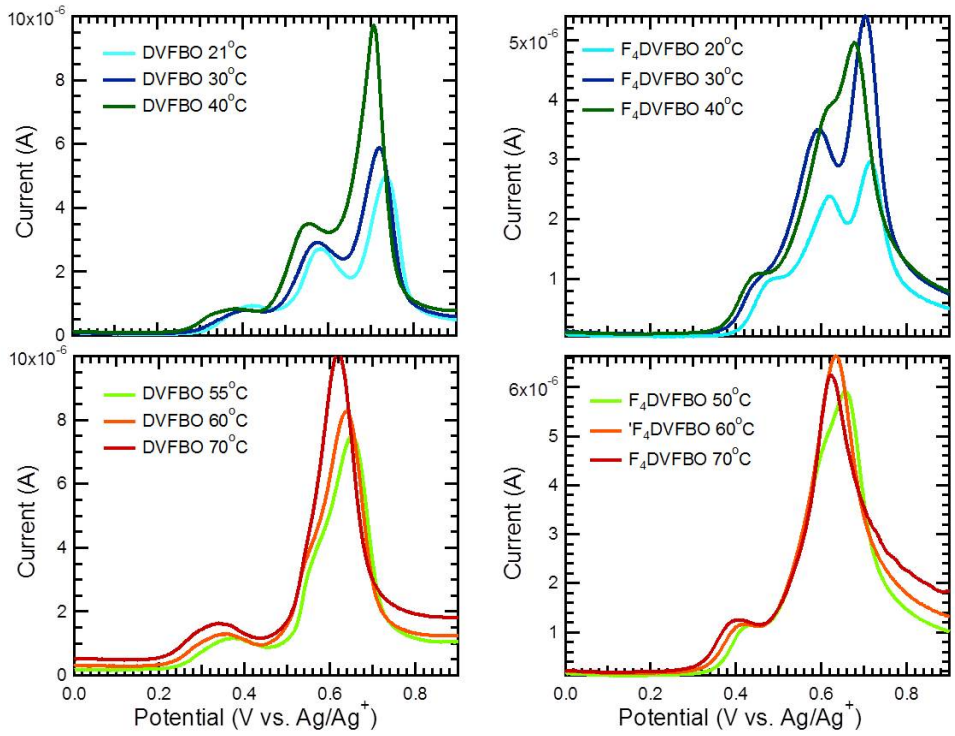


Figure 3.6: Temperature dependent DPV scans of DVFBO and F4DVFBO in PB at 50 $\mu$M in 100 mM PB.

traces were taken as a function of temperature the two high-energy peaks converged upon one another (see 3.6), while the lower energy peak shifted to lower potentials according to Nernstian behavior. These experiments suggest that the appearance of high energy peaks in the DPV traces are due to burying of the redox centers, which are hydrophobic, into the interior of an aggregate or micelle like structure.

To further probe the existence of aggregates, we reasoned that once compounds **DVFBO** and **$F_4$-DVFBO** formed an aggregate or micellular structure, there should be a detectable signal from a zeta potential measurement, as the hydrophobic core of the molecule should be surrounded by the appended cationic functionalities.[119, 120, 121] Indeed, zeta potential signals of a positive magnitude were detected in the same concentration ranges that afforded the DPV traces in 3.7. We were encouraged to find that the

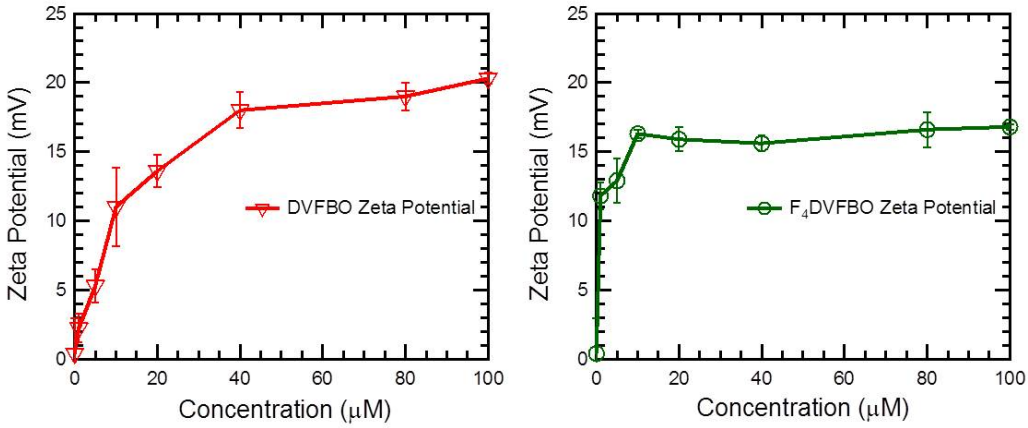


Figure 3.7: Zeta Potential of **DVFBO** and **$F_4$-DVFBO** at varying concentraions in 100 mM PB.

trend in zeta potential correlated nicely with the concentration dependent DPV study and that the zeta potential decreased in magnitude as the concentration of **DVFBO** and **$F_4$-DVFBO** was lowered in solution. Considering that the samples were in a solution containing phosphate buffer of at least three orders of magnitude higher in concentration (phosphate buffer was kept invariant at 100 mM), the change in zeta potential as a function of COE concentration is highly suggestive of aggregation or micelle formation in solution.

Interestingly, cryo-TEM of **DVFBO** in pure water was found to have ordered ribbon like structures that persisted across micron length scales, indicating supramolecular order (3.8-**A** and **B**). However, cryo-TEM images **DVFBO** (3.8-**C**) and **$F_4$-DVFBO** (3.8-**D**) in PB show aggregates on the order of 100 nm that were clearly disordered and composed themselves of smaller aggregates. The local environment around these molecules affects intermolecular interactions, distorting single molecule properties, which is highlighted by the fact that cryo-TEM images of **DVFBO** are drastically different when PB is used as the solvent, rather than water, yet **DVFBO** and **$F_4$-DVFBO** have similar morphologies in PB. Additionally, this sheds light on the presence of two high energy peaks in the

DPV traces (which are taken in PB), where we attribute the lower energy peak to the oxidation of smaller aggregates and the higher energy peak to the oxidation of the clusters of aggregates. The cryo-TEM images also help to explain the zeta potential data, as the concentration of COE is increased in the solution the molecules aggregate and at higher concentrations, those aggregates start to form larger aggregates, leading to an increased magnitude of the measured zeta potential.

## 3.4 Conclusions

These results have important implications into the design of redox active COEs for use in bioelectronics applications. We have developed a modular synthetic route for the synthesis of COEs capped with ferrocene units that requires minimal purification, uses mild reagents, and has a respectable overall synthetic yield. We have shown that fluorination is one possible way to affect the redox properties of ferrocene derivatives without changing optical properties in the situation where the main absorption band is not the lowest energy band.

The results of our electrochemical experiments show that the two ferrocene units are not in communication electronically although they are connected by a $\pi$-delocalized bridge. The reason for this is due to a mismatch in the energy levels of the ferrocene unit and the $\pi$-delocalized bridge of the molecule. Additionally, we have shown that the more complex electrochemical features observed for **DVFBO** and **$F_4$-DVFBO** in buffered water are due to aggregation and not to actual features of the molecular entity. The reason for such pronounced aggregation of **DVFBO** and **$F_4$-DVFBO** compared to previous reports on COEs is likely due to their lower number of ionic functionalities. Having a lower number of ionic functionalities will likely increase the affinity of **DVFBO** and **$F_4$-DVFBO** for a biological membrane, which is desirable from a practical stand-

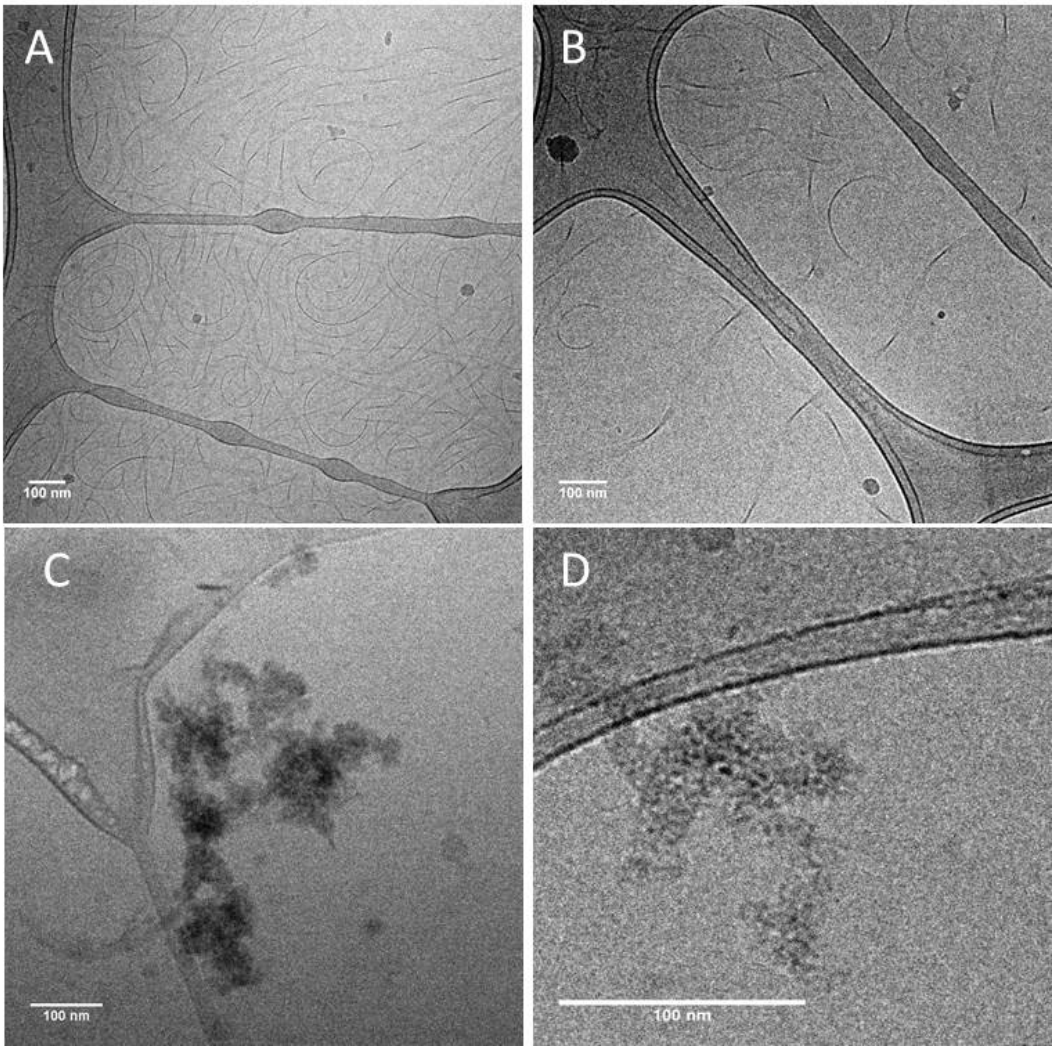


Figure 3.8: TEM Micrographs of (a/b) **DVFBO** in deionized water, (c) **DVFBO** in 100 mM PB, and **$F_4$-DVFBO** in 100 mM PB.

point. The fact that the oxidation of both iron centers in **DVFBO** and **$F_4$-DVFBO** are equienergetic has important consequences in potential applications, as it shows that both redox sites are available for redox cycling (e.g. catalytic electron transfer) in a biological situation, invariant of the oxidation state of the entire molecule.

## 3.5 Preliminary Performance in MECs

## 3.6 Supplemental Experimental Procedures

**General Information** Unless otherwise noted, materials were purchased from suppliers (Sigma Aldrich, Acros, Strem, and TCI) and were used without further purification. 1H and 13C NMR spectra were recorded on either a Bruker DMX 500 MHz or Varian VNMRS 600 MHz spectrometer and all chemical shifts are reported in ppm values ($\Delta$) versus tetramethylsilane. Dry, inhibitor-free THF was taken from a solvent purification system, using packed alumina columns under Argon. Silica gel was purchased from Dynamic Adsorbents Inc. and had particle size of 32-64 $\mu$M. Compounds **2**, **3a**, and **3b** were prepared according to literature procedures.[122, 123, 124]

**Preparation of 1,4-bis-(2-ethenyl-(1-formylferrocen-1-yl))benzene (3a)** A dry 100 mL schlenck flask was charged with 500 mg (1.0 eq, 1.32 mmol) of compound **2a** and 736 mg (2.3 eq, 3.04 mmol) of compound **1**. The flask was capped with a septum and placed under an inert Argon atmosphere by 3 vacuum/argon cycles. 50 mL of dry THF was added via syringe to give a deep brick red homogeneous solution. Then, 326 mg of Potassium tert-butoxide (2.2 eq, 2.91 mmol) was added in one portion by taking of the septum and adding the solid against an argon flow at room temperature. The solution immediately turned a bright red color and was allowed to stir under Argon for 2 hours. An aliquot of the reaction mixture showed consumption of the limiting reagent by thin

layer chromatography (TLC) using 1:1 (v/v) dichloromethane (DCM) and Ethyl Acetate (EtOAc) as the mobile phase. The reaction is quenched with 10 mL of water and poured into 100 mL of water to give a red heterogeneous mixture. The solid was collected by vacuum filtration through a Buchner filter, washed with methanol, and dried to afford **3a** of mass 656 mg in 90% yield. 1H NMR (600 MHz, CD2Cl2) $\Delta$ = 9.88 (s, 2H), 7.43 (s, 5H), 6.80 (d, J=16.2, 3H), 6.74 (d, J=16.1, 3H), 4.76 (t, J=1.9, 4H), 4.60 (t, J=1.9, 4H), 4.58 (t, J=1.9, 4H), 4.40 (t, J=1.8, 4H). 13C NMR (600 MHz, CDCl3) $\Delta$= 193.79, 136.36, 127.75, 126.39, 124.75, 85.46, 79.79, 74.41, 70.63, 70.50, 68.16. HRMS m/z (ESI) calcd for C32H26Fe2O2H [M+H]+ 553.0757, found 553.0771

**Preparation of 1,4-bis-(2-ethenyl-(1-formylferrocen-1-yl))-2,3,5,6-tetrafluorobenzene (3b)**

A dry 100 mL schlenck flask was charged with 500 mg (1.0 eq, 1.11 mmol) of compound **2b** and 618 mg (2.3 eq, 2.55 mmol) of compound **1.** The flask was capped with a septum and placed under an inert Argon atmosphere by 3 vacuum/argon cycles. 50 mL of dry THF was added via syringe to give a deep brick red homogeneous solution. Then, 274 mg of Potassium tert-butoxide (2.2 eq, 2.44 mmol) was added in one portion by removing the septum and adding the solid against an argon flow at room temperature. The solution immediately turned a bright red color and was allowed to stir under Argon for 2 hours. An aliquot of the reaction mixture shows consumption of the limiting reagent by thin layer chromatography (TLC) using 1:1 (v/v) dichloromethane (DCM) and Ethyl Acetate (EA) as the mobile phase. The reaction was quenched with 10 mL of water and poured into 100 mL of water to give a red heterogeneous mixture. The solid was collected by vacuum filtration through a Buchner filter, washed with methanol, and dried to afford **3b** of mass 378 mg in 54% yield. 1H NMR (600 MHz, $CD_2Cl_2$) $\Delta$ = 9.87 (s, 1H), 7.19 (d, J=16.5, 2H), 6.70 (d, J=16.6, 2H), 4.77 (s, 4H), 4.64 (s, 4H), 4.60 (s, 4H), 4.47 (s, 4H). 13C NMR (600 MHz, CDCl3) $\Delta$ =193.30, 145.34-143.53 (dm, J= 249), 134.20 (t,

J= 3.5), 114.49, 112.87, 84.31, 80.05, 74.53, 71.27, 70.77, 68.57. HRMS m/z (ESI) calcd for C32H22F4Fe2O2H [M+H]+ 625.0380, found 625.0386

**Preparation of 1,4-bis-(2-ethenyl-(1-hydroxymethylferrocen-1-yl))benzene (4a)**

A 3-neck 150 mL round bottom flask was charged with 719 mg of compound **3a** (1.0 eq, 1.30 mmol), 70 mL of 1,2-dichloroethane, 7 mL of methanol (10 vol %), and placed under a blanket of Argon. 108 mg of sodium borohydride (2.2 eq, 2.85 mmol) was dissolved in a minimal amount of methanol and quickly added to the stirring, homogeneous, red solution. Bubbles of hydrogen were observed to form and continued for 3.5 hrs, at which time an aliquot analyzed by TLC showed consumption of the starting material using 20% (v/v) EA, 30%(v/v) DCM, in hexanes as the mobile phase. The reaction mixture was slowly quenched with 5 mL saturated ammonium chloride solution at room temperature. The mixture was diluted with water and extracted with DCM two times, washed with water and brine, and dried over sodium sulfate. Decanting the solution to remove the drying agent, followed by removal of solvent in vacuo, afforded 714 mg of compound **4a** in 99% yield. 1H NMR (600 MHz, $CD_2Cl_2$) $\Delta$ = 7.41 (s, 4H), 6.89 (d, J=16.1, 2H), 6.73 (d, J=16.1, 2H), 4.49 (t, J=1.8, 4H), 4.32 (t, J=1.8, 4H), 4.29 (s, 4H), 4.22 (t, J=1.8, 4H), 4.17  4.09 (m, 4H). 13C NMR (600 MHz, CDCl3) $\Delta$= 136.32, 126.32, 126.17, 125.90, 88.97, 83.81, 69.41, 69.39, 68.81, 67.11, 60.61. HRMS m/z (ESI) calcd for C32H30Fe2O2 [M]+ 556.0992, found 556.0972

**Preparation of 1,4-bis-(2-ethenyl-(1-hydroxymethylferrocen-1-yl))- 2,3,5,6-tetrafluorobenzene (4b)**

A 3-neck 150 mL round bottom flask was charged with 513 mg of compound **3b** (1.0 eq, 0.819 mmol), 50 mL of 1,2-dichloroethane, 5 mL of methanol (10 vol %), and placed under a blanket of Argon. 68 mg of sodium borohydride (2.2 eq, 1.80 mmol) was dissolved in a minimal amount of methanol and quickly added to the stirring, homogeneous, red

solution. Bubbles of hydrogen were observed to form and continued for 3.5 hrs, at which time an aliquot analyzed by TLC showed consumption of the starting material using 20% (v/v) EA, 30%(v/v) DCM, in hexanes as the mobile phase. The reaction mixture was slowly quenched with 5 mL saturated ammonium chloride solution at room temperature. The mixture was diluted with water and extracted with DCM three times, the organic layer was washed with water and brine, and dried over sodium sulfate. Decanting the solution to remove the drying agent, followed by removal of solvent in vacuo, afforded 714 mg of compound **4b** in 89% yield. 1H NMR (600 MHz, $CD_2Cl_2$) $\Delta$ = 7.27 (d, J=16.5, 2H), 6.68 (d, J=16.5, 2H), 4.54 (t, J=1.9, 4H), 4.40 (t, J=1.8, 4H), 4.30 (d, J=5.8, 4H), 4.24 (t, J=1.8, 4H), 4.17 (t, J=1.8, 4H). 13C NMR (600 MHz, CDCl3) $\Delta$= 145.29-143.45 (dm, J= 251), 135.61 (t, J= 3.3), 114.33, 111.35, 88.94, 82.84, 70.26, 69.74, 69.13, 67.61, 60.54. HRMS m/z (ESI) calcd for C32H26F4Fe2O2 [M]+ 628.0615, found 628.0613

**Preparation of 1,4-bis-(2-ethenyl-(1-((6-bromohexoxy)methyl)ferrocen-1-yl))benzene (5a)**

300 mg of compound **4a** (1.0 eq, 0.537 mmol) was weighed into a 2 mL microwave tube and capped. 2.2 mL of DCM ( 0.25M solution) was added via syringe and the flask purged with argon. Then, 148$\mu$L of 6-bromohex-1-ol (2.1 eq, 1.13 mmol) was added *via* microsyringe, followed by 3.1 $\mu$L of glacial acetic acid (10 mole %, 0.054 mmol) and the solution was allowed to stir vigorously for 2 hours. An aliquot analyzed by TLC showed consumption of the starting material using 20% (v/v) EA, 30%(v/v) DCM, in hexanes as the mobile phase. At this time, 0.1 mL trimethylamine was added to quench the reaction. The mixture was diluted with DCM and filtered through a silica plug. Column chromatography using a small gradient of 5 to 7% (v/v) EA in hexane was performed to remove the trimer generated in the first synthetic transformation. Removal of solvent afforded 262 mg of **5a** in 55% yield. 1H NMR (600 MHz, $CD_2Cl_2$) $\Delta$ = 7.41 (s, 4H), 6.85 (d, J=16.1, 2H), 6.69 (d, J=16.1, 2H), 4.45 (t, J=1.8, 4H), 4.30  4.26 (m, 4H), 4.18

(m, 8H), 4.13 (m, 4H), 3.40 (t, J=6.9, 4H), 3.35 (t, J=6.6, 4H), 1.83 (p, J=7.0, 4H), 1.50 (p, J=7.1, 4H), 1.40 (p, J=7.4, 4H), 1.35  1.28 (m, 4H). 13C NMR (600 MHz, CDCl3) Δ 136.41, 126.14, 126.08, 126.06, 84.47, 84.17, 70.64, 69.79, 69.75, 69.69, 68.82, 67.30, 33.92, 32.71, 29.47, 27.94, 25.33. HRMS m/z (ESI) calcd for C44H52Br2Fe2O2 [M]+ 880.1082, found 880.1086

**Preparation of 1,4-bis-(2-ethenyl-(1-((6-bromohexoxy)methyl)ferrocen-1-yl))-2,3,5,6-tetrafluorobenzene (5b)**

300 mg of compound **4b** (1.0 eq, 0.537 mmol) was weighed into a 2 mL microwave tube and capped. 2.2 mL of DCM ( 0.25M solution) was added via syringe and the flask purged with argon. Then, 131 $\mu$L of 6-bromohex-1-ol (2.1 eq, 1.00 mmol) was added *via* microsyringe, followed by 2.7 $\mu$L of glacial acetic acid (10 mole %, 0.047 mmol) and the solution was allowed to stir vigorously for 2 hours. An aliquot analyzed by TLC showed consumption of the starting material using 20% (v/v) EA, 30%(v/v) DCM, in hexanes as the mobile phase. At this time, 0.1 mL trimethylamine was added to quench the reaction. The mixture was diluted with DCM and filtered through a silica plug. Column chromatography using a small gradient of 5 to 7% (v/v) EA in hexane was performed to remove the trimer generated in the first synthetic transformation. Removal of solvent afforded 246 mg of **5b** in 48% yield. 1H NMR (600 MHz, $CD_2Cl_2$) Δ = 7.25 (d, J=16.5, 2H), 6.66 (d, J=16.5, 2H), 4.51 (t, J=1.9, 4H), 4.36 (t, J=1.8, 4H), 4.20 (t, J=1.9, 4H), 4.17 (s, 4H), 4.15 (t, J=1.8, 4H), 3.41 (t, J=6.9, 4H), 3.38 (t, J=6.6, 4H), 1.88  1.79 (m, 4H), 1.53 (m, 4H), 1.45  1.38 (m, 4H), 1.37  1.30 (m, 4H). 13C NMR (600 MHz, CDCl3) Δ = 150.09  139.40 (dm, J=250), 135.84, 114.34 (d, J=11.3), 111.09, 84.65, 82.85, 70.72, 70.46, 69.87, 69.85, 68.62, 67.78, 33.87, 32.72, 29.48, 27.94, 25.34. HRMS m/z (ESI) calcd for C44H48F4Fe2O2Br2 [M]+ 952.0704, found: 952.0710.

**Preparation of 1,4-bis-(2-ethenyl-(1-((6-iodohexoxy)methyl)ferrocen-1-yl)) benzene (6a)**

50 mg of compound **5a** (1.0 eq, 0.057 mmol), 85 mg of sodium iodide (10 eq, 0.565 mmol), and 5 mL of dry acetone were refluxed in a 10 mL round bottom flask, equipped with a stir bar and condenser, for 18 hours. Dilution of the reaction mixture with DCM and filtration through a silica plug afforded 55 mg of compound **6a** in quantitative yield. 1H NMR (600 MHz, $CD_2Cl_2$) $\Delta$ = 7.41 (s, 4H), 6.86 (d, J=16.2, 2H), 6.70 (d, J=16.1, 2H), 4.46 (s, 4H), 4.29 (s, 4H), 4.19 (d, J=7.5, 8H), 4.14 (s, 4H), 3.36 (t, J=6.6, 4H), 3.19 (t, J=7.1, 4H), 1.79 (q, J=7.1, 4H), 1.51 (p, J=6.7, 4H), 1.38  1.30 (m, 8H). 13C NMR (600 MHz, CDCl3) $\Delta$ = 136.41, 126.06, 84.29, 83.80, 70.49, 69.78, 69.58, 69.53, 68.82, 67.24, 62.78, 33.42, 32.48, 30.25, 29.45, 25.13, 24.69. HRMS m/z (ESI) calcd for C44H52Fe2O2I2 [M]+ 976.0803, found: 976.0766.

**Preparation of 1,4-bis-(2-ethenyl-(1-((6-iodohexoxy)methyl)ferrocen-1-yl))-2,3,5,6-tetrafluorobenzene (6b)**

50 mg of compound **5b** (1.0 eq, 0.052 mmol), 85 mg of sodium iodide (10 eq, 0.520 mmol), and 5 mL of dry acetone were refluxed in a 10 mL round bottom flask, equipped with a stir bar and condenser, for 18 hours. Dilution of the reaction mixture with DCM and filtration through a silica plug afforded 55 mg of compound **6b** in quantitative yield. 1H NMR (600 MHz, $CD_2Cl_2$) $\Delta$ = 7.26 (d, J=16.5, 2H), 6.66 (d, J=16.5, 2H), 4.54  4.48 (m, 4H), 4.37 (t, J=1.8, 4H), 4.21 (t, J=1.9, 4H), 4.18 (s, 4H), 4.16 (t, J=1.9, 4H), 3.38 (t, J=6.6, 4H), 3.19 (t, J=7.1, 4H), 1.80 (p, J=7.1, 4H), 1.52 (p, J=6.8, 4H), 1.41  1.29 (m, 8H). 13C NMR (600 MHz, CDCl3) $\Delta$ = 145.26-143.42 (dm, J = 250), 135.87-135.82 (t, J=3.52), 114.40 (m), 111.09, 84.62, 82.80, 70.70, 70.44, 69.87, 69.83, 68.62, 67.76, 33.44, 30.25, 29.46, 25.11, 7.12. HRMS m/z (ESI) calcd for C44H48F4Fe2O2I2 [M]+ 1048.0426, found: 1048.0430.

**Preparation of 1,4-bis-(2-ethenyl-(1-((6-trimethylammoniumhexoxy)methyl)ferrocen-1-yl))benzene (DVFBO)**

63 mg of compound **6a** (1.0 eq, 0.064 mmol) was dissolved in 5 mL of dry, inhibitor

free THF and placed under a blanket of argon. 0.4 mL of a trimethylamine solution in methanol (20 eq, 1.20 mmol, 3.2M) was added and the solution was left to stir at room temperature for 24 hours in the dark. The resulting red heterogeneous solution was diluted with methanol to afford a homogeneous solution, another 0.4 mL portion of trimethylamine solution was added and the left to stir for another 24 hours. The excess trimethylamine and THF was removed via reduced pressure distillation to give a red oil. The oil was sonicated in the presence of hexane, centrifuged for 10 min, and the solvent decanted off. This process was repeated with a 1:1 (v/v) mixture of acetone:hexane, followed by inhibitor free diethyl ether to give 50 mg of a red solid in 70% yield. 1H NMR (600 MHz, $CD_3OD$) $\Delta$ = 7.46 (s, 4H), 6.92 (d, J=16.2, 2H), 6.76 (d, J=16.2, 2H), 4.54 4.47 (m, 4H), 4.32 4.26 (m, 4H), 4.24 4.17 (m, 8H), 4.16 4.11 (m, 4H), 3.36 (t, J=6.6, 4H), 3.27 3.21 (m, 4H), 3.05 (s, 18H), 1.72 1.62 (m, 4H), 1.47 (m, 4H), 1.29 (m8H). 13C NMR (600 MHz, $CD_3OD$) $\Delta$ = 136.52, 125.90, 125.84, 125.81, 83.87, 83.69, 70.36, 69.51, 69.33, 69.18, 68.76, 67.07, 66.42, 52.30 (t, J= 3.7), 28.79, 25.57, 25.28, 22.44. HRMS m/z (ESI) calcd for C50H70Fe2N2O2I [M-I]+ 967.3228, found: 967.3276

**Preparation of 1,4-bis-(2-ethenyl-(1-((6-trimethylammoniumhexoxy)methyl)ferrocen-1-yl)) ))- 2,3,5,6-tetrafluorobenzene diiodide ($F_4$-DVFBO)**

63 mg of compound **6b** (1.0 eq, 0.064 mmol) was dissolved in 5 mL of dry, inhibitor free THF and placed under a blanket of argon. 0.4 mL of a trimethylamine solution in methanol (20 eq, 1.20 mmol, 3.2M) was added and the solution was left to stir at room temperature for 24 hours in the dark. The resulting red heterogeneous solution was diluted with methanol to afford a homogeneous solution, another 0.4 mL portion of trimethylamine solution was added and the left to stir for another 24 hours. The excess trimethylamine and THF was removed via reduced pressure distillation to give a red oil. The oil was sonicated in the presence of hexane, centrifuged for 10 min, and the solvent decanted off. This process was repeated with a 1:1 (v/v) mixture of acetone:hexane,

followed by inhibitor free diethyl ether to give 49 mg of a red solid in 70% yield. 1H NMR (600 MHz, $CD_3OD$:D2O) $\Delta$ = 7.24 (d, J=16.5, 2H), 6.66 (d, J=16.4, 2H), 4.56 (t, J=2.0, 4H), 4.40 (t, J=2.0, 4H), 4.31  4.19 (m, 8H), 4.19  4.16 (m, 4H), 3.41 (t, J=6.5, 4H), 3.33  3.29 (m, 4H), 3.10 (s, 18H), 1.74 (m, 4H), 1.54 (m, 4H), 1.43  1.31 (m, 8H). 1H NMR (600 MHz, $CD_3OD$) $\Delta$ = 144.24 (dm, J= 247), 136.42, 114.37, 110.13, 84.09, 82.52, 70.56, 70.40, 69.57, 69.48, 68.51, 67.62, 66.40, 52.26 (t, J=3.9), 28.90, 25.60, 25.32, 22.43. HRMS m/z (ESI) calcd for 3276 C50H66F4Fe2N2O2I [M-I]+ 1039.2852, found: 1039.2863

**Ultraviolet-Visible Absorbance Spectroscopy** Solutions were illuminated at 1 nm wavelength intervals at a scan rate of 20 nm/s (Beckman Coulter DU 800 Spectrophotometer) in a quartz cuvette with 1 cm path length.

**Differential Pulse Voltammetry** DPV traces were collected using a glass carbon electrode, silver wire reference electrode and platinum counter electrode. The working electrode was cleaned and polished before each scan with successive rubbing with a paste of 0.3 $\mu$M Alumina particles in water on a polishing cloth, a 0.05 $\mu$M Alumina paste on a polishing cloth, washing with water then acetone and allowed to air dry. The parameters for DPV scans were as follows: The scan window (low E to High E) was chosen as needed and the following parameters were kept invariant, Incr E (V) = 0.002, Amplitude (V) = 0.05, Pulse Width (sec) = 0.2, Sample Width (sec) = 0.02, Pulse Period (sec) = 0.4. Chloroform solutions utilized 100 mM tetrabutylammonium hexafluorophosphate and aqueous solutions used 100 mM pH 7.2 phosphate buffer (PB) as the supporting electrolyte.

**Zeta Potential Measurents** Zeta potentials were measured using a Malvern Zetasizer Nano ZS equipped with a He-Ne 4mW 633 nm laser.

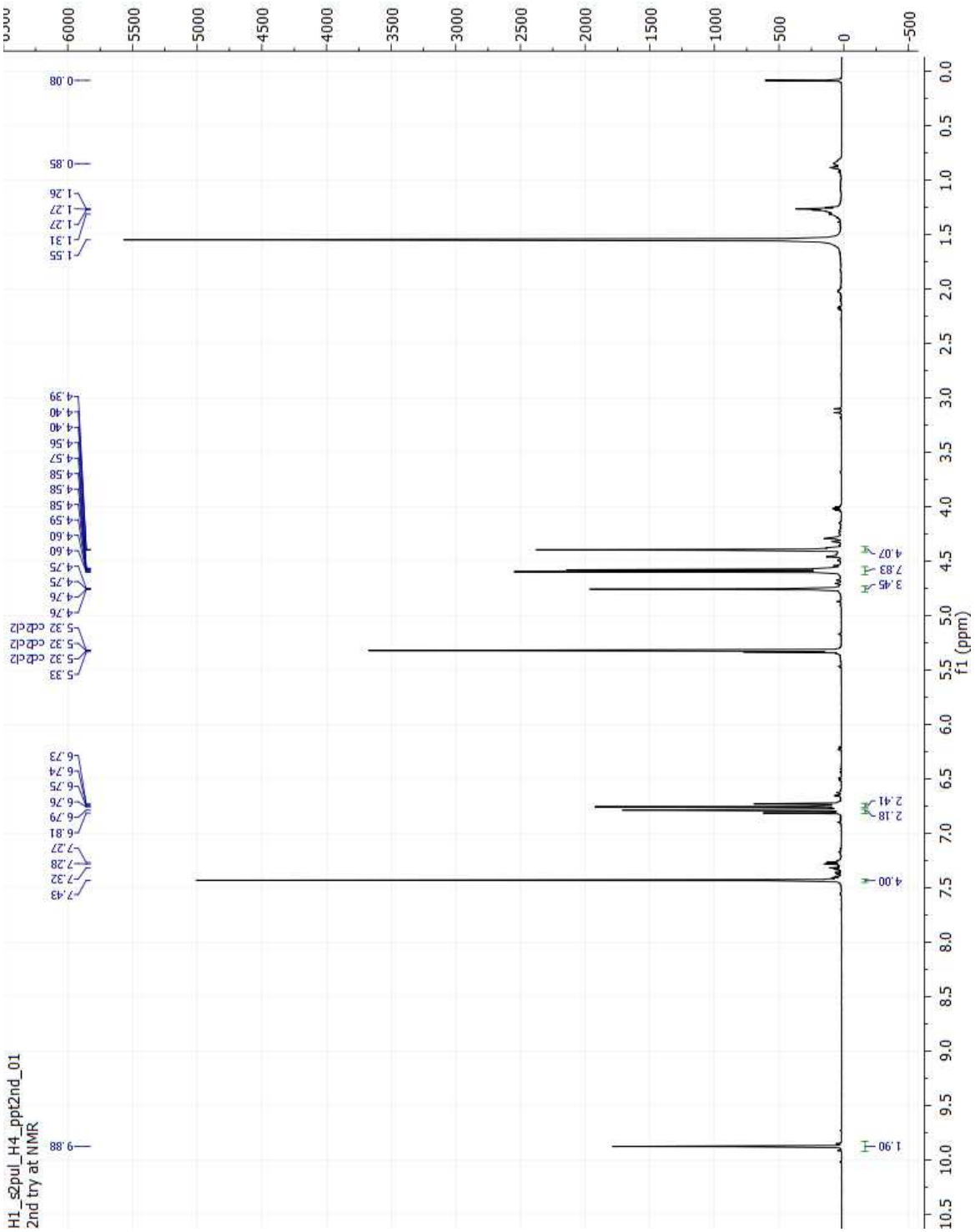


Figure 3.9: $^{1}$H NMR of compound **3a**.

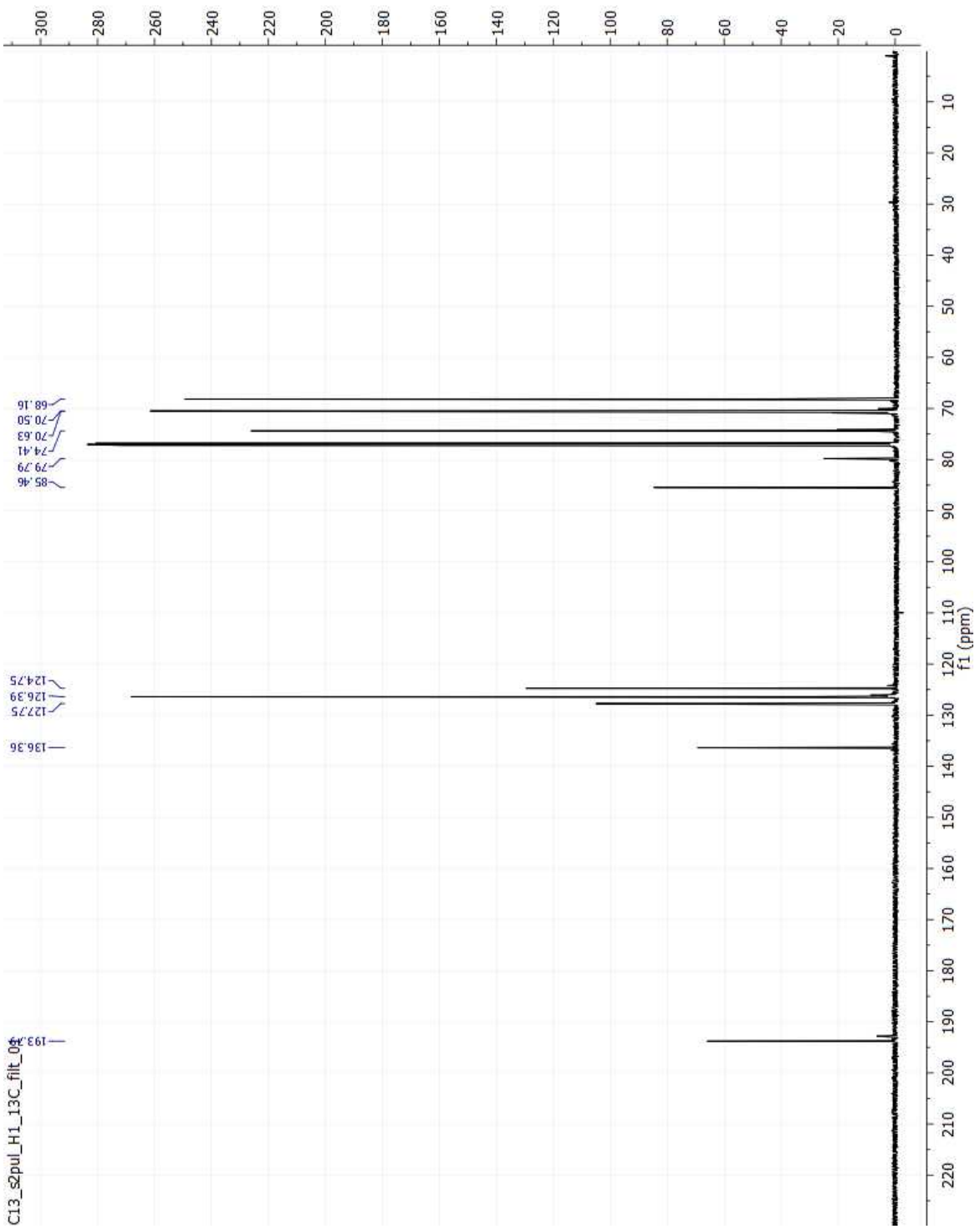


Figure 3.10: $^{13}$C NMR of compound **3a**.

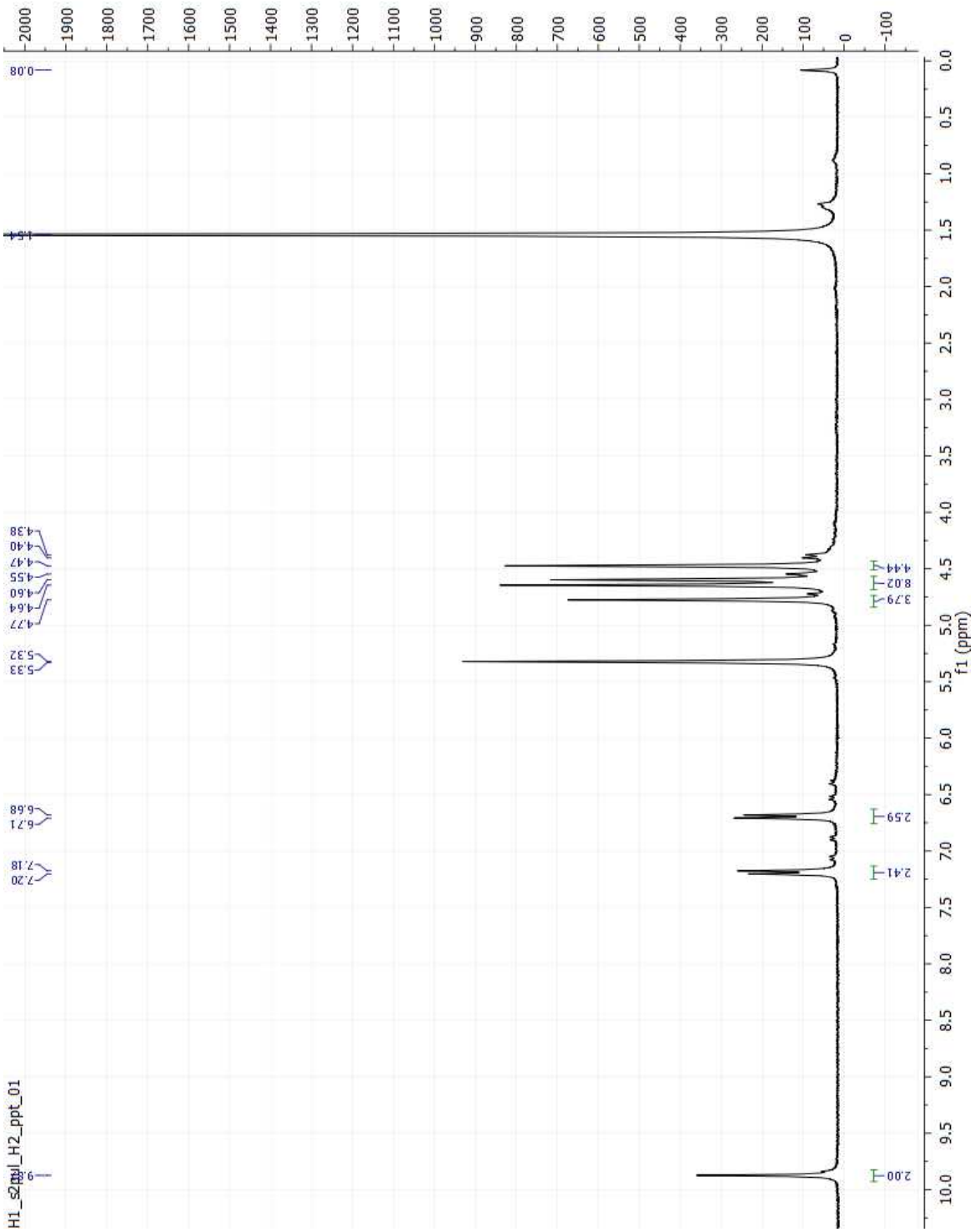


Figure 3.11: $^{1}$H NMR of compound **3b**.

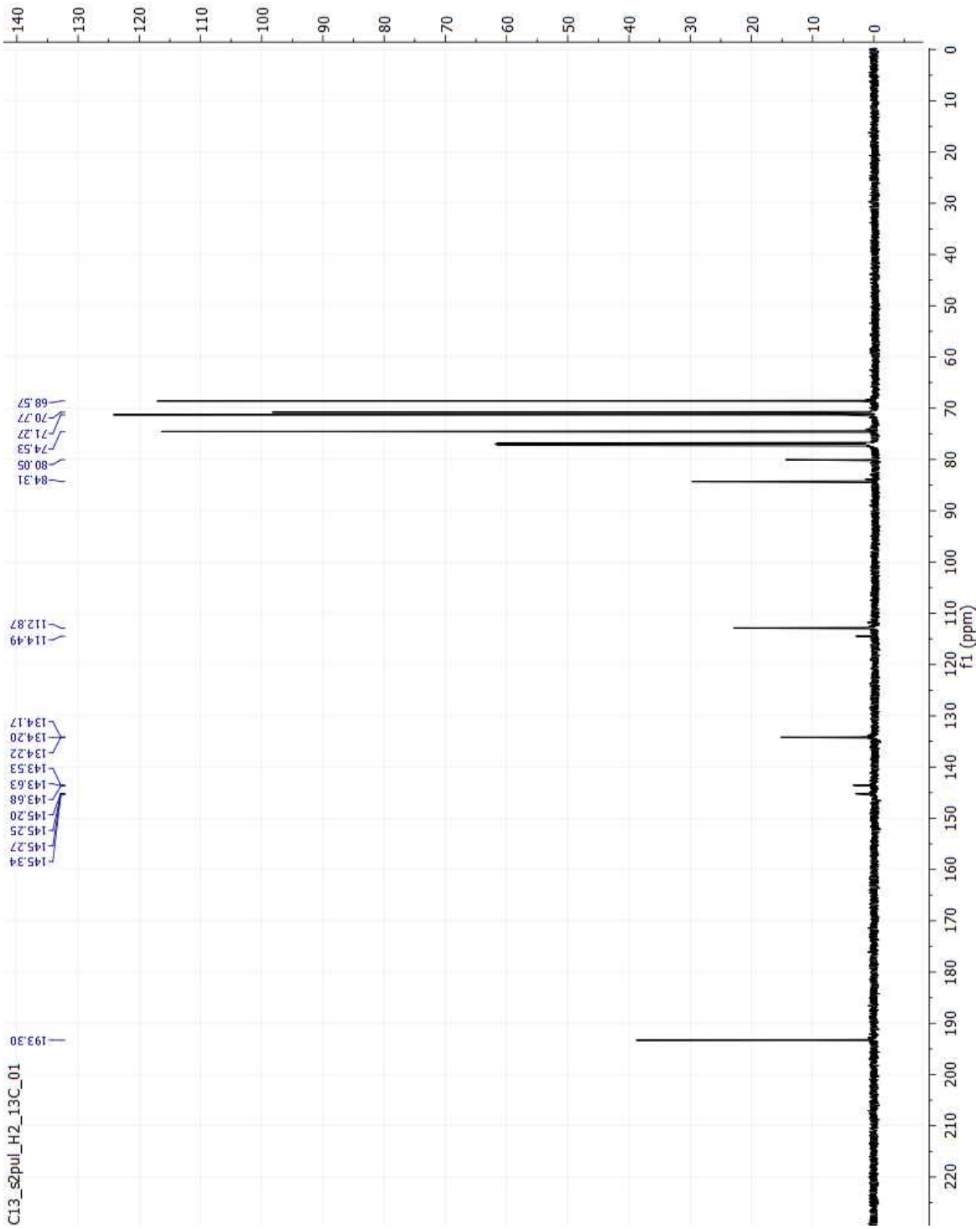


Figure 3.12: $^{13}$C NMR of compound **3b**.

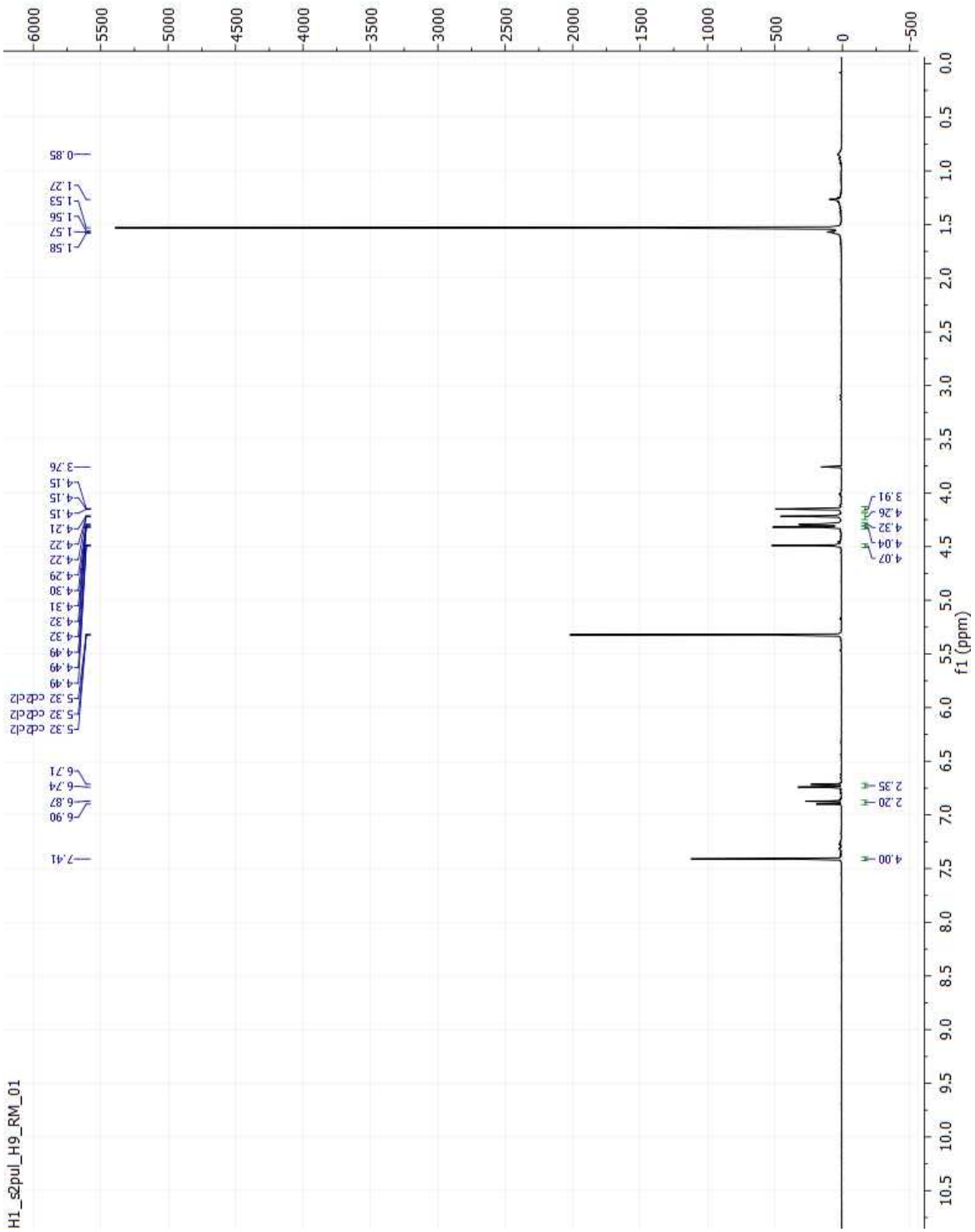


Figure 3.13: $^{1}$H NMR of compound **4a**.

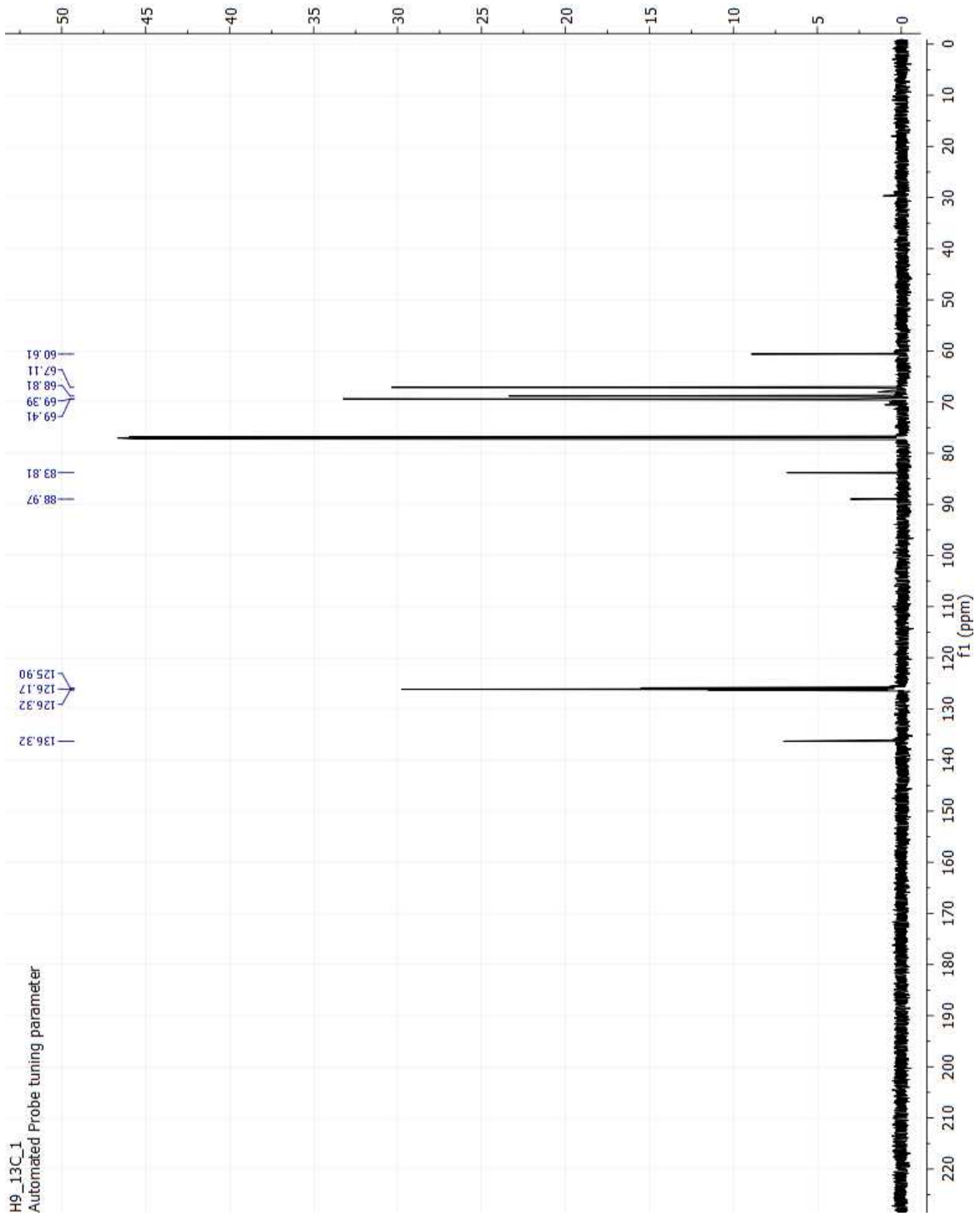


Figure 3.14: $^{13}$C NMR of compound **4a**.

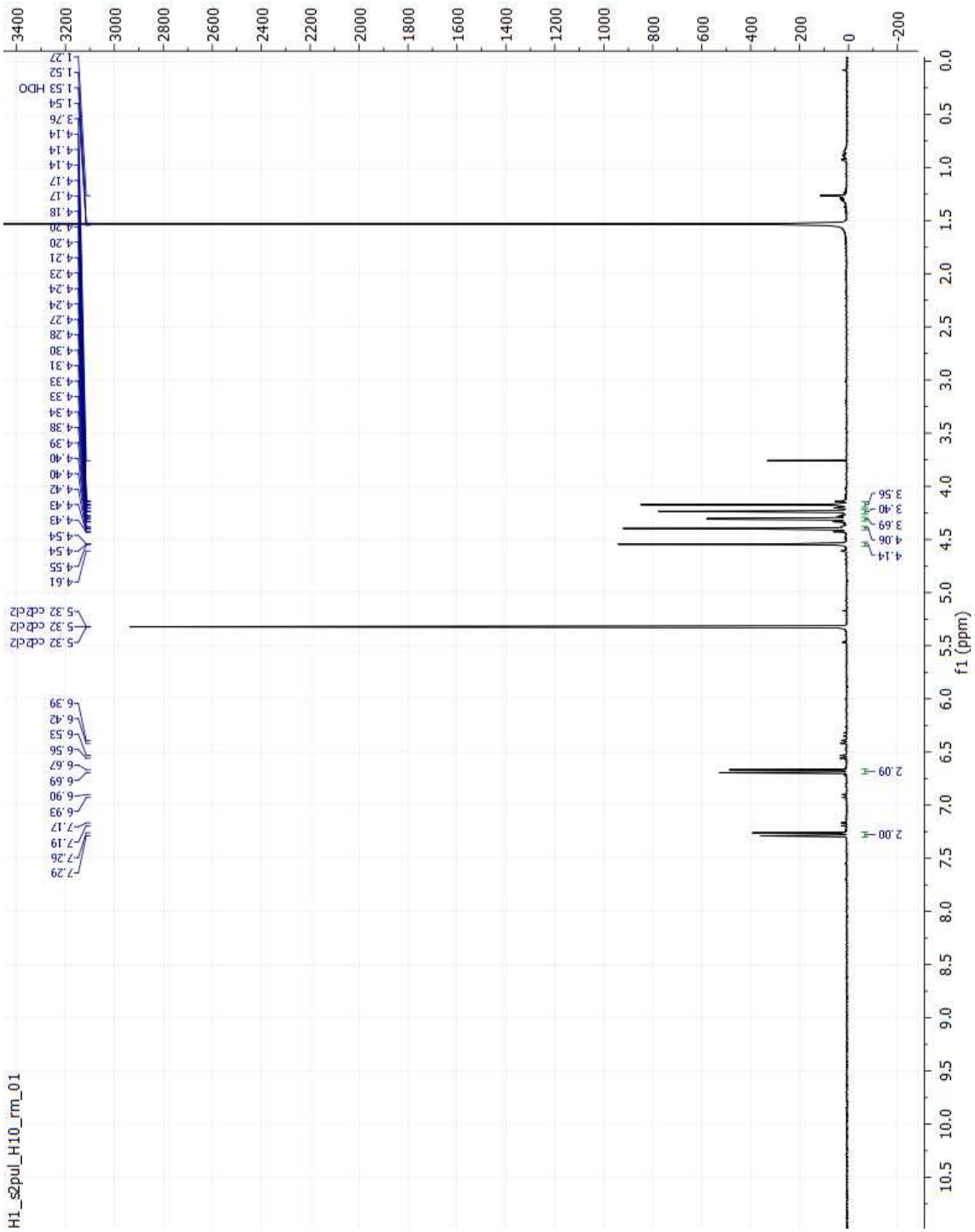


Figure 3.15: $^{1}$H NMR of compound **4b**.

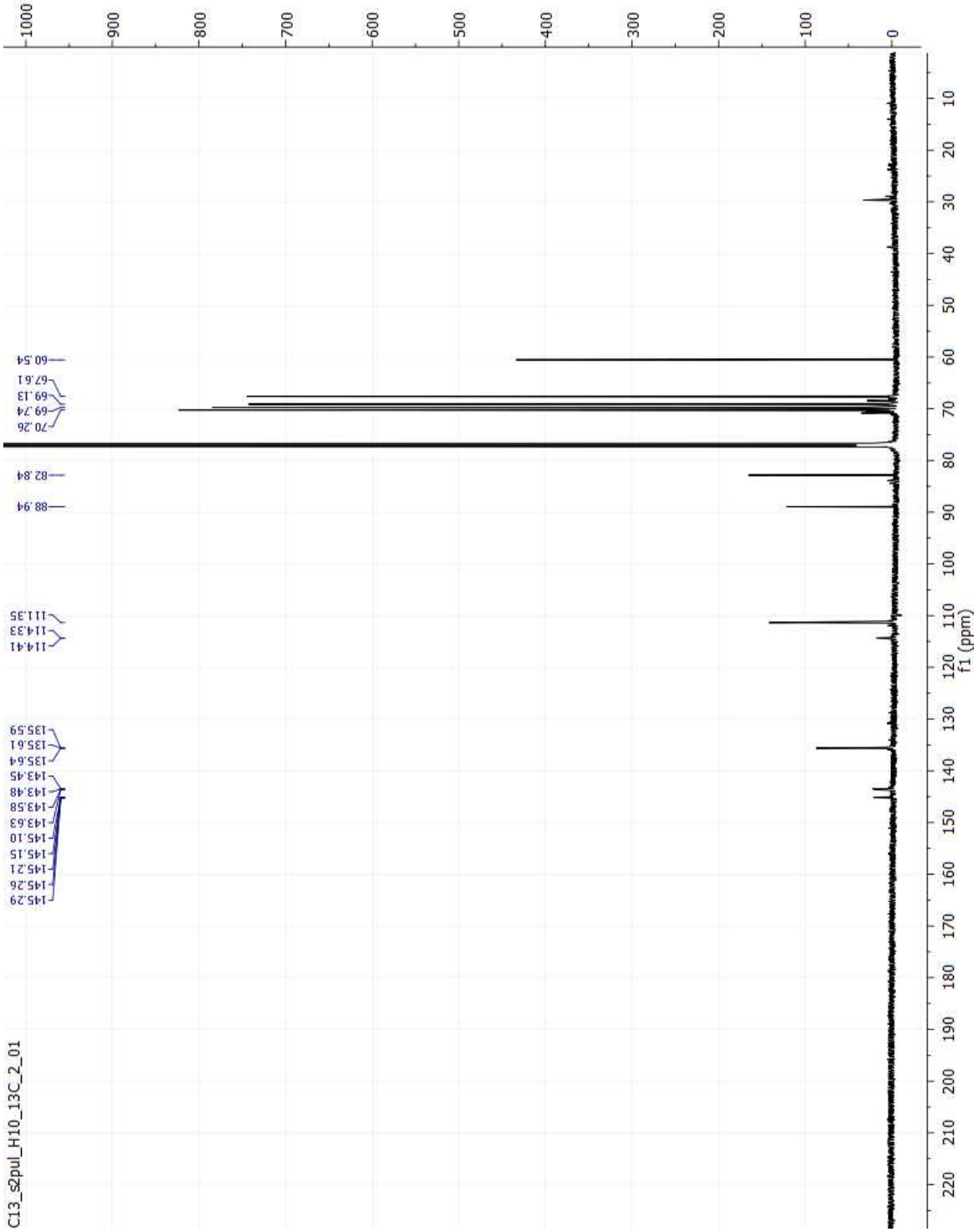


Figure 3.16: $^{13}$C NMR of compound **4b**.

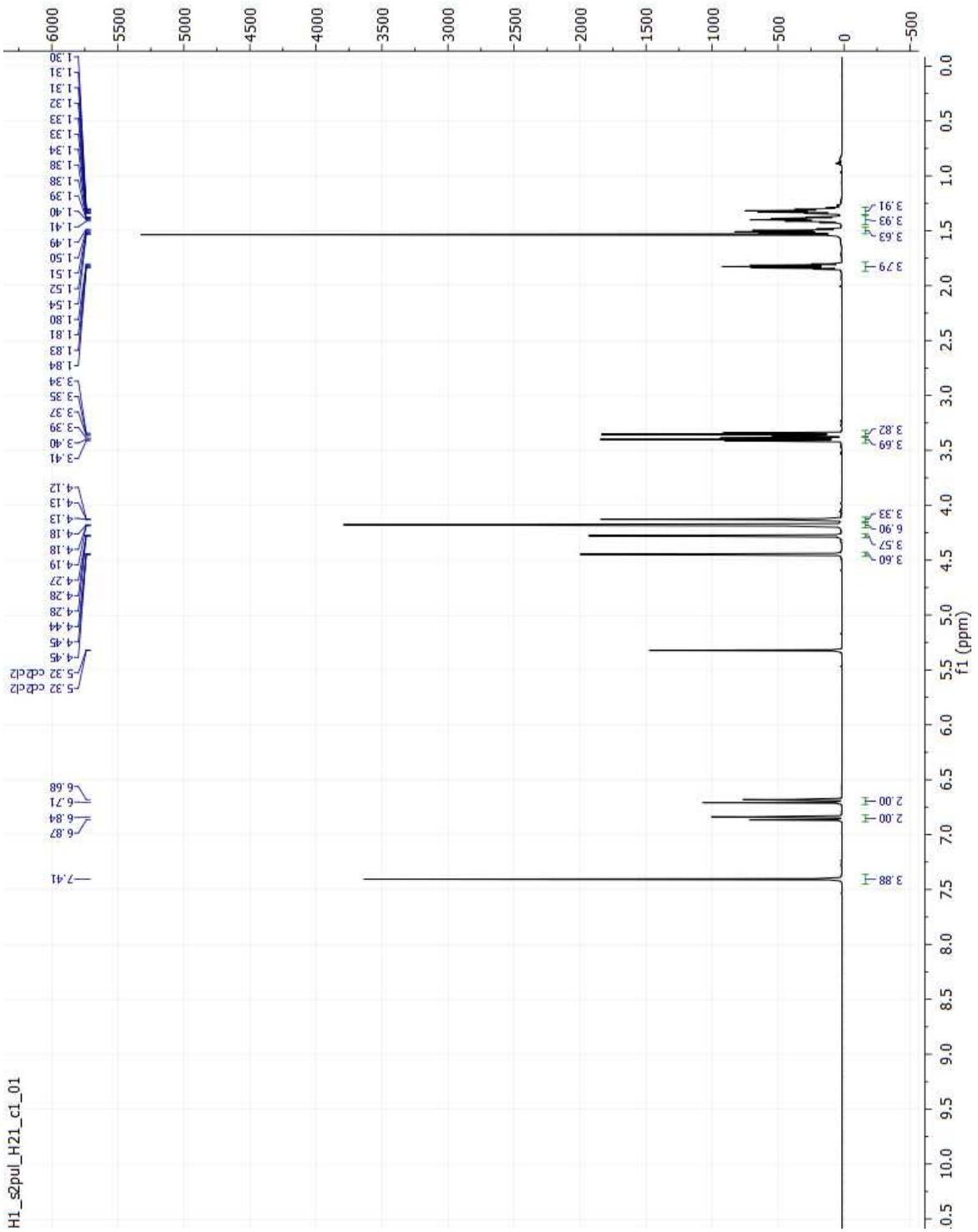


Figure 3.17: $^{1}$H NMR of compound **5a**.

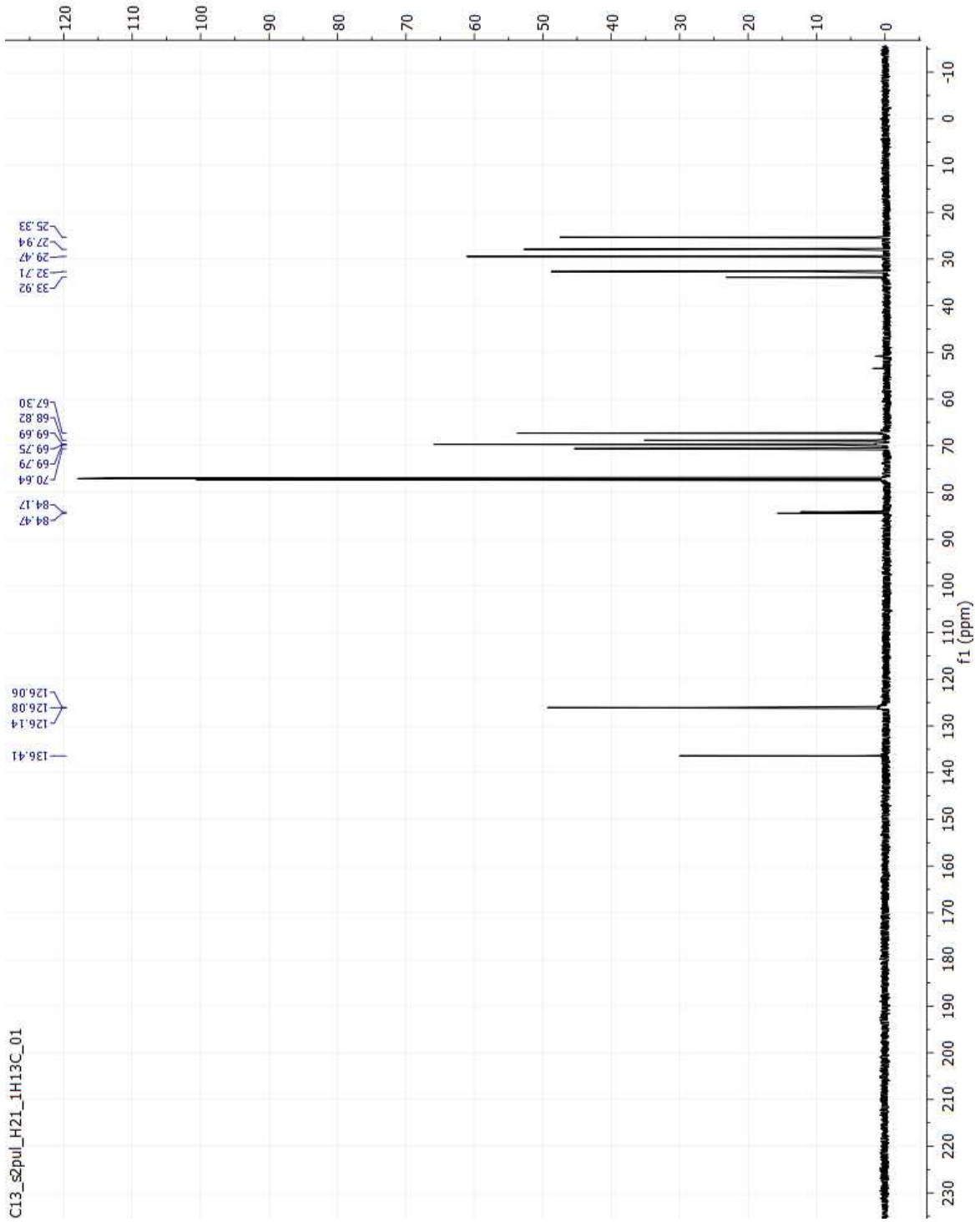


Figure 3.18: $^{13}$C NMR of compound **5a**.

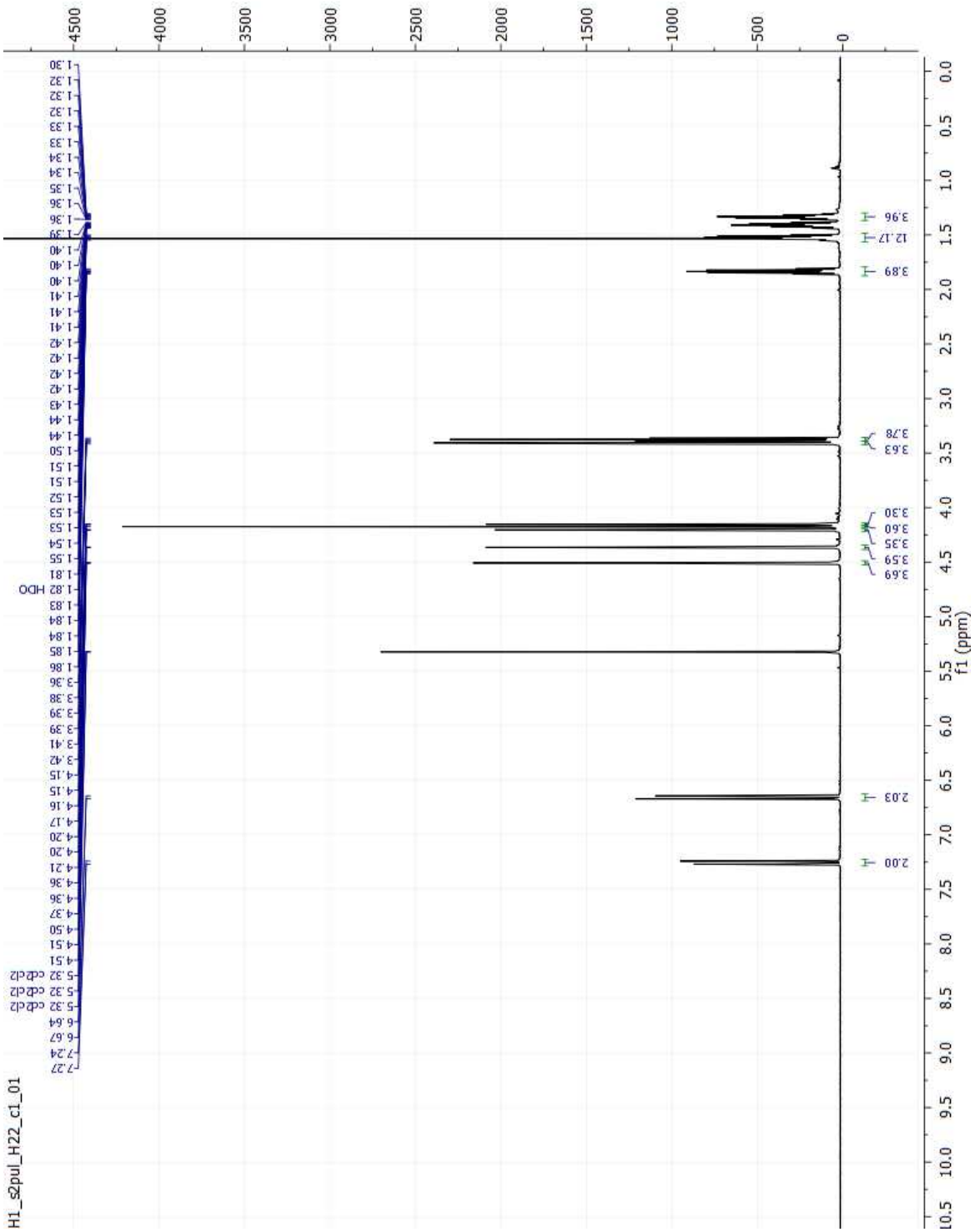


Figure 3.19: $^{1}$H NMR of compound **5b**.

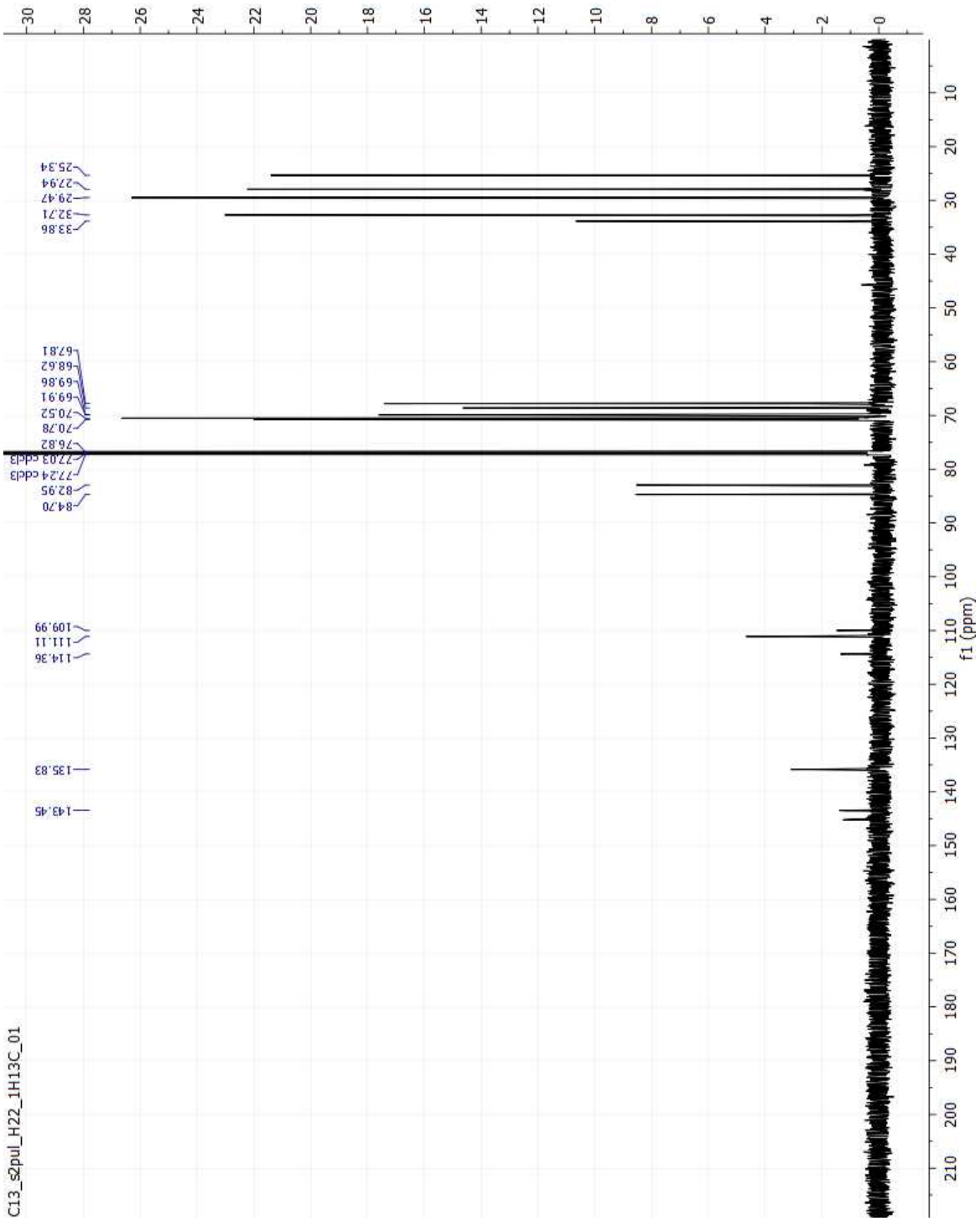


Figure 3.20: $^{13}$C NMR of compound **5b**.

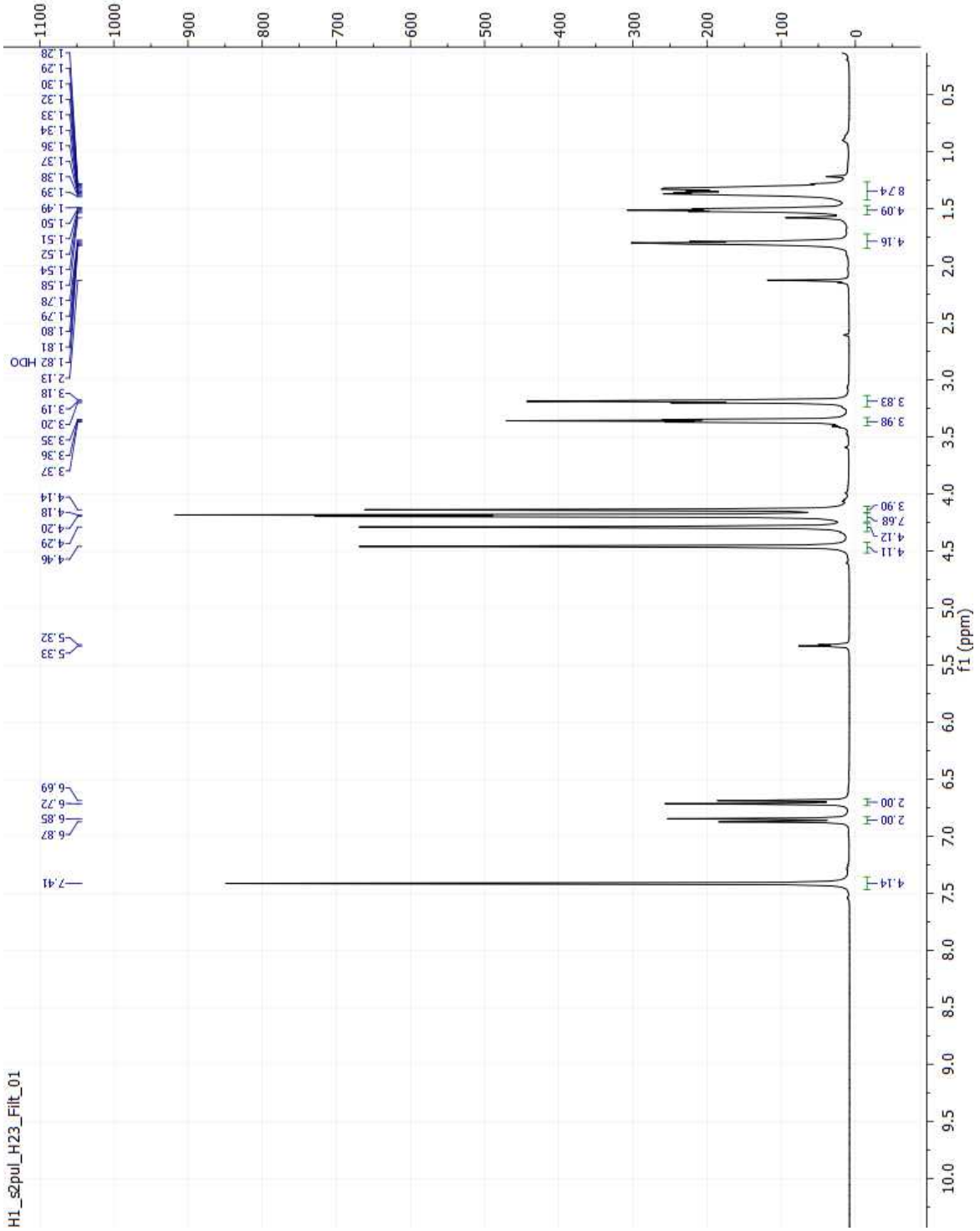


Figure 3.21: $^{1}$H NMR of compound **6a**.

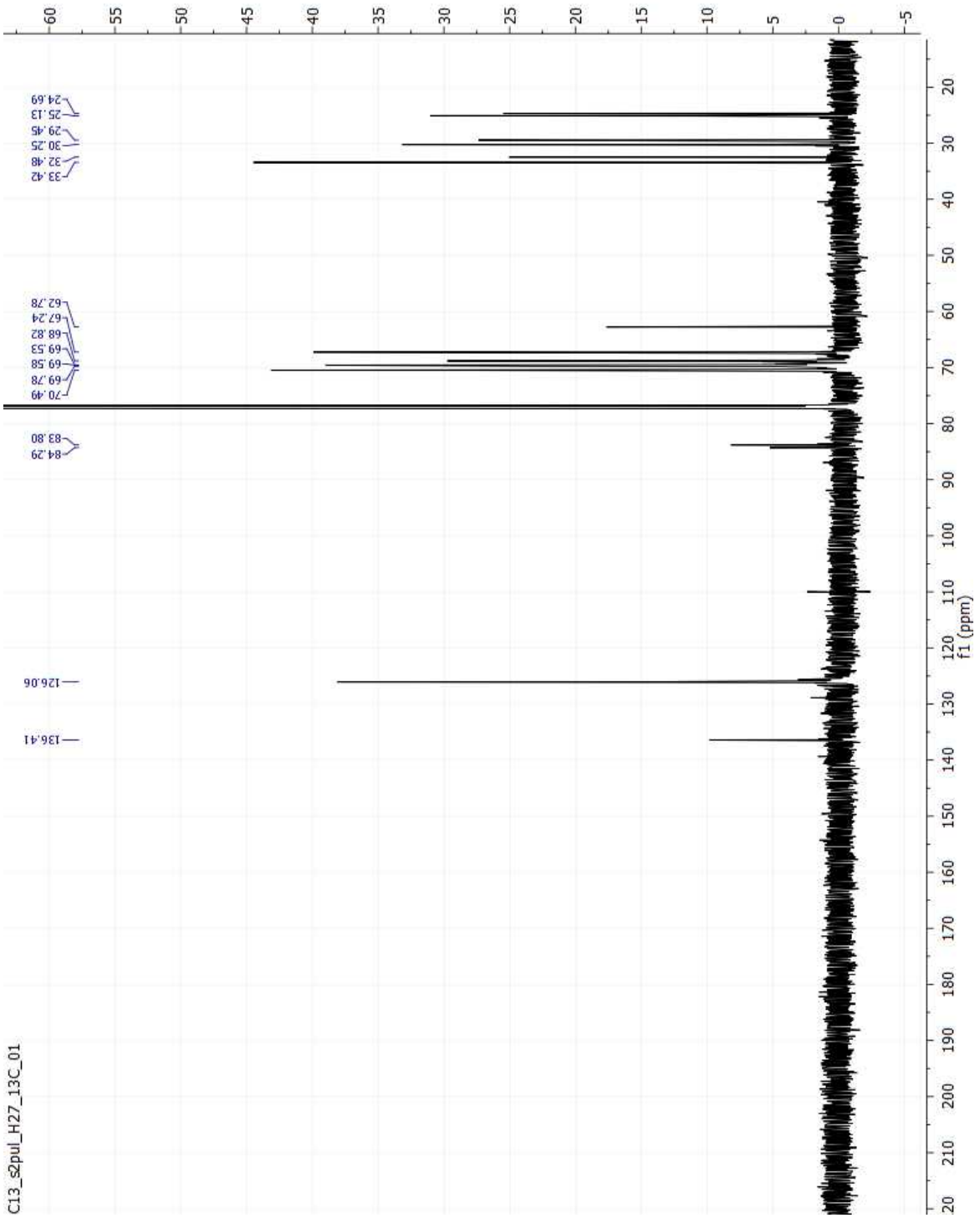


Figure 3.22: $^{13}$C NMR of compound **6a**.

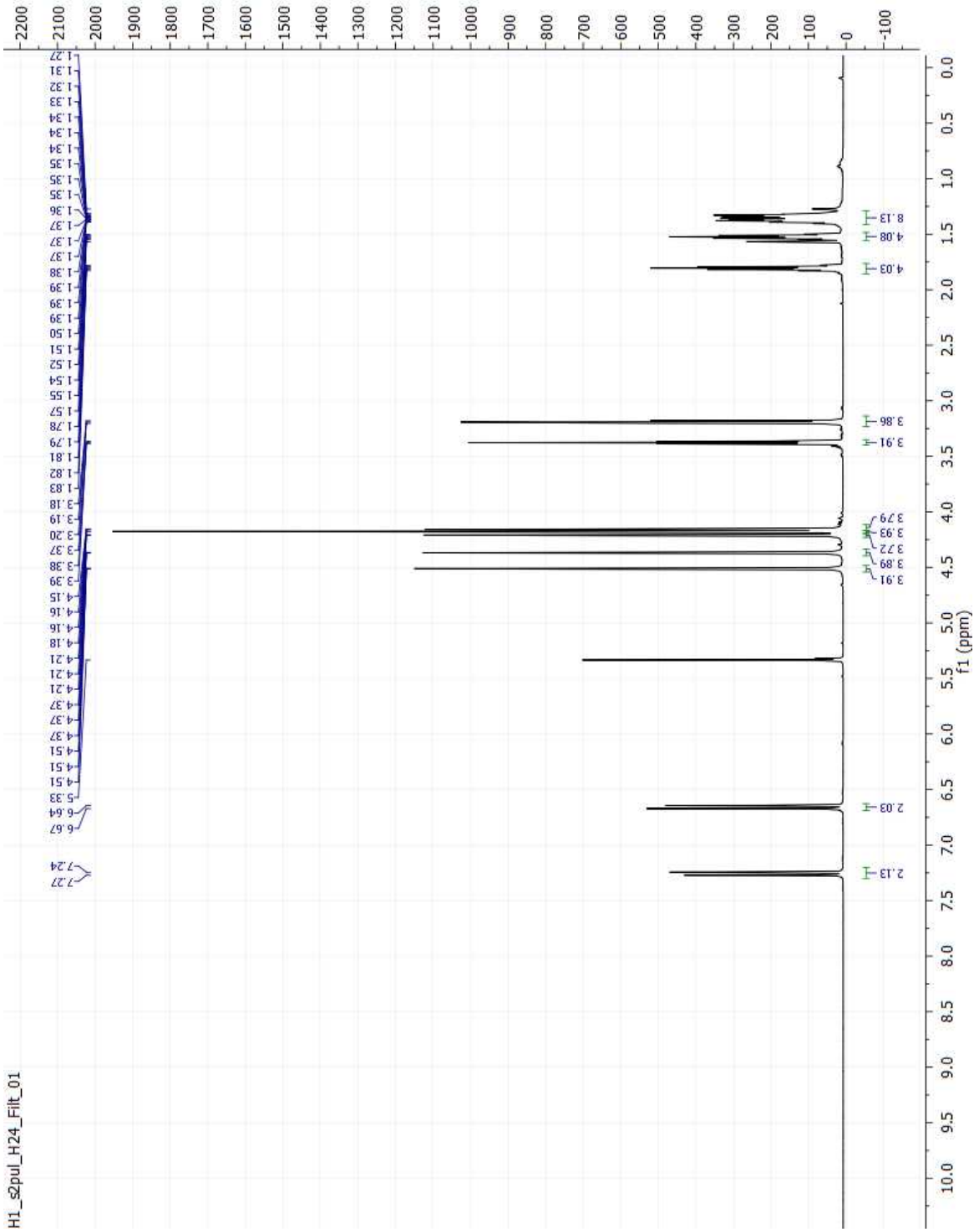


Figure 3.23: $^{1}$H NMR of compound **6b**.

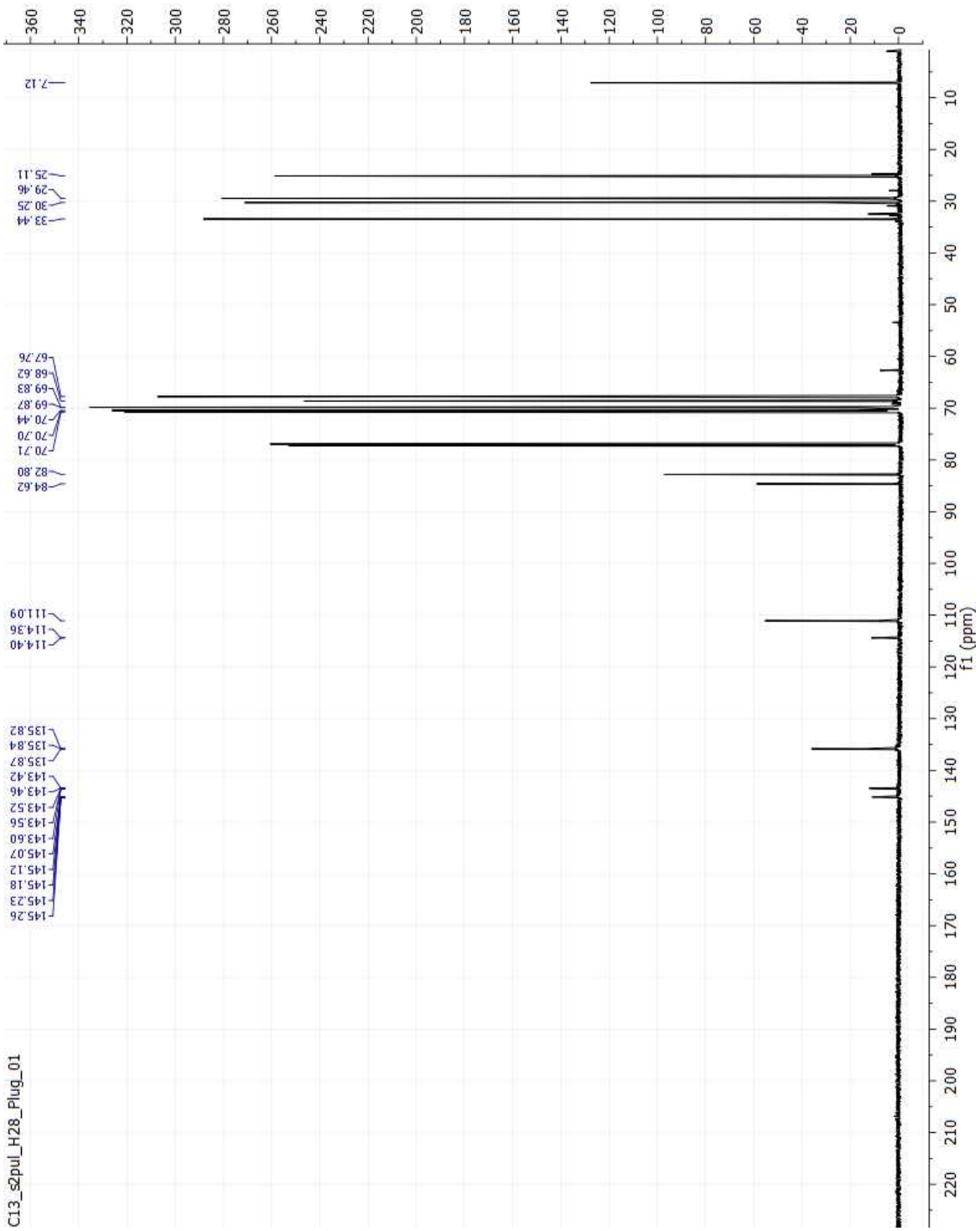


Figure 3.24: $^{13}$C NMR of compound **6b**.

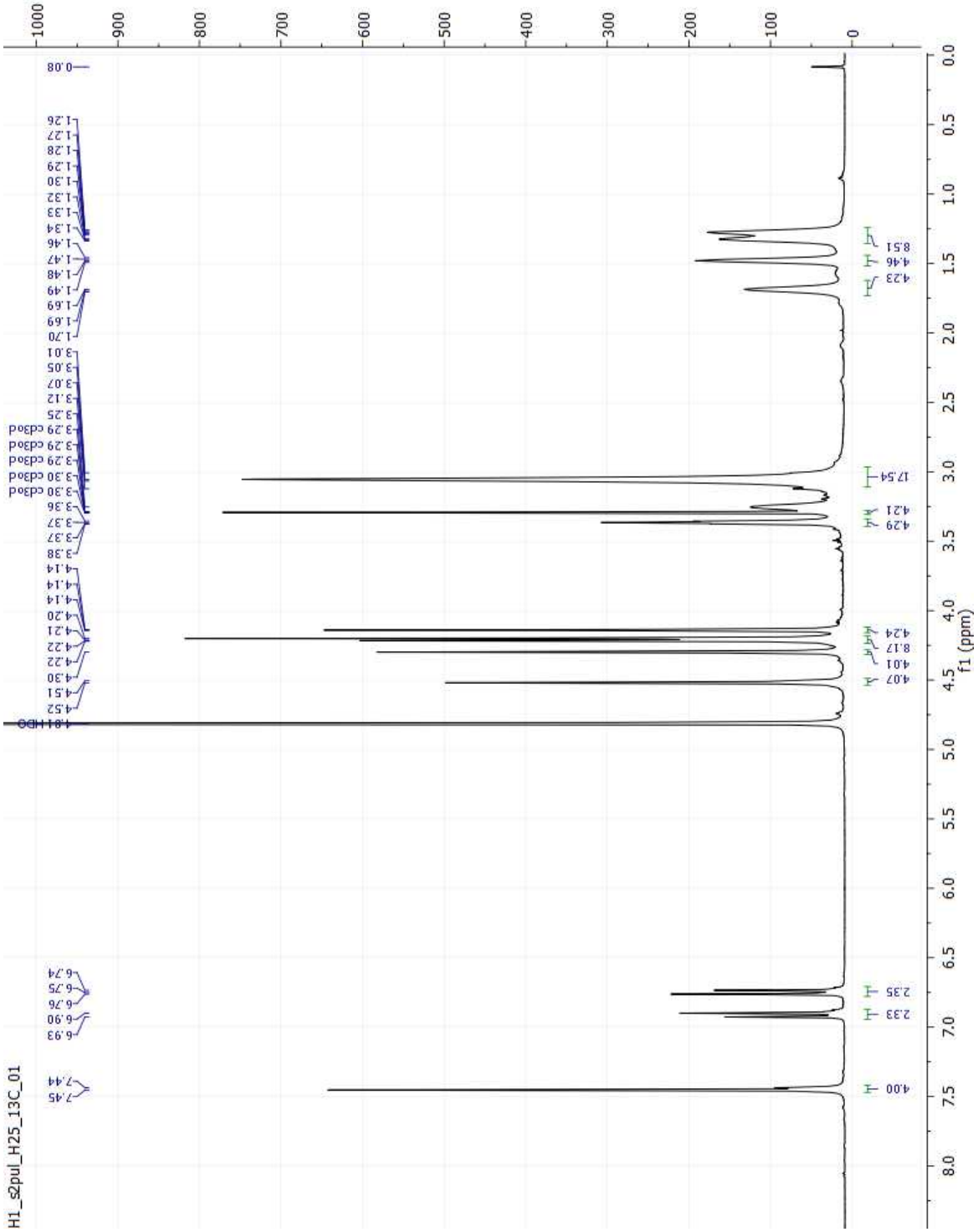


Figure 3.25: $^{1}$H NMR of compound **DVFBO**.

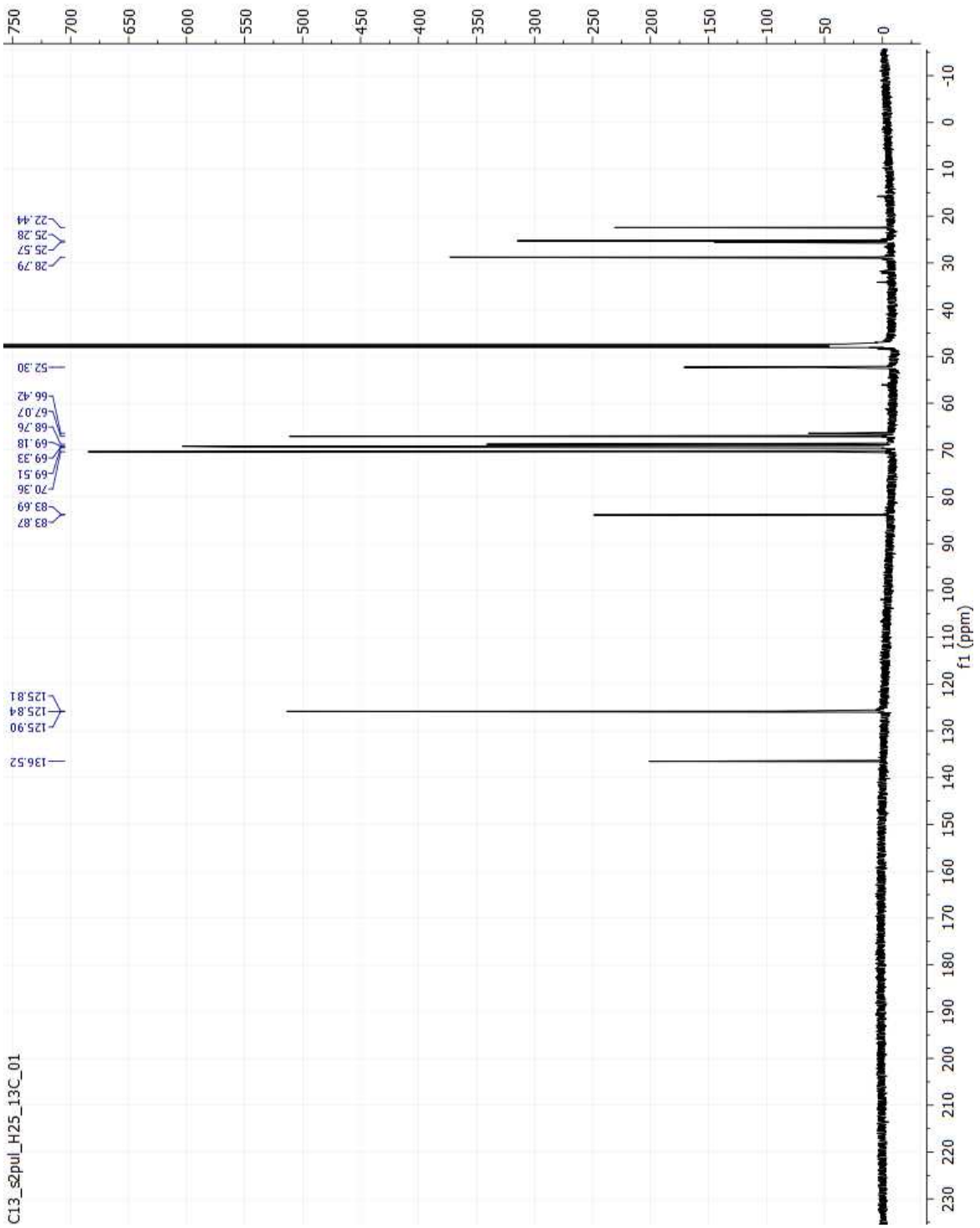


Figure 3.26: $^{13}$C NMR of compound **DVFBO**.

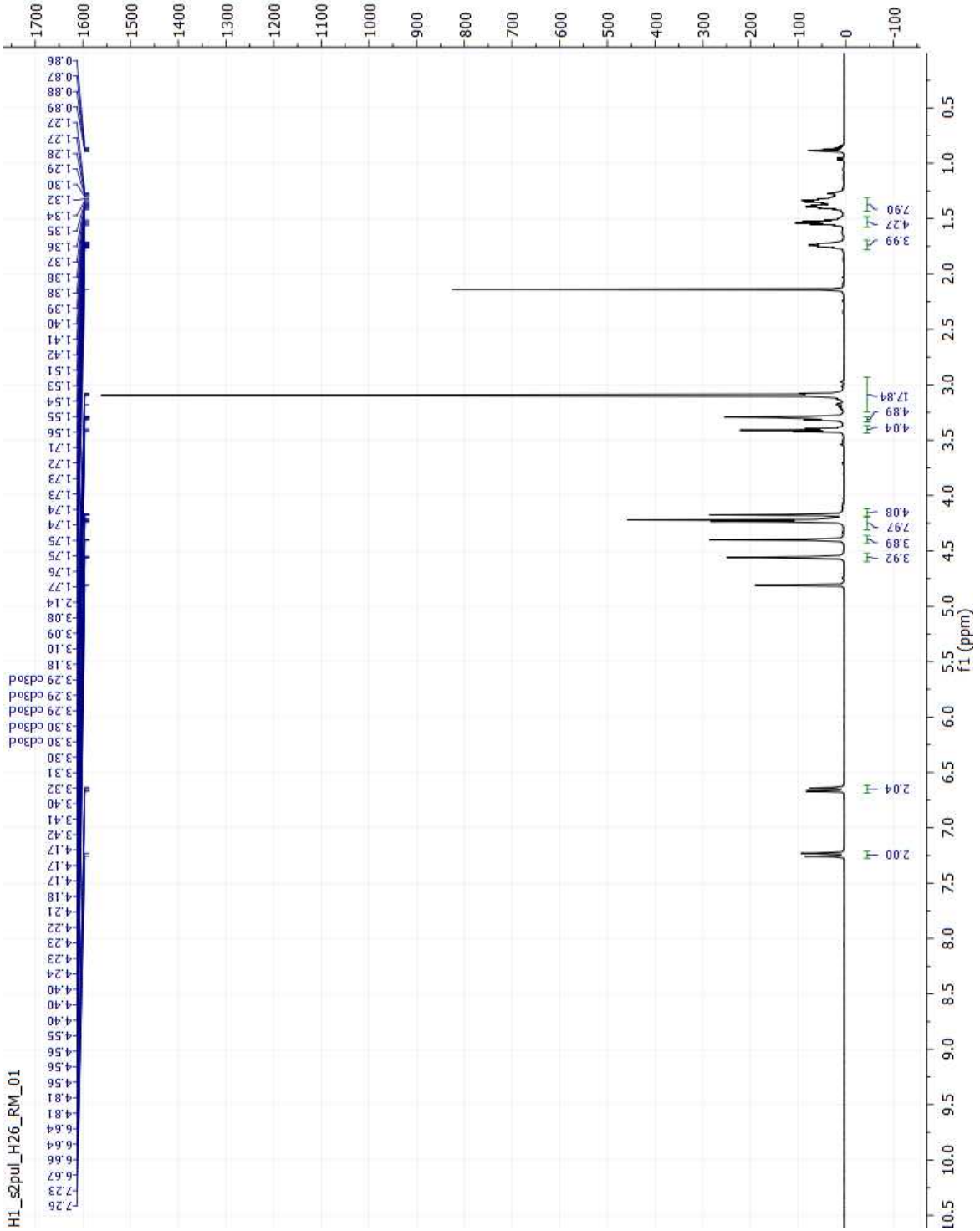


Figure 3.27: $^{1}$H NMR of compound **$F_4$-DVFBO**.

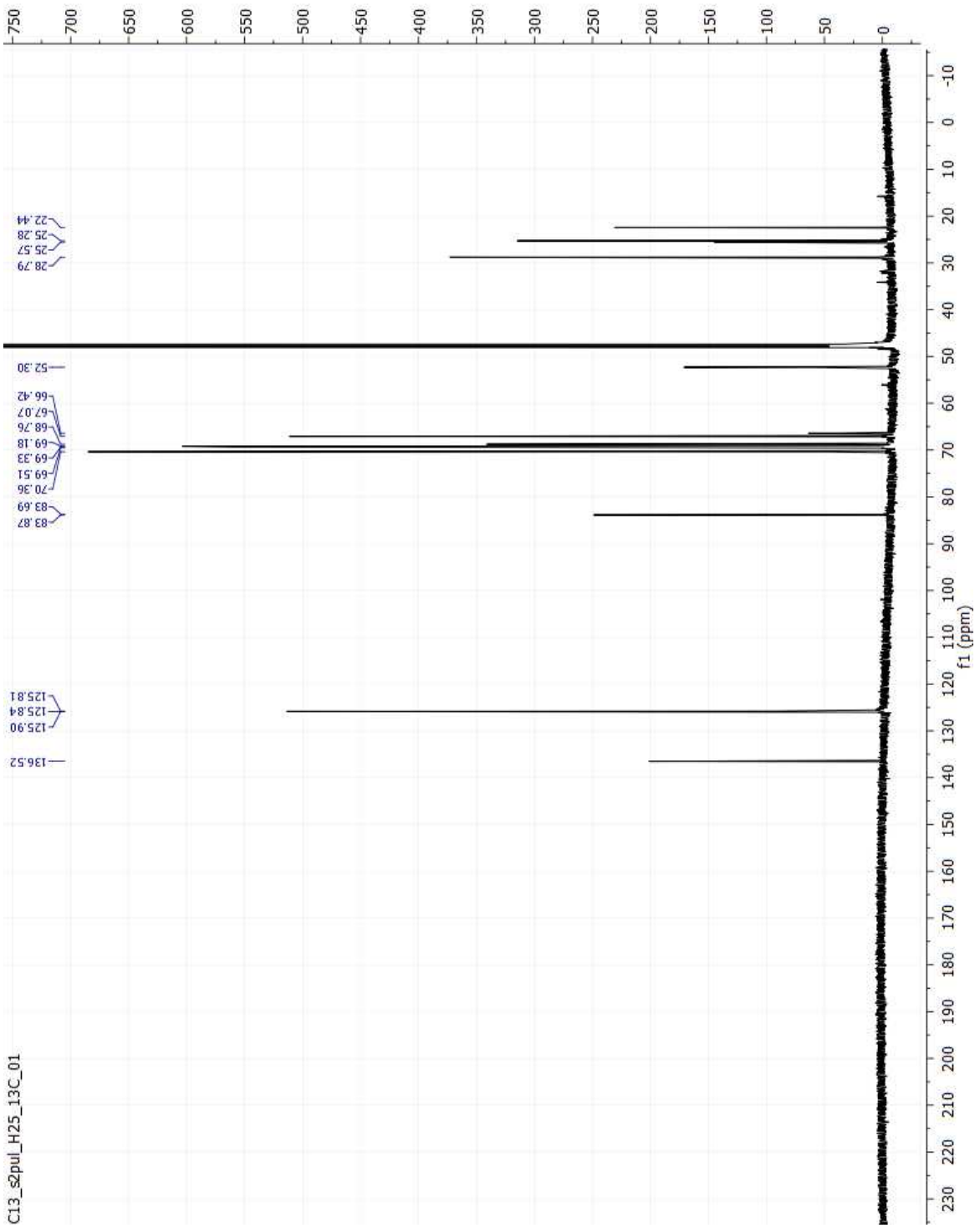


Figure 3.28: $^{13}$C NMR of compound **$F_4$-DVFBO**.

# Chapter 4

# Interactions of COEs With Model Lipid Systems

*Where do the COEs really go??*

## 4.1 Preface

For the majority of my Ph.D. I was focused on developing new redox active COEs. As the previous chapters have indicated, the motivation for imparting redox character in COEs was fueled by experiments that showed our previous COEs changed the physical properties of membranes, likely through a convolution of multiple effects, but that they were not acting as molecular wires. Towards the end of my Ph.D., we started to think of how we could determine what these previous COEs were really doing. As a chemist,

sometimes the complexity of biology can be a bit overwhelming and this motivated me to try to find some sort of "model system" to study the interactions of COEs with lipid membranes and to compare these results with that of living cell studies. The following discussion pertains to this effort and aims to gain insight into the governing mechanisms that surround molecules that have physical properties similar to COEs, *e.g.* bolaphiles containing semiconducting cores and appended ionic groups of varying identities. The hope is that the conclusions for this type of study are pertinent to both COEs with and without redox character.

## 4.2 Abstract

Neutral and Anionic liposomes were constructed to investigate the role of electrostatic interactions in conjugated oligoelectrolyte (COE) association with model lipid bilayer systems. Intermolecular electrostatic interactions between COE head groups limit the maximum association in neutral liposome systems. Cationic COEs are electrostatically attracted to anionic liposomes, affording nearly quantitative association, while an anionic COE shows minimal association. In the concentration ranges investigated, COEs associate to a maximum of 1.5 mole % in neutral liposomes and 6 mole% in anionic liposomes. A linear relationship between amount of COE associated and change in liposome zeta potential was observed, with no dependence on molecular length.

## 4.3 Introduction

Conjugated oligoelectrolytes (COEs) are small molecules characterized by an oligomeric conjugated core flanked on both ends by alkyl chains terminated with ionic functionalities. [114, 125, 126] COEs have gained considerable interest for improving performance in

bioelectrochemical systems (e.g. microbial fuel cells), biofuel production, bioremediation, and membrane-based photosynthetic systems, with these benefits attributed to their ability to modify microbial membrane properties. [109, 48, 127, 108, 128, 49, 129, 52, 130] Seminal studies have demonstrated that COEs spontaneously insert and align into membranes due to their amphiphilic nature and affinity for the non-polar environment of the lipid bilayer. The molecular design of COEs was originally inspired by oligophenelynevinylene molecular wires, and have thus been added to lipid bilayers for the specific purpose of improving transmembrane electron transfer.[131] However, increasing evidence is pointing away from this original proposed mechanism of action and towards a conglomeration of membrane property effects that could explain increases in bioelectrochemical performance. It is generally accepted that improved performance in these bioelectrochemical systems relies on the ability of COEs to intercalate in the membrane, and the magnitude of improvement varies with molecular structure and concentration.[127, 51] The concentration and chemical composition of semiconducting repeat units, number of repeat units, and nature of pendant ionic functionalities has been shown to influence important properties such as membrane permeability, surface potential, favorability of membrane interactions and toxicity effects.[125, 51, 118, 110] For example, it has been shown that cationic COEs can reduce the negative surface potentials of gram-negative bacteria and the magnitude of modulation is dependent on the length of the semiconducting core.16 Interestingly, it was found that the amount of COE associated with the cell approached, or exceeded, a 1:1 molar ratio of COE to membrane lipid. The maximum association concentration of COEs decreased with backbone length, where almost all of the 3-repeat unit COEs were able to associate. This result suggests COE-cell associations are not limited to the lipid bilayer, as its integrity would undoubtedly be compromised. Differences between toxicity effects in Gram-negative and Gram-positive bacteria underlie COE-cell envelope interactions of greater complexity than just intercalation in the lipid

membrane. While most membrane-intercalating molecules, such as arylamide oligomers, polycarbonate polymers, and cationic steroids, have similar antimicrobial function according to Gram-type, COEs have been shown to be at least 4 times more toxic to Gram-positive bacteria than to Gram-negative bacteria.[118, 132, 133, 134, 135] While mechanistic studies on cationic phenylene ethynylene oligomers and polymers demonstrate importance of electrostatic interactions for initial bonding of molecules with lipids, lipid composition can also be an important factor in determining sensitivity.[136, 137] Membrane permeability may be a factor in bacterial sensitivity to COEs. The permeability of membranes to cations, small molecules and proteins has been shown to increase with the concentration of incorporated COEs.[138, 139] Additionally, charge permeability has been shown to be dependent on interactions with other membrane additives, such as cholic acid and cholesterol.[59] It has been hypothesized that the interaction of cationic COEs with lipopolysaccharides (LPS) in the outer leaflet of the lipid bilayer could play an important role in COE association and permeability effects, as LPS is a polyanion and is the first physical barrier a COE would encounter before intercalation in the lipid bilayer. With the above information in mind, we sought to gain insight into the mechanism of COE-membrane interactions by using a model liposome system, containing only lipids, in order to eliminate association effects contributed from LPS, proteins (both membrane bound and cytosolic/extracellular), and other biological components. Two unilamellar liposome model systems were utilized; 1,2-dimyristoyl-sn-glycero-3-phosphocholine (DMPC) liposomes and Escherichia coli total lipid extract, representative of liposomes with near zero surface charge dominated by hydrophobic interactions and net negative liposomes composed of lipids naturally found in E. coli, respectively. By using model liposomes, we remove the complexity of alternative interactions between COEs and other membrane components and can thus probe the role of electrostatic forces in COE-lipid interactions.

## 4.4 Results and Discussion

The electrostatic properties of liposomes comprised of DMPC or E. coli extract (ECE) lipids are considerably different due to the ionic nature of the substituent lipids from these two populations. DMPC is zwitterionic, while ECE is comprised of neutral and anionic lipids. DMPC liposomes afforded a zeta potential of -3.7 ± 0.5 mV with a diameter of 130 ± 2.5 nm, while liposomes prepared from ECE exhibited a zeta potential of -45.6 ± 1.2 mV with a diameter of 144 ± 1.5 nm. There is a large difference in electrostatic properties of these two lipid systems, although the sizes of the particles are quite similar. Thus, DMPC and ECE liposomes offer two contrasting systems to study the modulation of zeta potential changes upon COE association.

The interaction of COEs with liposomes was studied with COEs that had both a difference in conjugation length and type of alkyl linker. COE1-3, COE1-4, and COE1-5 possess alkyl linkers comprised of aniline groups in the para positions and differ in conjugation length by 3, 4, and 5 rings, respectively. COE2-3, COE2-4, and COE2-5 possess alkoxy linkers in both meta positions and differ in conjugation length by 3, 4, and 5 rings, respectively. COE2-4-COOK was used to provide an anionic COE with dimensions similar to COE2-4. The chemical structures of all seven molecules can be found in 4.1. The following discussion focuses on the difference between these two COE classes, three COE lengths, and difference between cationic and anionic pedant groups in DMPC and ECE liposomes.

To investigate whether COEs associate with model lipid liposomes in a similar manner to living cells, we stained liposomes with varying concentrations of COE to measure COE uptake and resulting zeta potentials of the liposomes. We found the interaction of COEs with DMPC liposomes, shown in 4.2, displays a trend qualitatively similar to those found in whole cell studies of E. coli.[110] As the staining concentration of COEs

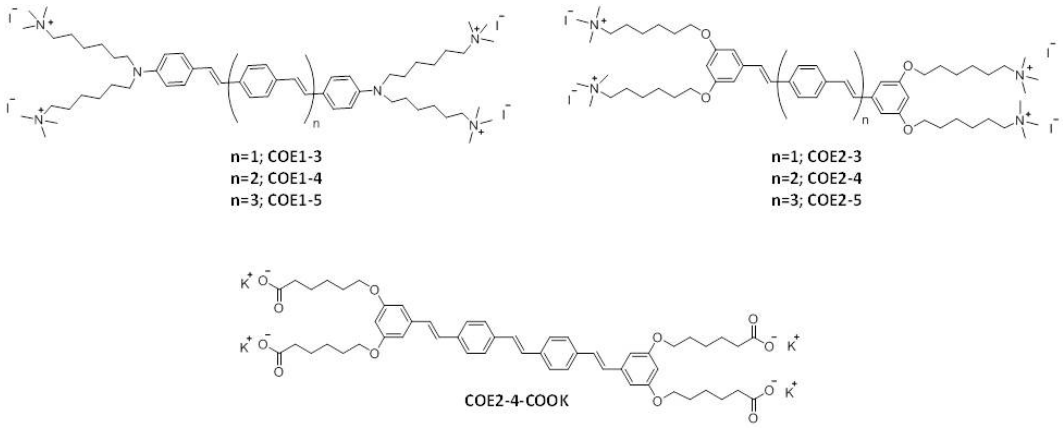


Figure 4.1: Chemical Structures of COEs.

with DMPC liposomes is increased, the amount of COE associated with the liposomes increases until a critical point is reached. At this critical concentration, saturation in COE association was observed for all six molecules between 20-30 $\mu$M, indicating a max loading of COEs into a liposome of DMPC. There is a relationship between COE length and max loading, such that COE1-5 is able to associate into DMPC liposomes less than COE1-3 and COE1-4. Interestingly, COE2-4 is able to associate more than COE2-3 and COE2-5. These trends in COE association with DMPC liposomes suggest a length dependence of intercalation, where COEs of intermediate length are the appropriate size, with respect to lipid bilayer thickness, for intercalation and can thus incorporate to a larger extent than their larger/smaller counterparts. The only outlier in this set of experiments is found in the highest staining concentration of COE1-5, where zero association was found even after multiple attempts. It is known that COE1-3 can aggregate in deionized water above 510 $\mu$M, so it is possible that COE1-5, being much less soluble than COE1-3, could show aggregation at even 50 $\mu$M in PBS.[140] If COE1-5 is aggregated in solution prior to staining with liposomes, there may be no driving force for intercalation, as the non-polar backbone of the COE is already shielded from the bulk solution. Attempts

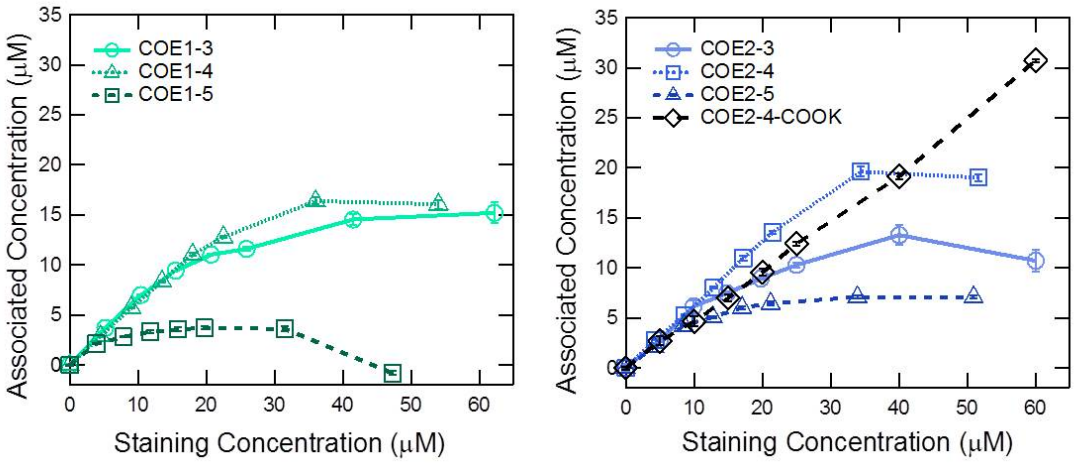


Figure 4.2: Association of COEs in DMPC liposomes as a function of COE staining concentration. Error bars represent one standard deviation from the average of triplicate measurements.

to determine aggregation using DLS and centrifugation of stock solutions showed no evidence for aggregation, but these techniques are unlikely to detect smaller aggregates, especially if they are disordered. The amount of COE2-4-COOK associated into DMPC liposomes was comparable to that of its cationic counterparts, except that a plateau in association was not observed in a similar concentration range, although the slope of association versus supplied COE concentration was similar for all COEs. The cationic choline functionality of the zwitterionic head group is likely to be closest to the water interface and an electrostatic attraction between the carboxylate group of COE2-4-COOK and the trimethylammonium head group of DMPC may exist, offering one possible explanation for the lack of plateau in the case of COE2-4-COOK.

The association of COEs with ECE lipid liposomes was performed in a similar manner to DMPC liposomes to probe the relation of liposome surface charge to the trends observed in COE association. The surface potential of ECE liposomes is considerably more negative than both living cells and DMPC liposomes. For all seven COEs, a linear

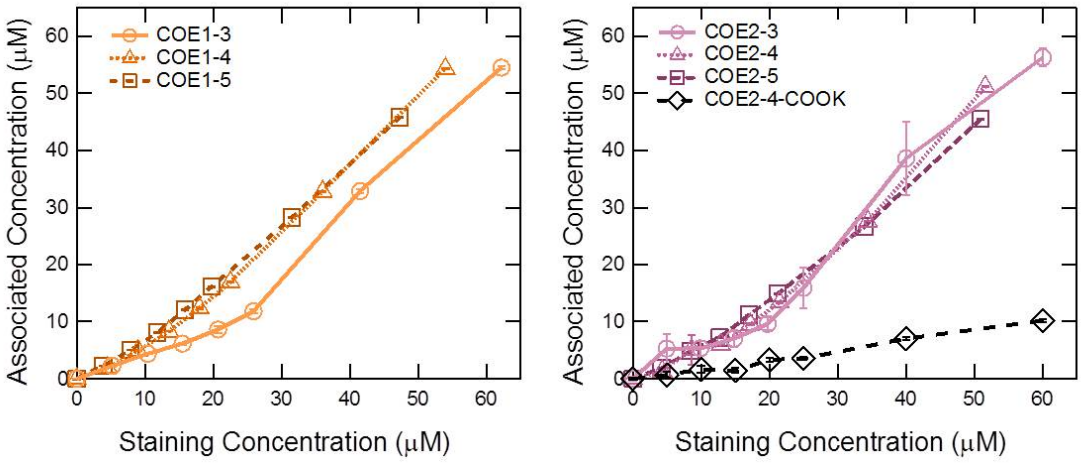


Figure 4.3: Association of COEs in ECE liposomes as a function of COE staining concentration. Error bars represent one standard deviation from the average of triplicate measurements.

relationship between COE association and staining concentration was observed and no plateau effect observed in the concentration ranges investigated, as shown in 4.3. There was no discernable difference between the two classes of COEs or their length, with the amount associated approaching 10%. However, COE2-4-COOK displayed a smaller slope than the rest of the molecules and did not associate as much as the other COEs, with association maximizing at 10 $\mu$M. The smaller slope of COE2-4-COOK is likely due to the unfavorable interaction of its anionic head groups with the anionic head groups in ECE lipids. The lack of plateau in membrane association of ECE liposomes is explained by the differences in electrostatic nature between DMPC and ECE liposomes, *vide infra*.

To examine the ability of COEs to affect the surface charge of liposomes and compare these observations to the association data, we measured the zeta potential of liposomes as a function of COE staining concentration. Due to the zwitterionic nature of DMPC, the zeta potential of native liposomes had a near zero value. We found that the addition of cationic COEs increased the magnitude of the zeta potential in a positive manner,

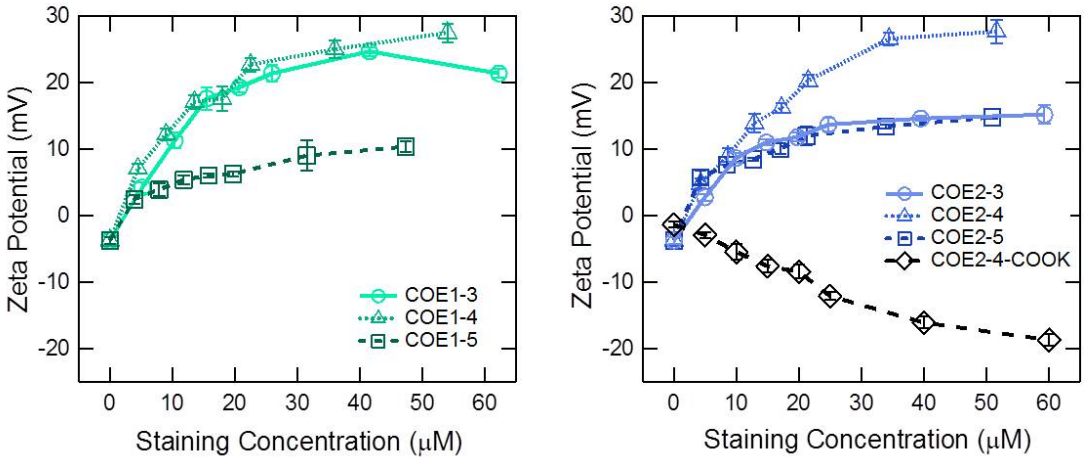


Figure 4.4: Effect of COE staining concentration on the Zeta Potential of DMPC liposomes. Error bars represent one standard deviation from the average of triplicate measurements.

while addition of COE2-4-COOK gave a negative shift in zeta potential. 4.4 shows the influence of COE staining concentration on the zeta potential of DMPC liposomes. The measured zeta potential increases with increasing COE staining and exhibits a plateau very similar to that of the COE association experiments. COE1-3 and COE1-4 staining saturated at a zeta potential of 25 mV and COE1-5 saturated at 10 mV, while COE2-4 saturates at 30 mV and COE2-5/COE2-3 saturate at 10 mV. These trends nicely reflect the observations from COE association in 4.2. For the case of COE2-4COOK, the maximum change in zeta potential was found to be approximately -20 mV, which is similar in magnitude to the cationic COEs, but of opposite sign due to its anionic head groups.

To compare the zeta potential change in DMPC liposomes and association in ECE liposomes, zeta potential measurements of COEs in ECE liposomes were undertaken in the same manner as in DMPC liposomes. 4.5 shows a linear relationship between COE staining and zeta potential for ECE liposomes, again mirroring the trends observed for COE association (refer to 4.3). When liposomes were stained with 50 $\mu$M COE, COE1-4

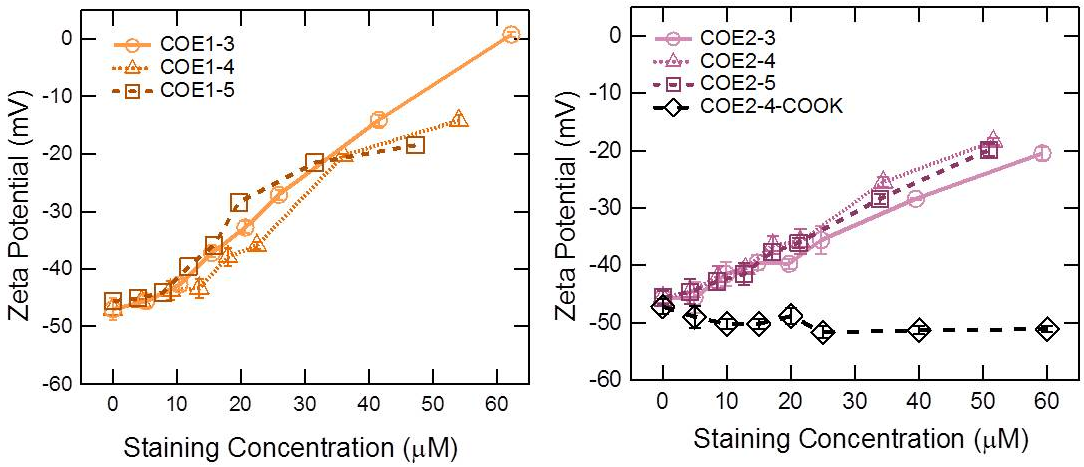


Figure 4.5: Effect of COE staining concentration on the Zeta Potential of ECE liposomes. Error bars represent one standard deviation from the average of triplicate measurements.

and COE1-5 gave zeta potentials of around -20 mV and COE1-3 rendered liposomes to have a neutral zeta potential. When ECE liposomes were treated with similar amounts of COE2-4-COOK, the zeta potential of the liposomes was found to change by only 4 mV to around -50 mV.

The correlation between COE association and zeta potential, as a function of COE staining, suggests that electrostatic interactions between the charged head groups of COEs and lipids in liposomes play an important role in governing the favorability of COE association. For DMPC liposomes, this effect becomes repulsive in nature as the concentration of COE in the lipid bilayer becomes sufficiently high, decreasing the favorability of further COE intercalation. The plateau effect observed in DMPC liposomes is a result of intermolecular electrostatic repulsions between cationic head groups as the COE concentration increases. This electrostatic repulsion has a dependence on the length of the COE backbone and type of alkyl linker because these two factors will affect the equilibrium separation of covalently linked cationic groups residing on the outer edge of the

lipid bilayer. For ECE liposomes, an attractive electrostatic interaction between cationic groups of the COE and the anionic groups of lipid molecules in liposome exists. This suggests why there is no plateau affect observed in COE association with ECE liposomes, because even at the highest staining concentrations of COE, the zeta potential of the liposomes is negative, indicating that COE association is in an attractive regime from an electrostatic viewpoint. The only difference between COE2-4 and COE2-4-COOK is the appended ionic head groups, yet a very drastic difference in interaction is observed when they are used to stain ECE liposomes, with COE2-4-COOK being unable to modulate the zeta potential or associate. Therefore, intermolecular electrostatic interactions play a significant role in governing the favorability of COE association in model liposome systems.

Previous reports on E. coli cells have shown trends in which COE intercalation and zeta potential modulation increases as a function of conjugation length, where in the present study we have found that COEs of intermediate length are the superior at intercalation and zeta potential modulation. One possible explanation for this discrepancy may arise from interactions of COEs with membrane proteins or lipopolysaccharides found in the membrane of E. coli cells. Additionally, it has been shown previously that apparent COEs associations can approach and even surpass a 1:1 lipid to COE ratio, which seems impossible from a simple model of membrane intercalation. Therefore we were interested to see how this would manifest in model membrane systems of DMPC and ECE, and how these factors would affect the geometrical considerations of these liposomes. To ascertain information about the COE to lipid ratio in the liposomes constructed in this study, it is necessary to know the moles of lipid per liposome. For DMPC liposomes, it was possible to calculate the moles of lipid in a liposome by knowing the size of the liposomes, molecular weight of the lipid, length of the bilayer, and concentration of lipid in solution.[141] For the case of ECE liposomes, this calculation is more

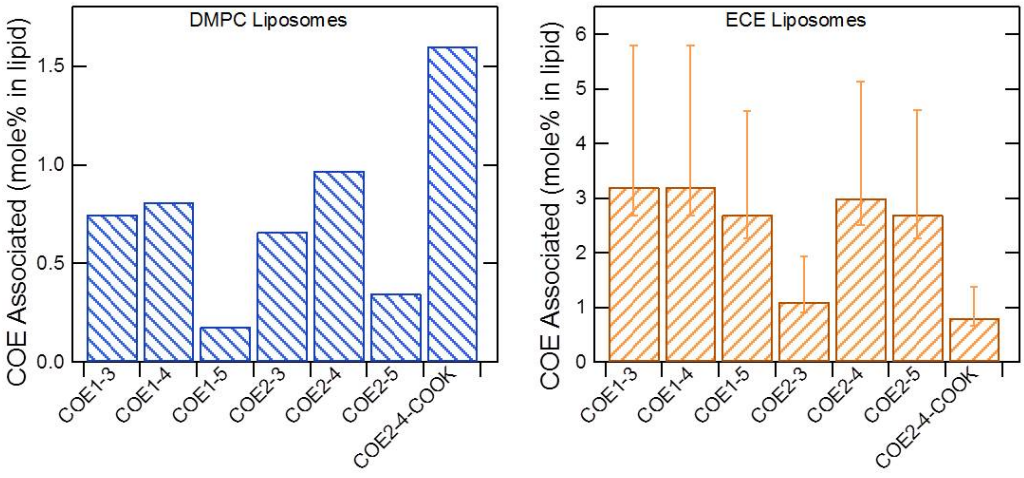


Figure 4.6: Maximum mole percent of COEs in liposomes. Error bars in the ECE plot represent upper and lower estimates due to varying composition of lipids.

complicated, as the exact molecular weights and percentages of lipids in the mixture are unknown. Therefore, we calculated a lower, average, and upper bound for the moles of lipids in an ECE liposome, by using the molecular weight of the lightest lipid, average of the known lipids, and the heaviest lipid, respectively (see the SI for more details). As shown in 4.6, it is obvious that the ratio of COE to lipid in the liposome is far below the 1:1 (50 mole %) value determined for live E. coli cells. In fact, the maximum amount of COE was found to be 1.5 mole % for DMPC liposomes and 6 mole % for ECE liposomes (when using the upper estimate, not average). This observation highlights a stark difference in COE interactions between liposome and E. coli cells. Interactions between COEs and lipids in a model bilayer, both from hydrophobic and electrostatic interactions, cannot account for the observations seen in living cells, pointing at contributions from components other than lipids to play an important role in COE uptake.

The interaction between living E. coli cells and COEs was previously found to have a linear dependence on the relationship between associated concentration of COE and the resulting zeta potential of the liposome. Furthermore, the slope of this linear dependence

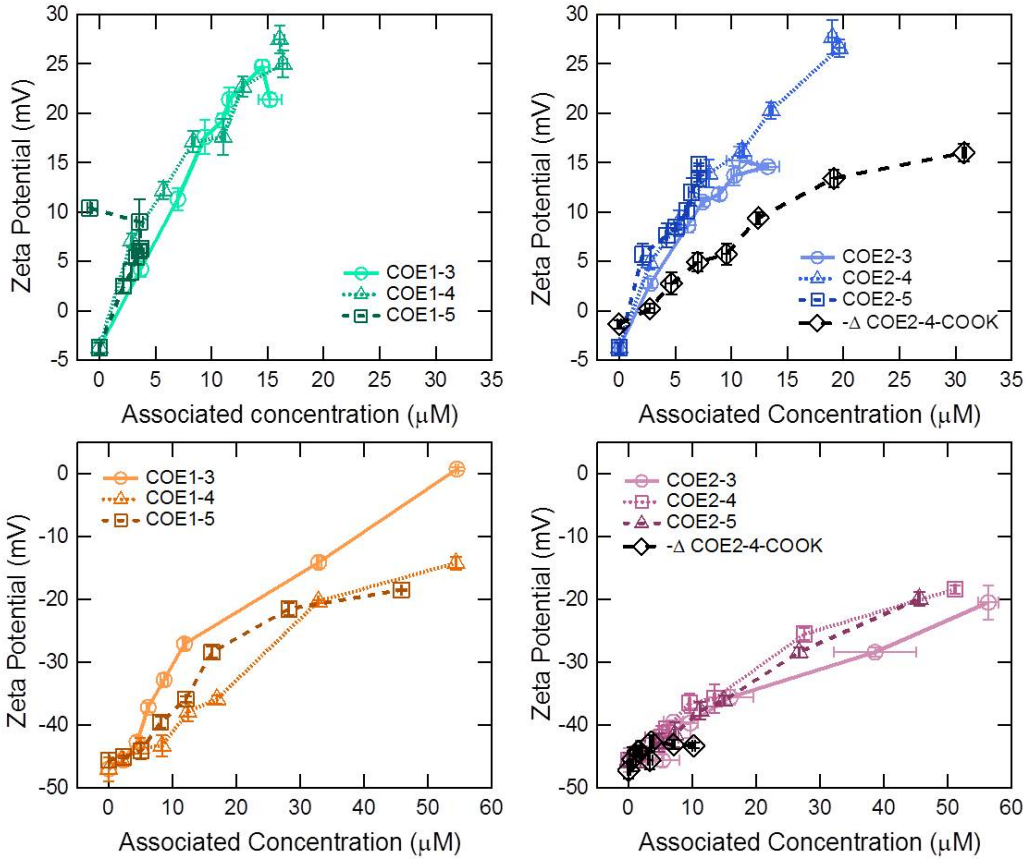


Figure 4.7: Zeta Potential of Liposomes vs. Amount of incorporated COE. Error bars were taken from previous figures.

was heavily influenced by the length of the COE, with longer COEs giving a steeper slope, and not strongly influenced by the nature of the alkyl liner present in the COE. As shown in 4.7, we found both DMPC and ECE liposomes show a linear dependence on zeta potential as a function of associated COE in the liposome. Interestingly, there was no observed length dependence for COE modulation of zeta potential, with all molecules giving similar slopes in both DMPC and ECE liposomes.

## 4.5 Conclusions

The results presented here highlight the difference between the membranes of living cells, whose constituents are complex and dynamic, and simple liposomes. In DMPC liposomes, we found a weak dependence on the length of COEs and the amount associated into a liposome, but in ECE liposomes no such trend was observed, with all COEs incorporating to about the same extent. The amount of COE incorporated into ECE liposomes was up to 4 times that of the DMPC liposomes. It was observed that COEs of intermediate lengths were incorporated the most into liposomes of DMPC, hinting at the fact that the packing of the COE backbones and appended ionic groups are sensitive to the overall length of the molecule and that if the COE is too short or too long, the favorability of intercalation is diminished. This agrees with previous computational studies on the membrane effects of COEs, as well as studies on the overall efficacy of COEs as a function of their length.[48, 142] Additionally, the use of anionic COE2-4-COOK emphasizes the role of electrostatic interactions in COE-liposome association, as COE2-4-COOK was able to incorporate much less in ECE liposomes compared to both the cationic COEs in ECE liposomes and COE2-4COOK in DMPC liposomes. Zeta potential measurements provided insight into the trends observed in the association studies, where by the nature of electrostatic intermolecular interactions between COEs themselves, as well as between COEs and lipids has a measurable effect on the zeta potential of the liposome. The changes found in zeta potential measurements correlated well with those found in the association studies and explain why cationic COEs incorporate much more in ECE liposomes than DMPC liposomes. The maximum amount of COE estimated in liposomes is far below what was observed in living cells, where a maximum loading in DMPC and ECE vesicles was 1.5 mole % and 6 mole %, respectively. Due to the unknown nature of the exact lipid composition of ECE liposomes, we estimated the mole

percent of COEs in these vesicles by using a lower, average, and upper bound. The 1:1 mole ratio of COEs to lipids in E. coli studies must originate from interactions outside of the classical lipid bilayer intercalation model. In fact, the association of COEs may be dominated by these other factors and the classical membrane intercalation picture may only be a minor contributor to the total amount of associated COE. How these observations relate to changes in microbial properties and their applications is not clear yet, nor is it known how influential other COE-cellular component interactions are to the previously explored applications of COEs. The ability of COEs to change the zeta potential of living cells as a function of incorporated COE was found to be dependent on the length of COEs, in previous work. We found no such correlation in the liposome systems studied here. All of the cationic COEs showed the same slope in their plots of zeta potential as a function of associated COE. Anionic COE2-4-COOK showed a lower slope in the DMPC system, possibly due to electrostatic interactions between the cationic choline group of DMPC and the anionic carboxylate of COE2-4-COOK. COE interactions with other components of the cell, such as entities in close proximity to the cellular envelope, are likely to play an important role in the favorability of COE association and display dependencies on COE length. LPS represent one candidate for influencing the interactions of COEs with the membrane of gram-negative bacteria. It is known that LPS is decorated with multiple phosphate groups, is highly enriched in the other leaflet of the outer membrane, and is sensitive to the presence of cations such as magnesium and calcium. The observations of this work show that COEs interact with model lipid bilayers by two competing factors, the second of which was underappreciated before this study. The first is solubilization of the hydrophobic semiconducting backbone and the second is intermolecular electrostatic COE-COE head group interactions and COE-lipid head group interactions. The relative energetic contributions and kinetic factors influencing these two factors are not currently well understood. There exists

clear research opportunities to further explore the thermodynamics and kinetics of these processes in both model systems and in living organisms. Additionally, the role LPS plays in the intercalation of COEs and how this changes the properties of cells is currently under investigation in our laboratory.

## 4.6 Experimental

All COEs used in this study were prepared according to published literature procedures. [114, 48, 51] Liposomes were prepared via extrusion.[143] Briefly, lipids (either DMPC or E. coli total lipid extracts) were first dissolved in chloroform. The chloroform was removed under reduced pressure and the lipid was dried overnight under vacuum. The resulting film was suspended in pH 7.4, 50 mM phosphate buffer saline (PBS) (10 mg/mL), with the aid of a vortex mixer, and shaken at 36 $^{o}$C for an hour in an incubator. The resulting milky colored suspension was kept at 40 $^{o}$C and passed through a 200 nm filter 11 times, followed by passing through a 100 nm filter 11 times, affording a translucent solution of monodisperse liposomes. This solution was diluted to 1.35 mg/mL and incubated with an appropriate concentration of COE for 2 hours with shaking at 36 $^{o}$C. The solutions were then split in two aliquots for DLS/zeta potential measurements and supernatant analysis. The aliquot for supernatant analysis was centrifuged at 17 kG for 1 hour at 4 $^{o}$C. The supernatant was transferred to a 96-well plate and the concentration of the COE left in the supernatant was determined using UV-Vis spectroscopy with the aid of a plate reader, using an internal calibration curve. All analysis of the liposomes (DLS, zeta potential, and UV-Vis) was performed at 20 $^{o}$C. DLS and zeta potential measurements were conducted using a Malvern Zetasizer Nano ZS, equipped with a 633 nm He-Ne laser and a polystyrene dip-cell. The 96-well plate reader used in the study was a

Tecan M220 Infinite Pro.

$$N_{tot} = \frac{4\pi(\frac{d}{2})^2 + 4\pi(\frac{d}{2} + h)^2}{a} \tag{4.1}$$

$$M_{tot} = \frac{N_{tot}}{N_a} \tag{4.2}$$

$$M_{COE-liposome} = \frac{M_{COE-assocaited}}{M_{COE-assocaited} + M_{tot}} \times 100 \tag{4.3}$$

In order to determine the mole percent of COEs in a liposome, we first determined the number of lipids in a liposome ($N_{tot}$) using equation 4.1. Where $d$ is the diameter of the liposome (nm), $h$ is the thickness of the bilayer itself (nm), and $a$ is the surface area of the lipid head group ($nm^2$). For the purposes of this discussion, we will simplify the calculations for ECE liposomes by using the same parameters is in DMPC.[141] Then equation 4.2 is used to determine the moles of lipid per liposome ($M_{tot}$), where $N_a$ is Avogadro's number. Finally, equation 4.3 was used to determine the mole percent of COE in a liposome ($M_{COE-liposome}$), where $M_{COE-assocaited}$ is determined from the association studies, e.g. figures 4.2 and 4.3. The purpose of this calculation is to give an estimate of the mole percent of COEs in liposomes and is not intended to be the most rigorous treatment of this problem, mainly due to the fact that the exact lipid compositions of the ECE liposomes is unknown.

# Bibliography


[1] "Universal Declaration of Human Rights — United Nations." http://www.un.org/en/universal-declaration-human-rights/.

[2] "Water scarcity — International Decade for Action 'Water for Life' 2005-2015." http://www.un.org/waterforlifedecade/scarcity.shtml.

[3] "Water quality — International Decade for Action 'Water for Life' 2005-2015." http://www.un.org/waterforlifedecade/quality.shtml.

[4] "Water: Facts and trends — WBCSD publications library." http://wbcsdpublications.org/project/water-facts-and-trends/.

[5] B. E. Logan, *Microbial Fuel Cells*. John Wiley & Sons.

[6] E. Marsili, J. B. Rollefson, D. B. Baron, R. M. Hozalski, and D. R. Bond, *Microbial Biofilm Voltammetry: Direct Electrochemical Characterization of Catalytic Electrode-Attached Biofilms*, *Applied and Environmental Microbiology* **74** (Dec., 2008) 7329–7337.

[7] N. A. Campbell and J. B. Reece, *Cellular Respiration: Harvesting Chemical Energy*, in *Biology*, pp. 160–178. Benjamin Cummings, 7th ed.

[8] T. A. Clarke, M. J. Edwards, A. J. Gates, A. Hall, G. F. White, J. Bradley, C. L. Reardon, L. Shi, A. S. Beliaev, M. J. Marshall, Z. Wang, N. J. Watmough, J. K. Fredrickson, J. M. Zachara, J. N. Butt, and D. J. Richardson, *Structure of a bacterial cell surface decaheme electron conduit*, *PNAS* **108** (July, 2011) 9384–9389.

[9] R. S. Hartshorne, C. L. Reardon, D. Ross, J. Nuester, T. A. Clarke, A. J. Gates, P. C. Mills, J. K. Fredrickson, J. M. Zachara, L. Shi, A. S. Beliaev, M. J. Marshall, M. Tien, S. Brantley, J. N. Butt, and D. J. Richardson, *Characterization of an electron conduit between bacteria and the extracellular environment*, *PNAS* **106** (Dec., 2009) 22169–22174.

[10] D. J. Richardson, J. N. Butt, J. K. Fredrickson, J. M. Zachara, L. Shi, M. J. Edwards, G. White, N. Baiden, A. J. Gates, S. J. Marritt, and T. A. Clarke, *The*

*'porin–cytochrome' model for microbe-to-mineral electron transfer*, *Molecular Microbiology* **85** (July, 2012) 201–212.

[11] "Synthesis of Organic Semiconductors - CleanEnergyWIKI." `http://photonicswiki.org/index.php?title=Synthesis_of_Organic_Semiconductors`.

[12] K. Mullen and U. Scherf, *Organic Light Emitting Devices: Synthesis, Properties and Applications*. John Wiley & Sons.

[13] C. Brabec, U. Scherf, and V. Dyakonov, *Organic Photovoltaics: Materials, Device Physics, and Manufacturing Technologies*. John Wiley & Sons.

[14] A. A. Virkar, S. Mannsfeld, Z. Bao, and N. Stingelin, *Organic Semiconductor Growth and Morphology Considerations for Organic Thin-Film Transistors*, *Adv. Mater.* **22** (Sept., 2010) 3857–3875.

[15] W. Hu, F. Bai, and X. Gong, *Organic Optoelectronics*. John Wiley & Sons.

[16] E. V. Anslyn and D. A. Dougherty, *Modern Physical Organic Chemistry*. University Science Books, 5th ed., 2006.

[17] J. E. Coughlin, Z. B. Henson, G. C. Welch, and G. C. Bazan, *Design and Synthesis of Molecular Donors for Solution-Processed High-Efficiency Organic Solar Cells*, *Acc. Chem. Res.* **47** (Jan., 2014) 257–270.

[18] P. Atkins and J. de Paula, *Physical Chemistry*. Macmillan Learning:, 10th ed., 2014.

[19] M. Born and R. Oppenheimer, *Zur Quantentheorie der Molekeln*, *Ann. Phys.* **389** (Jan., 1927) 457–484.

[20] E. U. Condon, *Nuclear Motions Associated with Electron Transitions in Diatomic Molecules*, *Phys. Rev.* **32** (Dec., 1928) 858–872.

[21] E. Condon, *A Theory of Intensity Distribution in Band Systems*, *Phys. Rev.* **28** (Dec., 1926) 1182–1201.

[22] J. Franck and E. G. Dymond, *Elementary processes of photochemical reactions*, *Trans. Faraday Soc.* **21** (Jan., 1926) 536–542.

[23] J. Lakowicz, *Principles of Fluorescence Spectroscopy*. Springer, 3rd ed., 2006.

[24] M. Kasha, *Characterization of electronic transitions in complex molecules*, *Discuss. Faraday Soc.* **9** (Jan., 1950) 14–19.

[25] D. A. Skoog, D. M. West, F. J. Holler, and S. R. Crouch, *Analytical Chemistry: An Introduction*. Saunders College Pub., 7th ed., 2000. Google-Books-ID: ii8vAQAAIAAJ.

[26] J. C. Poggendorff, *Annalen der Physik*. J.A. Barth, 1852. Google-Books-ID: PNmXAAAAIAAJ.

[27] "Ultraviolet-Visible (UV-Vis) Spectroscopy – Limitations and Deviations of Beer-Lambert's Law — Analytical Chemistry." `http://pharmaxchange.info/press/2012/05/ultraviolet-visible-uv-vis-spectroscopy-%e2%80%93-limitations-and-deviations-of-beer-lambert-law/`, May, 2012.

[28] A. Bard and L. Faulkner, *Electrochemical Methods: Fundamentals and Applications*. 2nd ed.

[29] B. J. Berne and R. Pecora, *Dynamic Light Scattering: With Applications to Chemistry, Biology, and Physics*. Courier Corporation, July, 2013. Google-Books-ID: xg3CAgAAQBAJ.

[30] R. J. Hunter, *Zeta Potential in Colloid Science: Principles and Applications*. Academic Press, Sept., 2013.

[31] D. R. Bond, D. E. Holmes, L. M. Tender, and D. R. Lovley, *Electrode-Reducing Microorganisms That Harvest Energy from Marine Sediments*, *Science* **295** (Jan., 2002) 483–485.

[32] D. R. Lovley, *Bug juice: Harvesting electricity with microorganisms*, *Nat Rev Micro* **4** (July, 2006) 497–508.

[33] D. R. Lovley, *Extracellular electron transfer: Wires, capacitors, iron lungs, and more*, *Geobiology* **6** (June, 2008) 225–231.

[34] C. I. Torres, R. Krajmalnik-Brown, P. Parameswaran, A. K. Marcus, G. Wanger, Y. A. Gorby, and B. E. Rittmann, *Selecting Anode-Respiring Bacteria Based on Anode Potential: Phylogenetic, Electrochemical, and Microscopic Characterization*, *Environ. Sci. Technol.* **43** (Dec., 2009) 9519–9524.

[35] B. E. Logan, *Exoelectrogenic bacteria that power microbial fuel cells*, *Nat Rev Micro* **7** (May, 2009) 375–381.

[36] D. Lovely, *Electromicrobiology*, *Annual Review of Microbiology* **66** (2012), no. 1 391–409.

[37] H. M. Jensen, A. E. Albers, K. R. Malley, Y. Y. Londer, B. E. Cohen, B. A. Helms, P. Weigele, J. T. Groves, and C. M. Ajo-Franklin, *Engineering of a synthetic electron conduit in living cells*, *PNAS* **107** (Sept., 2010) 19213–19218.

[38] C. P. Goldbeck, H. M. Jensen, M. A. TerAvest, N. Beedle, Y. Appling, M. Hepler, G. Cambray, V. Mutalik, L. T. Angenent, and C. M. Ajo-Franklin, *Tuning Promoter Strengths for Improved Synthesis and Function of Electron Conduits in Escherichia coli*, *ACS Synth. Biol.* **2** (Mar., 2013) 150–159.

[39] A. Sydow, T. Krieg, F. Mayer, J. Schrader, and D. Holtmann, *Electroactive bacteria—molecular mechanisms and genetic tools*, *Appl Microbiol Biotechnol* **98** (Oct., 2014) 8481–8495.

[40] J. Du, C. Catania, and G. C. Bazan, *Modification of Abiotic–Biotic Interfaces with Small Molecules and Nanomaterials for Improved Bioelectronics*, *Chem. Mater.* **26** (Jan., 2014) 686–697.

[41] G. Malliaras and M. R. Abidian, *Organic Bioelectronic Materials and Devices*, *Adv. Mater.* **27** (Dec., 2015) 7492–7492.

[42] W. Brutting and C. Adachi, *Physics of Organic Semiconductors*. John Wiley & Sons, 2nd ed.

[43] L. Bin and G. Bazan, *Conjugated Polyelectrolytes: Fundamentals and Applications*. John Wiley & Sons.

[44] M. Leclerc and J.-F. Morin, *Design and Synthesis of Conjugated Polymers*. John Wiley & Sons.

[45] L. E. Garner, J. Park, S. M. Dyar, A. Chworos, J. J. Sumner, and G. C. Bazan, *Modification of the Optoelectronic Properties of Membranes via Insertion of Amphiphilic Phenylenevinylene Oligoelectrolytes*, *J. Am. Chem. Soc.* **132** (July, 2010) 10042–10052.

[46] L. E. Garner, A. W. Thomas, J. J. Sumner, S. P. Harvey, and G. C. Bazan, *Conjugated oligoelectrolytes increase current response and organic contaminant removal in wastewater microbial fuel cells*, *Energy Environ. Sci.* **5** (Oct., 2012) 9449–9452.

[47] V. B. Wang, J. Du, X. Chen, A. W. Thomas, N. D. Kirchhofer, L. E. Garner, M. T. Maw, W. H. Poh, J. Hinks, S. Wuertz, S. Kjelleberg, Q. Zhang, J. S. C. Loo, and G. C. Bazan, *Improving charge collection in Escherichia coli–carbon electrode devices with conjugated oligoelectrolytes*, *Phys. Chem. Chem. Phys.* **15** (Mar., 2013) 5867–5872.

[48] H. Hou, X. Chen, A. W. Thomas, C. Catania, N. D. Kirchhofer, L. E. Garner, A. Han, and G. C. Bazan, *Conjugated Oligoelectrolytes Increase Power Generation in E. coli Microbial Fuel Cells*, *Adv. Mater.* **25** (Mar., 2013) 1593–1597.

[49] A. W. Thomas, L. E. Garner, K. P. Nevin, T. L. Woodard, A. E. Franks, D. R. Lovley, J. J. Sumner, C. J. Sund, and G. C. Bazan, *A lipid membrane intercalating conjugated oligoelectrolyte enables electrode driven succinate production in Shewanella*, *Energy Environ. Sci.* **6** (May, 2013) 1761–1765.

[50] V. B. Wang, N. D. Kirchhofer, X. Chen, M. Y. L. Tan, K. Sivakumar, B. Cao, Q. Zhang, S. Kjelleberg, G. C. Bazan, S. C. J. Loo, and E. Marsili, *Comparison of flavins and a conjugated oligoelectrolyte in stimulating extracellular electron transport from Shewanella oneidensis MR-1*, *Electrochemistry Communications* **41** (Apr., 2014) 55–58.

[51] A. W. Thomas, C. Catania, L. E. Garner, and G. C. Bazan, *Pendant ionic groups of conjugated oligoelectrolytes govern their ability to intercalate into microbial membranes*, *Chem. Commun.* **51** (May, 2015) 9294–9297.

[52] N. D. Kirchhofer, M. A. Rasmussen, F. W. Dahlquist, S. D. Minteer, and G. C. Bazan, *The photobioelectrochemical activity of thylakoid bioanodes is increased via photocurrent generation and improved contacts by membrane-intercalating conjugated oligoelectrolytes*, *Energy Environ. Sci.* **8** (Aug., 2015) 2698–2706.

[53] N. D. Kirchhofer, X. Chen, E. Marsili, J. J. Sumner, F. W. Dahlquist, and G. C. Bazan, *The conjugated oligoelectrolyte DSSN+ enables exceptional coulombic efficiency via direct electron transfer for anode-respiring Shewanella oneidensis MR-1—a mechanistic study*, *Phys. Chem. Chem. Phys.* **16** (Sept., 2014) 20436–20443.

[54] T. S. Arrhenius, M. Blanchard-Desce, M. Dvolaitzky, J.-M. Lehn, and J. Malthete, *Molecular devices: Caroviologens as an approach to molecular wires—synthesis and incorporation into vesicle membranes*, *PNAS* **83** (Jan., 1986) 5355–5359.

[55] W. B. Davis, W. A. Svec, M. A. Ratner, and M. R. Wasielewski, *Molecular-wire behaviour in p -phenylenevinylene oligomers*, *Nature* **396** (Nov., 1998) 60–63.

[56] V. Mujica, M. Kemp, A. Roitberg, and M. A. Ratner, *Current-voltage characteristics of molecular wires: Eigenvalue staircase, Coulomb blockade, and rectification*, *The Journal of Chemical Physics* **104** (May, 1996) 7296–7305.

[57] K. W. Hipps, *It's All About Contacts*, *Science* **294** (Oct., 2001) 536–537.

[58] J. Du, A. W. Thomas, X. Chen, L. E. Garner, C. A. Vandenberg, and G. C. Bazan, *Increased ion conductance across mammalian membranes modified with conjugated oligoelectrolytes*, *Chem. Commun.* **49** (Sept., 2013) 9624–9626.

[59] J. P. Jahnke, G. C. Bazan, and J. J. Sumner, *Effect of Modified Phospholipid Bilayers on the Electrochemical Activity of a Membrane-Spanning Conjugated Oligoelectrolyte*, *Langmuir* **31** (Oct., 2015) 11613–11620.

[60] R. Renslow, J. Babauta, A. Kuprat, J. Schenk, C. Ivory, J. Fredrickson, and H. Beyenal, *Modeling biofilms with dual extracellular electron transfer mechanisms*, *Phys. Chem. Chem. Phys.* **15** (Oct., 2013) 19262–19283.

[61] G. F. White, Z. Shi, L. Shi, Z. Wang, A. C. Dohnalkova, M. J. Marshall, J. K. Fredrickson, J. M. Zachara, J. N. Butt, D. J. Richardson, and T. A. Clarke, *Rapid electron exchange between surface-exposed bacterial cytochromes and Fe(III) minerals*, *PNAS* **110** (Apr., 2013) 6346–6351.

[62] D. Baron, E. LaBelle, D. Coursolle, J. A. Gralnick, and D. R. Bond, *Electrochemical Measurement of Electron Transfer Kinetics by Shewanella oneidensis MR-1*, *J. Biol. Chem.* **284** (Oct., 2009) 28865–28873.

[63] J. N. Roy, S. Babanova, K. E. Garcia, J. Cornejo, L. K. Ista, and P. Atanassov, *Catalytic biofilm formation by Shewanella oneidensis MR-1 and anode characterization by expanded uncertainty*, *Electrochimica Acta* **126** (Apr., 2014) 3–10.

[64] A. Okamoto, K. Hashimoto, K. H. Nealson, and R. Nakamura, *Rate enhancement of bacterial extracellular electron transport involves bound flavin semiquinones*, *PNAS* **110** (July, 2013) 7856–7861.

[65] D. J. Richardson, J. N. Butt, J. K. Fredrickson, J. M. Zachara, L. Shi, M. J. Edwards, G. White, N. Baiden, A. J. Gates, S. J. Marritt, and T. A. Clarke, *The 'porin–cytochrome' model for microbe-to-mineral electron transfer*, *Molecular Microbiology* **85** (July, 2012) 201–212.

[66] L. Shi, B. Chen, Z. Wang, D. A. Elias, M. U. Mayer, Y. A. Gorby, S. Ni, B. H. Lower, D. W. Kennedy, D. S. Wunschel, H. M. Mottaz, M. J. Marshall, E. A. Hill, A. S. Beliaev, J. M. Zachara, J. K. Fredrickson, and T. C. Squier, *Isolation of a High-Affinity Functional Protein Complex between OmcA and MtrC: Two Outer Membrane Decaheme c-Type Cytochromes of Shewanella oneidensis MR-1*, *J. Bacteriol.* **188** (Jan., 2006) 4705–4714.

[67] D. Coursolle, D. B. Baron, D. R. Bond, and J. A. Gralnick, *The Mtr Respiratory Pathway Is Essential for Reducing Flavins and Electrodes in Shewanella oneidensis*, *J. Bacteriol.* **192** (Jan., 2010) 467–474.

[68] E. Marsili, J. B. Rollefson, D. B. Baron, R. M. Hozalski, and D. R. Bond, *Microbial Biofilm Voltammetry: Direct Electrochemical Characterization of Catalytic Electrode-Attached Biofilms*, *Appl. Environ. Microbiol.* **74** (Jan., 2008) 7329–7337.

[69] M. Rosenbaum, F. Aulenta, M. Villano, and L. T. Angenent, *Cathodes as electron donors for microbial metabolism: Which extracellular electron transfer mechanisms are involved?*, *Bioresource Technology* **102** (Jan., 2011) 324–333.

[70] E. Marsili, D. B. Baron, I. D. Shikhare, D. Coursolle, J. A. Gralnick, and D. R. Bond, *Shewanella secretes flavins that mediate extracellular electron transfer*, *PNAS* **105** (Nov., 2008) 3968–3973.

[71] J. K. Fredrickson, M. F. Romine, A. S. Beliaev, J. M. Auchtung, M. E. Driscoll, T. S. Gardner, K. H. Nealson, A. L. Osterman, G. Pinchuk, J. L. Reed, D. A. Rodionov, J. L. M. Rodrigues, D. A. Saffarini, M. H. Serres, A. M. Spormann, I. B. Zhulin, and J. M. Tiedje, *Towards environmental systems biology of Shewanella*, *Nat Rev Micro* **6** (Aug., 2008) 592–603.

[72] H. H. Hau and J. A. Gralnick, *Ecology and Biotechnology of the Genus Shewanella*, *Annu. Rev. Microbiol.* (Sept., 2007).

[73] H. Werner, *At Least 60 Years of Ferrocene: The Discovery and Rediscovery of the Sandwich Complexes*, *Angew. Chem. Int. Ed.* **51** (June, 2012) 6052–6058.

[74] M. E. N.P.R.A. Silva, A. J. L. Pombeiro, J. J. R. Fraústo da Silva, R. Herrmann, N. Deus, and R. E.Bozak, *Redox potential and substituent effects in ferrocene derivatives: II*, *Journal of Organometallic Chemistry* **480** (Oct., 1994) 81–90.

[75] P. Stepnicka, *Ferrocenes: Ligands, Materials and Biomolecules*. John Wiley & Sons.

[76] A. M. Bond, E. A. McLennan, R. S. Stojanovic, and F. G. Thomas, *Assessment of conditions under which the oxidation of ferrocene can be used as a standard voltammetric reference process in aqueous media*, *Anal. Chem.* **59** (Dec., 1987) 2853–2860.

[77] C. M. Cardona, W. Li, A. E. Kaifer, D. Stockdale, and G. C. Bazan, *Electrochemical Considerations for Determining Absolute Frontier Orbital Energy Levels of Conjugated Polymers for Solar Cell Applications*, *Adv. Mater.* **23** (May, 2011) 2367–2371.

[78] N. G. Connelly and W. E. Geiger, *Chemical Redox Agents for Organometallic Chemistry*, *Chem. Rev.* **96** (Jan., 1996) 877–910.

[79] K. Rabaey and R. A. Rozendal, *Microbial electrosynthesis — revisiting the electrical route for microbial production*, *Nat Rev Micro* **8** (Oct., 2010) 706–716.

[80] K. P. Barry and C. Nataro, *A new synthesis and electrochemistry of 1,1′-bis(β-hydroxyethyl)ferrocene*, *Inorganica Chimica Acta* **362** (Apr., 2009) 2068–2070.

[81] A. N. Patwa, R. G. Gonnade, V. A. Kumar, M. M. Bhadbhade, and K. N. Ganesh, *Ferrocene-Bis(thymine/uracil) Conjugates: Base Pairing Directed, Spacer Dependent Self-Assembly and Supramolecular Packing*, *J. Org. Chem.* **75** (Dec., 2010) 8705–8708.

[82] A. Lin, A. C. Willis, and M. G. Banwell, *A chemoenzymatic and enantioselective total synthesis of the resorcylic acid lactone L-783,290, the trans-isomer of L-783,277*, *Tetrahedron Letters* **51** (Feb., 2010) 1044–1047.

[83] E. Mertz and S. C. Zimmerman, *Cross-Linked Dendrimer Hosts Containing Reporter Groups for Amine Guests*, *J. Am. Chem. Soc.* **125** (Mar., 2003) 3424–3425.

[84] R. J. Kassner, *Effects of Nonpolar Environments on the Redox Potentials of Heme Complexes*, *PNAS* **69** (Jan., 1972) 2263–2267.

[85] B. J. Marsh, L. Hampton, S. Goggins, and C. G. Frost, *Fine-tuning of ferrocene redox potentials towards multiplex DNA detection*, *New J. Chem.* **38** (Oct., 2014) 5260–5263.

[86] P. Blainey, M. Krzywinski, and N. Altman, *Points of Significance: Replication*, *Nat Meth* **11** (Sept., 2014) 879–880.

[87] J. P. Dilger, S. G. McLaughlin, T. J. McIntosh, and S. A. Simon, *The dielectric constant of phospholipid bilayers and the permeability of membranes to ions*, *Science* **206** (Dec., 1979) 1196–1198.

[88] G. Gramse, A. Dols-Perez, M. A. Edwards, L. Fumagalli, and G. Gomila, *Nanoscale Measurement of the Dielectric Constant of Supported Lipid Bilayers in Aqueous Solutions with Electrostatic Force Microscopy*, *Biophysical Journal* **104** (Mar., 2013) 1257–1262.

[89] J. C. Weaver and K. H. Schoenbach, *Biodielectrics*, *IEEE Transactions on Dielectrics and Electrical Insulation* **10** (Oct., 2003) 715–716.

[90] A. Kouzuma, X.-Y. Meng, N. Kimura, K. Hashimoto, and K. Watanabe, *Disruption of the Putative Cell Surface Polysaccharide Biosynthesis Gene SO3177 in Shewanella oneidensis MR-1 Enhances Adhesion to Electrodes and Current Generation in Microbial Fuel Cells*, *Appl. Environ. Microbiol.* **76** (Jan., 2010) 4151–4157.

[91] B. E. Logan, B. Hamelers, R. Rozendal, U. Schröder, J. Keller, S. Freguia, P. Aelterman, W. Verstraete, and K. Rabaey, *Microbial Fuel Cells: Methodology and Technology*, *Environ. Sci. Technol.* **40** (Sept., 2006) 5181–5192.

[92] B. E. Logan, *Essential Data and Techniques for Conducting Microbial Fuel Cell and other Types of Bioelectrochemical System Experiments*, *ChemSusChem* **5** (June, 2012) 988–994.

[93] C. R. Myers and J. M. Myers, *MtrB Is Required for Proper Incorporation of the Cytochromes OmcA and OmcB into the Outer Membrane of Shewanella putrefaciens MR-1*, *Appl. Environ. Microbiol.* **68** (Jan., 2002) 5585–5594.

[94] D. Coursolle and J. A. Gralnick, *Modularity of the Mtr respiratory pathway of Shewanella oneidensis strain MR-1*, *Molecular Microbiology* **77** (Aug., 2010) 995–1008.

[95] J. Hinks, Y. Wang, W. H. Poh, B. C. Donose, A. W. Thomas, S. Wuertz, S. C. J. Loo, G. C. Bazan, S. Kjelleberg, Y. Mu, and T. Seviour, *Modeling Cell Membrane Perturbation by Molecules Designed for Transmembrane Electron Transfer*, *Langmuir* **30** (Mar., 2014) 2429–2440.

[96] H. Yan, Z. D. Rengert, A. W. Thomas, C. Rehermann, J. Hinks, and G. C. Bazan, *Influence of molecular structure on the antimicrobial function of phenylenevinylene conjugated oligoelectrolytes*, *Chem. Sci.* **7** (Aug., 2016) 5714–5722.

[97] B. Cao, P. D. Majors, B. Ahmed, R. S. Renslow, C. P. Silvia, L. Shi, S. Kjelleberg, J. K. Fredrickson, and H. Beyenal, *Biofilm shows spatially stratified metabolic responses to contaminant exposure*, *Environ Microbiol* **14** (Nov., 2012) 2901–2910.

[98] B. Cao, L. Shi, R. N. Brown, Y. Xiong, J. K. Fredrickson, M. F. Romine, M. J. Marshall, M. S. Lipton, and H. Beyenal, *Extracellular polymeric substances from Shewanella sp. HRCR-1 biofilms: Characterization by infrared spectroscopy and proteomics*, *Environmental Microbiology* **13** (Apr., 2011) 1018–1031.

[99] J. M. Andrews, *Determination of minimum inhibitory concentrations*, *J Antimicrob Chemother* **48** (July, 2001) 5–16.

[100] E. Ji, T. S. Corbitt, A. Parthasarathy, K. S. Schanze, and D. G. Whitten, *Light and Dark-Activated Biocidal Activity of Conjugated Polyelectrolytes*, *ACS Appl. Mater. Interfaces* **3** (Aug., 2011) 2820–2829.

[101] K. Guo, S. Freguia, P. G. Dennis, X. Chen, B. C. Donose, J. Keller, J. J. Gooding, and K. Rabaey, *Effects of Surface Charge and Hydrophobicity on Anodic Biofilm Formation, Community Composition, and Current Generation in Bioelectrochemical Systems*, *Environ. Sci. Technol.* **47** (July, 2013) 7563–7570.

[102] K. Guo, A. Prévoteau, S. A. Patil, and K. Rabaey, *Engineering electrodes for microbial electrocatalysis*, *Current Opinion in Biotechnology* **33** (June, 2015) 149–156.

[103] K. Bahartan, J. Gun, S. Sladkevich, P. V. Prikhodchenko, O. Lev, and L. Alfonta, *Encapsulation of yeast displaying glucose oxidase on their surface in graphene oxide hydrogel scaffolding and its bioactivation*, *Chem. Commun.* **48** (Nov., 2012) 11957–11959.

[104] J. Du, C. Catania, and G. C. Bazan, *Modification of Abiotic–Biotic Interfaces with Small Molecules and Nanomaterials for Improved Bioelectronics*, *Chem. Mater.* **26** (Jan., 2014) 686–697.

[105] R. A. Bullen, T. C. Arnot, J. B. Lakeman, and F. C. Walsh, *Biofuel cells and their development*, *Biosensors and Bioelectronics* **21** (May, 2006) 2015–2045.

[106] K. Rabaey and R. A. Rozendal, *Microbial electrosynthesis — revisiting the electrical route for microbial production*, *Nat Rev Micro* **8** (Oct., 2010) 706–716.

[107] D. Coursolle, D. B. Baron, D. R. Bond, and J. A. Gralnick, *The Mtr Respiratory Pathway Is Essential for Reducing Flavins and Electrodes in Shewanella oneidensis*, *J. Bacteriol.* **192** (Jan., 2010) 467–474.

[108] N. D. Kirchhofer, X. Chen, E. Marsili, J. J. Sumner, F. W. Dahlquist, and G. C. Bazan, *The conjugated oligoelectrolyte DSSN+ enables exceptional coulombic efficiency via direct electron transfer for anode-respiring Shewanella oneidensis MR-1—a mechanistic study*, *Phys. Chem. Chem. Phys.* **16** (Sept., 2014) 20436–20443.

[109] L. E. Garner, J. Park, S. M. Dyar, A. Chworos, J. J. Sumner, and G. C. Bazan, *Modification of the Optoelectronic Properties of Membranes via Insertion of Amphiphilic Phenylenevinylene Oligoelectrolytes*, *J. Am. Chem. Soc.* **132** (July, 2010) 10042–10052.

[110] C. Catania, A. W. Thomas, and G. C. Bazan, *Tuning cell surface charge in E. coli with conjugated oligoelectrolytes*, *Chem. Sci.* **7** (Feb., 2016) 2023–2029.

[111] N. D. Kirchhofer, Z. D. Rengert, F. W. Dahlquist, T.-Q. Nguyen, and G. C. Bazan, *A Ferrocene-Based Conjugated Oligoelectrolyte Catalyzes Bacterial Electrode Respiration*, *Chem* **2** (Feb., 2017) 240–257.

[112] P. D. Byrne, P. Müller, and T. M. Swager, *Conducting Metallopolymers Based on Azaferrocene*, *Langmuir* **22** (Dec., 2006) 10596–10604.

[113] U. Salzner, *Quantitatively Correct UV-vis Spectrum of Ferrocene with TDB3LYP*, *J. Chem. Theory Comput.* **9** (Sept., 2013) 4064–4073.

[114] H. Y. Woo, B. Liu, B. Kohler, D. Korystov, A. Mikhailovsky, and G. C. Bazan, *Solvent Effects on the Two-Photon Absorption of Distyrylbenzene Chromophores*, *J. Am. Chem. Soc.* **127** (Oct., 2005) 14721–14729.

[115] S. Barlow, H. E. Bunting, C. Ringham, J. C. Green, G. U. Bublitz, S. G. Boxer, J. W. Perry, and S. R. Marder, *Studies of the Electronic Structure of Metallocene-Based Second-Order Nonlinear Optical Dyes*, *J. Am. Chem. Soc.* **121** (Apr., 1999) 3715–3723.

[116] M. E. N.P.R.A. Silva, A. J. L. Pombeiro, J. J. R. Fraústo da Silva, R. Herrmann, N. Deus, and R. E.Bozak, *Redox potential and substituent effects in ferrocene derivatives: II*, *Journal of Organometallic Chemistry* **480** (Oct., 1994) 81–90.

[117] B. Gharib and A. Hirsch, *Synthesis and Characterization of New Ferrocene-Containing Ionic Liquids*, *Eur. J. Org. Chem.* **2014** (July, 2014) 4123–4136.

[118] H. Yan, Z. D. Rengert, A. W. Thomas, C. Rehermann, J. Hinks, and G. C. Bazan, *Influence of molecular structure on the antimicrobial function of phenylenevinylene conjugated oligoelectrolytes*, *Chem. Sci.* **7** (Aug., 2016) 5714–5722.

[119] B. White, S. Banerjee, S. O'Brien, N. J. Turro, and I. P. Herman, *Zeta-Potential Measurements of Surfactant-Wrapped Individual Single-Walled Carbon Nanotubes*, *J. Phys. Chem. C* **111** (Sept., 2007) 13684–13690.

[120] L. Y. Qiu and Y. H. Bae, *Self-assembled polyethylenimine-graft-poly($\epsilon$-caprolactone) micelles as potential dual carriers of genes and anticancer drugs*, *Biomaterials* **28** (Oct., 2007) 4132–4142.

[121] G. V. Hartland, F. Grieser, and L. R. White, *Surface potential measurements in pentanol–sodium dodecyl sulphate micelles*, *J. Chem. Soc., Faraday Trans. 1* **83** (Jan., 1987) 591–613.

[122] G. G. A. Balavoine, G. Doisneau, and T. Fillebeen-Khan, *An improved synthesis of ferrocene-1,1′-dicarbaldehyde*, *Journal of Organometallic Chemistry* **412** (July, 1991) 381–382.

[123] M. J. Plater and T. Jackson, *Polyaromatic amines. Part 3: Synthesis of poly(diarylamino)styrenes and related compounds*, *Tetrahedron* **59** (June, 2003) 4673–4685.

[124] D. P. Flaherty, S. M. Walsh, T. Kiyota, Y. Dong, T. Ikezu, and J. L. Vennerstrom, *Polyfluorinated Bis-styrylbenzene $\beta$-Amyloid Plaque Binding Ligands*, *J. Med. Chem.* **50** (Oct., 2007) 4986–4992.

[125] Y. Wang, E. Y. Chi, D. O. Natvig, K. S. Schanze, and D. G. Whitten, *Antimicrobial Activity of Cationic Conjugated Polyelectrolytes and Oligomers against Saccharomyces cerevisiae Vegetative Cells and Ascospores*, *ACS Appl. Mater. Interfaces* **5** (June, 2013) 4555–4561.

[126] Y. Wang, K. S. Schanze, E. Y. Chi, and D. G. Whitten, *When Worlds Collide: Interactions at the Interface between Biological Systems and Synthetic Cationic Conjugated Polyelectrolytes and Oligomers*, *Langmuir* **29** (Aug., 2013) 10635–10647.

[127] V. B. Wang, J. Du, X. Chen, A. W. Thomas, N. D. Kirchhofer, L. E. Garner, M. T. Maw, W. H. Poh, J. Hinks, S. Wuertz, S. Kjelleberg, Q. Zhang, J. S. C. Loo, and G. C. Bazan, *Improving charge collection in Escherichia coli–carbon electrode devices with conjugated oligoelectrolytes*, *Phys. Chem. Chem. Phys.* **15** (Mar., 2013) 5867–5872.

[128] J. Hinks, Y. Wang, A. Matysik, R. Kraut, S. Kjelleberg, Y. Mu, G. C. Bazan, S. Wuertz, and T. Seviour, *Increased Microbial Butanol Tolerance by Exogenous Membrane Insertion Molecules*, *ChemSusChem* **8** (Nov., 2015) 3718–3726.

[129] L. E. Garner, A. W. Thomas, J. J. Sumner, S. P. Harvey, and G. C. Bazan, *Conjugated oligoelectrolytes increase current response and organic contaminant removal in wastewater microbial fuel cells*, *Energy Environ. Sci.* **5** (Oct., 2012) 9449–9452.

[130] H. Yan, C. Catania, and G. C. Bazan, *Membrane-Intercalating Conjugated Oligoelectrolytes: Impact on Bioelectrochemical Systems*, *Adv. Mater.* **27** (May, 2015) 2958–2973.

[131] R. Huber, M. T. González, S. Wu, M. Langer, S. Grunder, V. Horhoiu, M. Mayor, M. R. Bryce, C. Wang, R. Jitchati, C. Schönenberger, and M. Calame, *Electrical Conductance of Conjugated Oligomers at the Single Molecule Level*, *J. Am. Chem. Soc.* **130** (Jan., 2008) 1080–1084.

[132] G. N. Tew, R. W. Scott, M. L. Klein, and W. F. DeGrado, *De Novo Design of Antimicrobial Polymers, Foldamers, and Small Molecules: From Discovery to Practical Applications*, *Acc. Chem. Res.* **43** (Jan., 2010) 30–39.

[133] R. F. Epand, P. B. Savage, and R. M. Epand, *Bacterial lipid composition and the antimicrobial efficacy of cationic steroid compounds (Ceragenins)*, *Biochimica et Biophysica Acta (BBA) - Biomembranes* **1768** (Oct., 2007) 2500–2509.

[134] Y. Qiao, C. Yang, D. J. Coady, Z. Y. Ong, J. L. Hedrick, and Y.-Y. Yang, *Highly dynamic biodegradable micelles capable of lysing Gram-positive and Gram-negative bacterial membrane*, *Biomaterials* **33** (Feb., 2012) 1146–1153.

[135] Q. Yu, W. Ge, A. Atewologun, A. D. Stiff-Roberts, and G. P. López, *Antimicrobial and bacteria-releasing multifunctional surfaces: Oligo (p-phenylene-ethynylene)/poly (N-isopropylacrylamide) films deposited by RIR-MAPLE*, *Colloids and Surfaces B: Biointerfaces* **126** (Feb., 2015) 328–334.

[136] L. Yang, V. Gordon, D. Trinkle, N. Schmidt, M. Davis, C. DeVries, A. Som, J. Cronan Jr., G. Tew, and G. Wong, *Mechanism of a prototypical synthetic membrane-active antimicrobial: Efficient hole-punching via interaction with negative intrinsic curvature lipids*, *Proc. Natl. Acad. Sci. U.S.A.* **105** (2008) 20595–20600.

[137] Y. Wang, Y. Tang, Z. Zhou, E. Ji, G. P. Lopez, E. Y. Chi, K. S. Schanze, and D. G. Whitten, *Membrane Perturbation Activity of Cationic Phenylene Ethynylene Oligomers and Polymers: Selectivity against Model Bacterial and Mammalian Membranes*, *Langmuir* **26** (Aug., 2010) 12509–12514.

[138] J. Du, A. W. Thomas, X. Chen, L. E. Garner, C. A. Vandenberg, and G. C. Bazan, *Increased ion conductance across mammalian membranes modified with conjugated oligoelectrolytes*, *Chem. Commun.* **49** (Sept., 2013) 9624–9626.

[139] C. Catania, C. M. Ajo-Franklin, and G. C. Bazan, *Membrane permeabilization by conjugated oligoelectrolytes accelerates whole-cell catalysis*, *RSC Adv.* **6** (Oct., 2016) 100300–100306.

[140] J. H. Ortony, T. Chatterjee, L. E. Garner, A. Chworos, A. Mikhailovsky, E. J. Kramer, and G. C. Bazan, *Self-Assembly of an Optically Active Conjugated Oligoelectrolyte*, *J. Am. Chem. Soc.* **133** (June, 2011) 8380–8387.

[141] C. Huang and J. T. Mason, *Geometric packing constraints in egg phosphatidylcholine vesicles*, *Proc. Natl. Acad. Sci. U.S.A.* **35** (Jan., 1978) 308–310.

[142] J. Hinks, Y. Wang, W. H. Poh, B. C. Donose, A. W. Thomas, S. Wuertz, S. C. J. Loo, G. C. Bazan, S. Kjelleberg, Y. Mu, and T. Seviour, *Modeling Cell Membrane Perturbation by Molecules Designed for Transmembrane Electron Transfer*, *Langmuir* **30** (Mar., 2014) 2429–2440.

[143] "Preparing Large, Unilamellar Vesicles by Extrusion (LUVET) — Avanti Polar Lipids."
`https://avantilipids.com/tech-support/liposome-preparation/luvet/`.